| | |
|---|---|
| **Titre:** Title: | Bi-stable Radiofrequency Rectangular Waveguide Switch with Magnetic Actuation |
| **Auteur:** Author: | Hassna Ouassal |
| **Date:** | 2011 |
| **Type:** | Mémoire ou thèse / Dissertation or Thesis |
| **Référence:** Citation: | Ouassal, H. (2011). Bi-stable Radiofrequency Rectangular Waveguide Switch with Magnetic Actuation [Master's thesis, École Polytechnique de Montréal]. PolyPublie. https://publications.polymtl.ca/531/ |

UNIVERSITÉ DE MONTRÉAL

# BI-STABLE RADIOFREQUENCY RECTANGULAR WAVEGUIDE SWITCH WITH MAGNETIC ACTUATION

HASSNA OUASSAL
DÉPARTEMENT DE GÉNIE ÉLECTRIQUE
ÉCOLE POLYTECHNIQUE DE MONTRÉAL

MÉMOIRE PRÉSENTÉ EN VUE DE L'OBTENTION
DU DIPLÔME DE MAÎTRISE ÈS SCIENCES APPLIQUÉES
(GÉNIE ÉLECTRIQUE)
AVRIL 2011

UNIVERSITÉ DE MONTRÉAL

ÉCOLE POLYTECHNIQUE DE MONTRÉAL

Ce mémoire intitulé:

# BI-STABLE RADIOFREQUENCY RECTANGULAR WAVEGUIDE SWITCH WITH MAGNETIC ACTUATION

Présenté par : OUASSAL Hassna
en vue de l'obtention du diplôme de : Maîtrise ès sciences appliquées
a été dûment accepté par le jury d'examen constitué de :

M. AKYEL Cevdet, Ph.D., président
M. LAURIN Jean-Jacques, Ph.D., membre et directeur de recherche
M. WU Ke, Ph.D., membre

*In the memory of my beloved father.*

# ACKNOWLEDGMENTS

I wish to express my sincere appreciation and gratitude to my research director, Professor Jean-Jacques Laurin for his scientific insight, invaluable guidance and patience throughout the course of this research. I always felt that he was there when I needed his help and that his door was always open. I consider myself fortunate to have him as my supervisor, I learnt a great deal from him.

A special thanks to professors Cevdet Akyel, and Ke Wu for serving on my thesis committee; the time and effort they put in reviewing my research work are greatly appreciated.

I would like to acknowledge the assistance from all technical staffs at Poly-Grames research centre. I also appreciate the help of all my friends and colleagues at our research center. Furthermore, I would like to thank Nathalie Lévesque and Ginette Desparois for their friendly and helpful service.

Extended thanks go to my mother, brothers and sisters for their encouragement, support and love.

# RÉSUMÉ

Ce mémoire présente une étude sur les utilisations possibles de nouveaux types de commutateurs radiofréquences (RF) bistables dans la réalisation d'antennes reconfigurables et de filtres à hautes fréquences. Ces commutateurs ont l'avantage d'être légers (fabriqués sur une membrane très mince) et d'avoir une consommation de puissance nulle dans les états stables. Les antennes reconfigurables et filtres actuels consomment plus de puissance à cause de l'intégration des commutateurs électroniques à base de semi-conducteurs ou MEMS qui nécessitent d'être polarisés en permanence. Les commutateurs proposés peuvent apporter une alternative, surtout dans des applications qui imposent des exigences strictes sur la consommation d'énergie ou le poids. Puisque ces interrupteurs sont des composants non-électroniques, ils présenteront moins d'interférences sur le comportement des antennes reconfigurables, le problème est particulièrement important lorsque plusieurs commutateurs sont intégrés à l'antenne.

Deux prototypes de configurations distinctes ont été fabriqués et testés expérimentalement afin de vérifier leurs fonctionnements et d'évaluer leurs performances. Le premier prototype est un commutateur membrane placé dans un guide d'onde rectangulaire ouvert (antenne à ondes de fuites). Le deuxième est un commutateur à réactance variable, placé dans un guide d'onde rectangulaire fermé. Une des extrémités de la membrane est fixée à la paroi basse du guide et l'autre extrémité est laissée libre. Les commutateurs sont réalisés à partir d'un substrat flexible *Pyralux* de *Dupont,* composé d'une couche diélectrique (polyimide), laquelle est recouverte d'une couche de cuivre sur une de ses deux faces. Les commutateurs utilisent un système d'actionnement magnétique et ne dépensent de l'énergie que lors du passage d'un état stable à l'autre.

Le commutateur à membrane est utilisé pour la conception d'une antenne à ondes de fuites commutable. Pour l'état ON, c'est-à-dire lorsque l'antenne rayonne, les simulations et les mesures ont montré des résultats similaires. Pour l'état OFF, c'est-à-dire lorsque l'antenne n'émet aucun rayonnement, une moins bonne concordance a été observée. La raison est due à un mauvais contact électrique entre la partie libre de l'interrupteur et la paroi haute du guide, lequel nécessiterait quelques améliorations. Globalement, le concept d'une antenne commutable en utilisant ce type de commutateur a été prouvé.

Le commutateur à réactance variable est intégré dans un guide d'onde rectangulaire fermé afin de démontrer un filtre coupe bande « notch ». Les résultats de mesures ont vérifié le concept en présentant des pertes d'insertion maximales de -29.7 dB à la fréquence de coupure 11.1 GHz et une largeur de bande à -20 dB de 0.2 GHz. Deux commutateurs similaires ont été placés en cascade et une largeur de bande de 0.9 GHz a été obtenue. Les temps de commutation de l'interrupteur ont été mesurés et sont de 80 ms pour le passage à l'état OFF et de 3 ms pour le passage à l'état ON.

# ABSTRACT

This M.Sc.A. thesis investigates the feasibility of using new types of bistable waveguide switches to implement reconfigurable antennas and filters. These switches have the advantages of being lightweight (made of very thin membrane) and have zero power consumption in their steady states. Current reconfigurable antennas and filters consume more power due to the integration of electronic switches; semiconductor and MEMS. The proposed switches can provide an alternative, especially in applications that impose stringent requirements on power consumption or weight. Since these switches are non-electronic components, they present less interference on the behaviour of reconfigurable antennas, the problem is particularly important when multiple switches are integrated into the antenna.

Two prototypes of distinct configurations are implemented and experimentally tested to verify and assess their performance. One is incorporated into a leaky rectangular waveguide to provide antenna switchability feature and the other is integrated into a closed rectangular waveguide to implement a switched filtering structure. Both switches are built from a flexible membrane *Pyralux Dupont*, composed of a dielectric layer (polyimide), which is covered with a layer of copper on one side. They are attached to the bottom wall of the waveguide at one part and free to move at the other part. They use a magnetic actuation system and consume energy only when moving from one stable state to the other.

The measured radiation patterns and return losses of the switched leaky wave antenna in the ON state agree quite well with the predictions obtained with a finite elements simulation tool (HFSS). However, there is a noticeable difference between the simulation and experimental results in the OFF state. This is mainly due to a non-uniform physical contact between the edge of the switched membrane and the inner

side of the waveguide's broad wall. Overall, the results of this proof of concept look promising. This technique provides an approach to implement reconfigurable antenna using bistable membrane built on a dielectric substrate.

A stop-band "notch" filter is demonstrated using a variable reactance membrane switch integrated into a closed rectangular waveguide. This structure can be used in an application that requires channel selection. Using only one switch, the measured $S_{21}$ at the notch frequency of 11.1 GHz is -29.7 dB, with a 20 dB insertion loss bandwidth of 0.2 GHz. By cascading two similar switches, the 20 dB stop-band is as wide as 0.9 GHz. The measured switching times are 3ms for the transition from the OFF to the ON state and 80 ms for the transition from the ON to the OFF state.

# CONDENSÉ EN FRANÇAIS

Le but du projet de recherche décrit dans ce mémoire est de concevoir et d'intégrer un nouvel interrupteur radiofréquence (RF) bistable actionné par un champ magnétique afin de déterminer son potentiel dans la réalisation d'antennes reconfigurables et filtres à hautes fréquences pour les systèmes de télécommunications. L'interrupteur proposé est construit sur une membrane flexible et intégré dans un guide d'onde rectangulaire. Pour parvenir à cela, nous avons choisi de développer deux configurations:

- Interrupteur dans un guide d'ondes rectangulaire ouvert (antenne à ondes de fuite) ;
- Interrupteur dans un guide d'onde rectangulaire fermé.

Ce mémoire s'articule autour de cinq chapitres. Le premier chapitre présente une vision globale des interrupteurs RF, leurs applications et leurs différents principes de fonctionnement. Le deuxième chapitre, présente la conception de l'interrupteur à membrane proposé. Le chapitre 3 porte sur l'intégration de l'interrupteur bistable dans une antenne à ondes de fuite. Le chapitre 4 est consacré à la réalisation d'une réactance variable placée dans un guide d'onde rectangulaire fermé dans le but d'accomplir un filtre commutable. Le dernier chapitre conclut ce mémoire et présente les travaux futurs.

Chapitre 1 : Introduction aux commutateurs RF

Ce chapitre présente de façon générale les commutateurs RF, le principe de fonctionnement de leurs mécanismes d'actionnement et leurs applications.

Chapitre 2: Commutateur RF à base d'une membrane de polyimide

Ce chapitre présente les deux commutateurs réalisés. Leurs dimensions physiques sont indiquées sur les Figures 2-1 et 2-2. La Figure 2-1 illustre le commutateur membrane et la Figure 2-2 présente le commutateur à réactance variable. Les interrupteurs sont constitués d'une membrane fixée à une extrémité, et sont réalisés à partir d'un substrat flexible *Pyralux* de *Dupont* composé d'une couche diélectrique (polyimide) recouverte de cuivre sur une face. Ils comportent une partie fixe et une partie mobile. Pour le commutateur membrane, la partie mobile comprend un ensemble de bandes de cuivres séparées par le diélectrique d'un côté et une pièce magnétique (Metglas) de très haute perméabilité de l'autre. Pour le commutateur à réactance variable, la partie mobile se compose d'une partie non métallisée (couche de polyimide) partiellement recouverte d'une mince plaque de matériau magnétique (Metglas).

Le substrat constituant le matériel de base de l'interrupteur comprend une couche de diélectrique d'une épaisseur de 25.4 μm (polyimide) et d'une couche métallique 35 μm (cuivre). Ce choix résulte d'un compromis entre la consommation en courant et l'épaisseur de substrat. Avec une faible épaisseur de substrat, l'interrupteur est instable lorsqu'il est soumis à des perturbations extérieures. Avec une épaisseur plus importante, le commutateur est moins sensible mais nécessite davantage de courant. Une analyse mécanique et magnétique a été élaborée afin de déterminer une formulation analytique de la densité du champ magnétique nécessaire pour un déplacement vertical de 2 mm de la partie mobile de l'interrupteur à l'intérieur du guide. Les calculs ont montré que ce champ devait être de 12.61 millitesla (mT), tandis que les mesures ont montré qu'un champ de 12 mT était suffisant.

Chapitre 3: Antenne à ondes de fuite utilisant un commutateur membrane

L'objectif de ce chapitre est d'utiliser le commutateur membrane pour commander une antenne à onde de fuite.

Dans un premier temps, des simulations avec le logiciel commercial d'éléments finis HFSS (*High Frequency Structure Simulator* de la compagnie Ansoft) ont été réalisées afin d'étudier le fonctionnement de l'interrupteur et l'effet de ce dernier sur le rayonnement de l'antenne. Les simulations présentées sur la Figure 3-5, ont montré de bons résultats. En effet, lorsque le commutateur est à la position horizontale (ON) l'antenne rayonne. Lorsqu'il est à la position verticale (OFF) l'antenne ne rayonne pas. Pour tester expérimentalement le système, un modèle réduit de l'interrupteur a été placé dans un guide d'onde. Le test a montré qu'à l'état OFF, l'interrupteur ne faisait pas un contact physique uniforme avec la surface du guide. Par conséquent, l'idée de réaliser une antenne reconfigurable avec un réseau de commutateurs n'a pas été poursuivie. Nous sommes alors tournés vers un autre design, présenté sur la Figure 3-6. Dans ce nouveau design, l'antenne est composée d'un guide d'onde rectangulaire de dimensions (900x80x9760) $mils^3$ muni d'une fente longitudinale et du commutateur membrane illustré à la même figure. La fente est d'une longueur de 6760 mils et large de 200 mils. Notre guide n'étant pas de dimensions standard, nous avons utilisés une transition permettant d'exciter le mode $TE_{10}$ comme l'indique la Figure 3-8(a). Un aimant permanent (très mince) produisant une densité de flux de 2.55 mT est collé à la paroi du guide (Fig.3-10) pour assurer la bi-stabilité, et deux bobines sont intégrées de chaque côté du guide pour permettre la commutation. Lorsqu'un courant est appliqué à la bobine de l'état OFF, la membrane est fléchie vers la position verticale (état stable 1) où elle établit un contact électrique avec l'intérieur de la paroi et reste maintenu à l'état OFF par l'aimant permanent. L'onde incidente est alors réfléchie et par conséquent, l'antenne ne rayonne pas. En excitant momentanément la bobine de l'état ON, la membrane est déplacée à la position horizontale (état stable 2). Le commutateur est à l'état ON et l'onde se

propage le long de l'antenne où l'énergie fuit à travers la fente. L'antenne commute avec un courant de 40 mA à l'état OFF et 140 mA à l'état ON, et l'interrupteur ne consomme aucun courant dans les deux états. Lorsque le commutateur est à l'état ON, les simulations des caractéristiques de l'antenne concordaient avec les mesures. Toutefois, une moins bonne concordance a été observée pour l'état OFF. La raison vient d'un mauvais contact électrique entre la membrane et la paroi du guide, lequel nécessiterait quelques améliorations. Globalement, le concept d'une antenne commutable par ce type de commutateur a été prouvé.

Chapitre 4 : Interrupteur membrane pour filtres de guide d'ondes commutable

Dans ce chapitre, le commutateur à réactance variable est intégré dans un guide d'onde rectangulaire fermé (Fig. 4-1). Il est situé à une distance d = 50 mils (Fig. 4-4) de la paroi latérale du guide d'onde. Nous avons conservé le même guide d'onde ainsi que le même mécanisme de commutation et de bistabilité utilisés pour démontrer l'antenne commutable. Cependant, une deuxième transition est ajoutée au guide d'onde afin de mesurer la transmission. À l'état ON, la membrane est en position basse et l'onde se propage à travers le guide. À l'état OFF, l'interrupteur est actionné pour que la membrane réalise un contact diélectrique-métal avec la paroi haute du guide. La réactance du guide d'onde est modifiée ce qui empêche une partie du signal de se propager jusqu'au port de sortie. Il est à mentionner que pour éviter le problème de contact électrique rencontré lorsque l'interrupteur était à l'état OFF dans la partie «Antenne à ondes de fuite utilisant un commutateur membrane », le commutateur dans sa position naturelle (état ON) est fixé de manière à ce que le côté polyimide de la membrane fasse face à la paroi haute, tandis que son côté métallique (Metglas) coïncide avec la paroi basse du guide d'onde. Dans les simulations HFSS, l'interrupteur est modélisé comme un conducteur électrique parfait. Donc, A l'état OFF, un écart de 1 mil (épaisseur polyimide) sépare la paroi métallique haute du guide et la membrane.

Cet interrupteur commute à partir de 30 mA en un temps de 80 ms pour l'état OFF, et de 110 mA en un temps de 3 ms pour l'état ON. À l'état OFF, le commutateur présente un comportement de filtre coupe bande. À la fréquence de coupure égale à 10.8 GHz, les pertes d'insertion sont de 33 dB. La largeur de bande pour une perte d'insertion de 20 dB est de 0.2 GHz. Ces résultats sont comparés avec les valeurs mesurées et une bonne concordance à été observée. Cependant, un léger décalage de la fréquence de coupure est observé. En effet, la fréquence de coupure est mesurée à 11.1 GHz au lieu de 10.8 GHz. Cela peut provenir d'un léger décalage dans le positionnement de l'interrupteur lors de son intégration dans le guide. En effet, comme le montre la Figure 4.5, un petit décalage de l'emplacement de l'interrupteur provoque une variation de la fréquence de coupure.

Il serait avantageux d'ajouter des commutateurs multiples pour obtenir une bande passante plus large. Pour ce faire, deux commutateurs similaires ont été placés en cascade dans le guide d'onde comme le présente la Figure 4-10. En commutant l'un des interrupteurs à l'état OFF, la largeur de bande simulée et mesurée est de 0.2 GHz. En forçant les deux interrupteurs à l'état OFF, la largeur de bande simulée et mesurée est de 0.9 GHz. On peut remarquer que les valeurs simulées concordent avec celles mesurées. Par contre, dans le cas ou les deux interrupteurs sont à l'état OFF, les pertes de retour mesurées dans la bande passante sont moins bonnes que celles modélisées. Ceci peut être dû à des pertes dans les transitions entre guides d'ondes de tailles différentes.

Finalement une discussion sur les améliorations possibles a été élaborée. Le temps de commutation de l'interrupteur à l'état OFF est long par rapport à celui à l'état ON. Ceci est dû à des rebonds (Fig. 4-15) de l'interrupteur qui apparaissent avant qu'il se stabilise. Il serait intéressant de minimiser ce temps de commutation en utilisant par exemple un matériau magnétique de plus haute perméabilité, ce qui réduirait la tension requise ainsi que le temps de commutation. En ce qui concerne

l’antenne commutable, les efforts futurs doivent être dirigés vers l'élaboration d'une technique pour améliorer le contact électrique lors de l’état OFF. Il serait aussi intéressant de réaliser un filtre ajustable en fréquence. Nous avons observé qu’en modifiant la dimension physique de la membrane, une modification de la fréquence de coupure pouvait être obtenue (Figs. 4-2 et 4-3). Aussi, en cascadant plusieurs membranes à réactances variables de dimensions différentes à l’intérieur du guide d’onde, la fréquence de coupure peut être modifiée dépendant de l’interrupteur actionné.

# CONTENTS

# LIST OF TABLES

# LIST OF FIGURES

# LIST OF ABBREVIATIONS AND NOTATIONS

| | |
|---|---|
| SAR | Synthetic Aperture Radar |
| RF | Radio-Frequency |
| MEMS | Micro-Electro-Mechanical Systems |
| FET | Field-Effect-Transistor |
| PIN | P-Type Intrinsic N-Type |
| DC | Direct Current |
| MIM | Metal-Insulator-Metal |
| GaAs | Gallium Arsenide |
| MESFETs | Metal-Semiconductor Field-Effect-Transistors |
| FETs | Field-Effect-Transistors |
| IDC | InterDigital Capacitors |
| Q | Quality Factor |
| PEC | Perfect Electric Conductor |
| $\mu_r$ | Relative Permeability |

# INTRODUCTION

Human involvement in space exploration and Earth science will bring new advanced sensing and communication systems to allow for higher data transmission rates and exploration of planets like Mars, Moon and beyond, as well as for more accurate earth and planetary remote sensing activities. Taking into account the cost of launching hardware into space (about $20K per kg), also the payload fairing space limitations, there is a need in finding new methods of fabricating large antennas which present lighter weight than conventional antennas to circumvent these limitations. Such large antennas [1] would seem to be impossible to launch into space, unless one considers innovative materials and lightweight structures that can be compactly packaged for launch and reliably deployed once in orbit.

To address this issue, deployable structures using inflatable or thin-membranes have presented a new possibility to satisfy the aforementioned requirements. This type of space structures, because of the use of membranes and lightweight components, provide a means to reduce the mass launch vehicle, stowage volume and overall program cost associated with the payload systems.

Membranes are made of thin, ultra lightweight polyimide[1] film. This implies, low Young's modulus, highly flexible material. Their low bending stiffness, allows them to be found in either tensioned or inflated configurations. Applications of such membranes include SAR membrane antennas [2-5], earth radiometers [6], solar sails [7], and deployable solar arrays. The missions may include deep space, low earth orbit or other Solar System Planets and satellites.

Additionally, these sheet-like membranes can also be used to fabricate prospective RF membrane switches. As example, RF MEMS switches which have been proven to be the most valuable technology compared to their solid-state counterparts

[1] The polyimide membranes used in this work are commercialized by DuPont under the names Kapton® and Pyralux®.

(FET transistor or PIN diodes) since they exhibit low loss, negligible power consumption and inter-modulation distortion. However, a major drawback of these devices is their limited power handling capability (maximum of 0.5W [8-11]), and this prevents them from being used in high power applications such as in transmitters in satellite and/or earth-based communications stations. Moreover, they are very sensitive to environmental conditions such as humidity, dust, vibration and temperature. Therefore, their RF performance can be severely degraded in such conditions.

Research in developing promising membrane switches that improve the disadvantages of MEMS switches, could open doors for a wide range of Earth-space applications.

The research described in this thesis is focused on the design and prototype of a new latching (bistable) RF waveguide membrane switch for the implementation of reconfigurable antennas and filters. To accomplish this, two different switch configurations are explored: One in a slotted waveguide (leaky wave antenna) that will provide the ON/OFF switching feature and the other in a closed waveguide will provide the switched filtering characteristic. In both implementations, the switches are built from thin flexible membrane and consume zero DC current in their quiescent states.

To date, only ferrite switches have showed the latching function with no power consumption. However a drawback of ferrite switches is their weights, especially if the switch is used in space (satellites) where weight consideration is crucial.

A brief outline of the contents of this thesis is as follows. The first chapter introduces RF switches and explores their types, their applications and methods of actuation. It also presents a discussion about power handling capability and linearity.
Chapter 2 reports on the design of the two switch configurations. By using a cantilever flexure, the operation principle, the mechanical and magnetic aspects of the theoretical models are described. The calculated and measured magnetic field are given.

Chapter 3 discusses the integration of a membrane switch into a leaky-wave antenna. Several design solutions to form a switchable antenna are presented. The principle of operation of the fabricated prototype is given. Theoretical and experimental results are presented.

Chapter 4 describes and demonstrates a stop-band (notch) filter based on a variable reactance membrane in a closed rectangular waveguide.

The last chapter provides a summary of the thesis and discussion of future work.

# CHAPTER 1. INTRODUCTION TO RF SWITCHES

This chapter provides an introduction to RF switches. Different types of switch are discussed, along with an emphasis on their applications. Then, a detailed survey of actuation mechanisms is presented, which includes the operation principles and example of some typical devices. The remaining part of this chapter discusses the power handling capability of commonly used switches and describes the nonlinear behavior caused by RF switches and other passive components.

## 1.1 RF Switches and Applications

RF switches are passive components that isolate RF signals when they are OFF, and allow RF signals to pass through when they are ON. Typical arrangements of these switches are single-pole single-throw (SPST), single-pole double-throw (SPDT), and single-pole quad-throw (SPQT), often with each arrangement using series and/or shunt combinations. Figure 1-1 shows two series MEMS switches developed by Analog Devices [12] and Lincoln Laboratory [13] respectively with their equivalent circuit model.

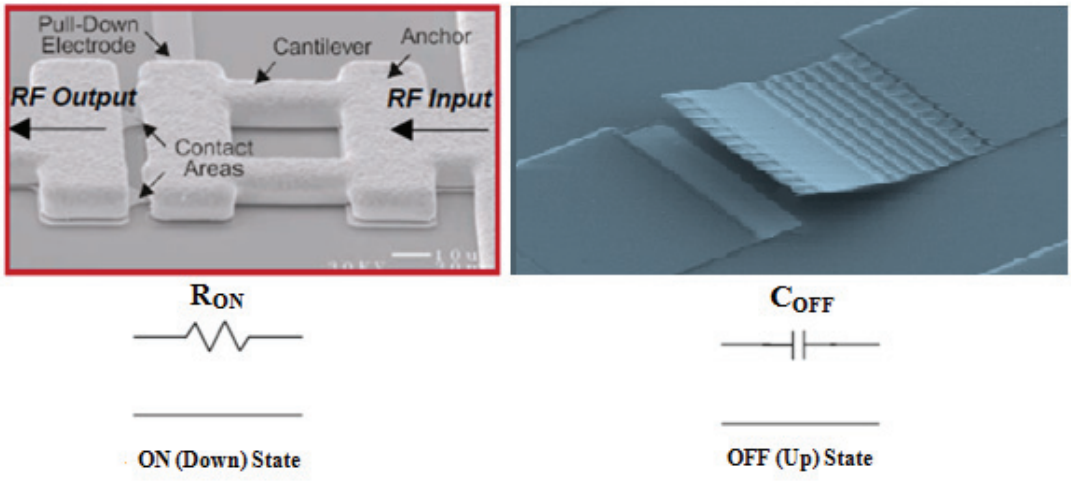


(a) (b)

Figure 1-1 Series switches developed by (a) Analog Devices [12] and (b) Lincoln Laboratory [13] with their equivalent circuits.

Series switches make an open circuit in the signal path ($C_{OFF}$) or a short circuit and a metal-to-metal contact is used to achieve an ohmic contact ($R_{ON}$). Series switches which utilize ohmic (metal-to-metal) contact are commonly used for low frequency applications.

For shunt switches, the principle is based on capacitive coupling. A capacitive (MIM) shunt switch consists of a thin metal membrane "bridge" suspended over a dielectric film deposited on top of the driving electrode with spacing, forming a capacitor (Fig. 1-2). The thin dielectric film is used for DC isolation when the bridge is actuated in downstate. When no DC bias is applied, the bridge remains in the upstate; the switch presents a very small capacitance ($C_{OFF}$), since air is separating the electrode and the bridge. This is referred to as "up or ON state" and the RF signal can propagate with negligible loss. However, when a DC voltage is applied, the switch membrane is pulled down, thus the capacitance is increased ($C_{ON}$); which

is equivalent to an RF short circuit. This is also referred to as "the down or OFF state" and the entire incident RF signal is reflected. Large "OFF" state capacitance and small negligible "ON" state capacitance are required to produce large capacitive ratio ($C_{ON}/C_{OFF}$) in order to achieve high tenability.

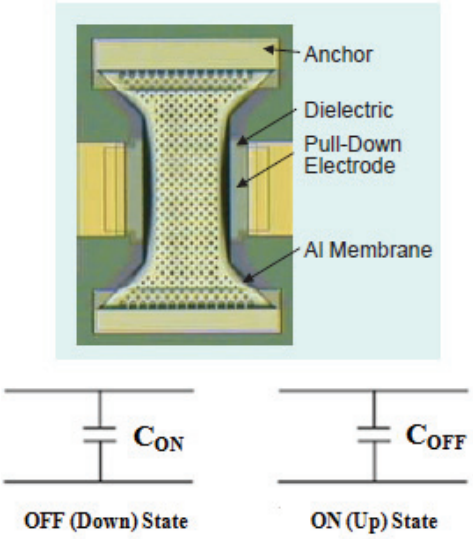


Figure 1-2 Shunt switch developed by Rytheon [14] with the equivalent circuit.

There are many parameters that are more or less critical when evaluating a switch performance. Such parameters are: insertion loss, isolation, DC power consumption, power handling capability, linearity, and switching speed. Traditional switches that include waveguide and coaxial switches show low insertion loss, high isolation, and good power handling capability but are power-consuming and slow. Solid-state electronic devices such as PIN diodes and GaAs MESFETs are used for their high switching speed, commercial availability, and low cost. However, at signal frequencies above 1 GHz, they exhibit large insertion loss in the ON state and poor isolation in the OFF state [15]. MEMS switches offer very low loss, high isolation and extreme linearity. However, disadvantages include increased actuation voltages,

slower switching speeds, and limited power handling. Table 1.1 shows a comparison between PIN, FET and MEMS switch technology [16].

Table 1.1 Performance comparison of RF MEMS, PIN diode, and FET based on [16].

| **Parameter** | **RF MEMS** | **PIN-Diode** | **FET** |
|---|---|---|---|
| Voltage (V) | 20-80 | ± 3-5 | 3-5 |
| Current (mA) | 0 | 3-20 | 0 |
| Power consumption (mW) | 0.05-1 | 5-100 | 0.05 – 0.1 |
| Switching time | 1-300 μs | 1-100 ns | 1-100 ns |
| Up-state capacitance (fF) | 1-6 | 40-80 | 70-140 |
| Series resistance (Ω) | 0.5 – 2 | 2-4 | 4-6 |
| Capacitance ratio | 40-500 | 10 | n/a |
| Isolation (1-10 GHz) | Very high | High | Medium |
| Isolation (10 – 40 GHz) | Very high | Medium | Low |
| Isolation (60 – 100 GHz) | High | Medium | None |
| Loss dB (1-100 GHz) | 0.05-0.2 | 0.3-1.2 | 0.4-2.5 |
| Power handling (W) | <1 | <10 | <10 |

RF switches are employed in a variety of commercial, aerospace and defence application areas including satellite communications systems, wireless communications systems and radar. One example is a simplified block diagram of a satellite payload (Fig. 1-3). It consists of receive/transmit antenna, a beam forming network (BFN), input filter assembly (IFA), high gain receiver (RCV), input and output multiplexers, high power amplifiers (HPA) as well as several switch matrices. In a satellite system of this type, switches are used in the form of the switch matrices to provide redundancy or signal routing. The receiver input/output and low power

switch matrices are typically implemented using coaxial switches while the high power switch matrix is implemented using waveguide switches.

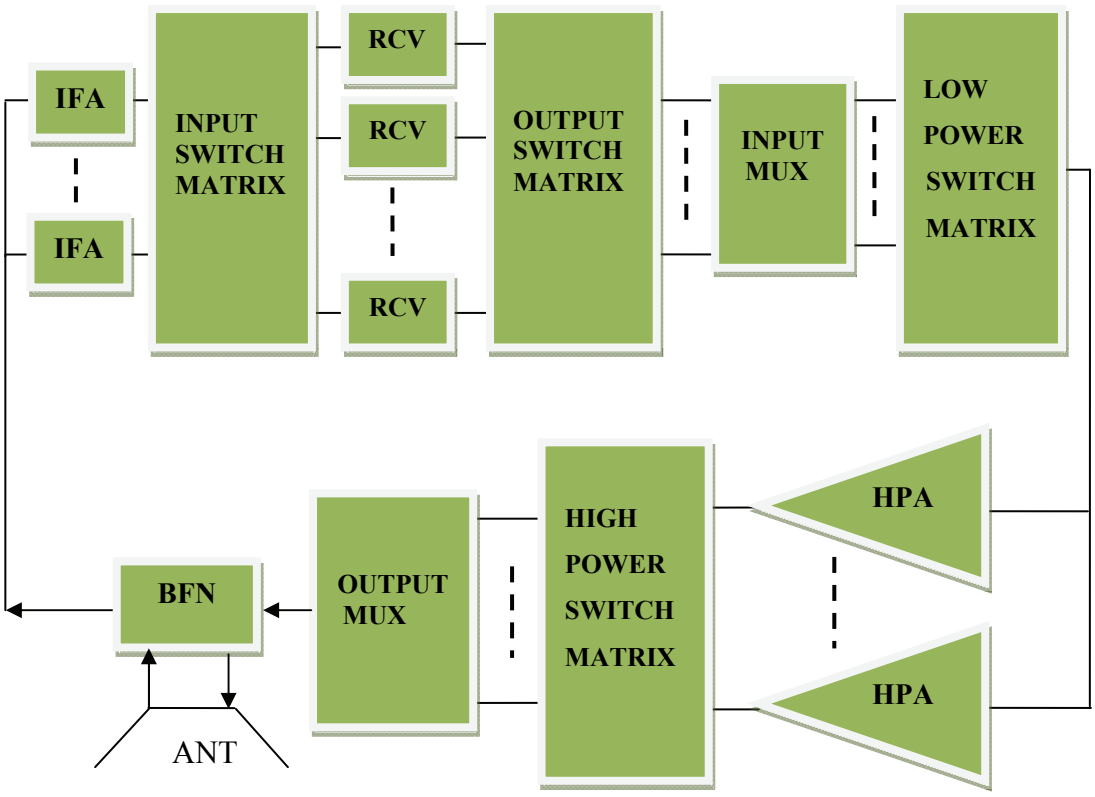


Figure 1-3 A simplified block diagram of a satellite payload [17].

RF switches are more than relays, since they can change the RF impedance of a transmission line. Capacitive membrane switches have been used to implement tunable capacitors (capacitors whose capacitance can be changed by an applied DC voltage) [18]. As the value of a capacitor in a circuit is changed, the impedance and phase in the circuit are likewise changed. Hence, these parameter changes can be employed to design tunable impedance matching networks, phase shifters, tunable filters and other functions where a variable capacitor, or varactor, is used.

Microwave tunable filters can be divided into two groups, filters with discrete tuning, and filters with continuous tuning. Filter configurations presenting a discrete tuning generally use PIN diodes or MEMS switches. On the other hand, filter topologies using varactor diodes, MEMS capacitors, ferroelectric materials or ferromagnetic materials are frequently used to obtain a continuous tuning device.

Zhang & Mansour, 2007 [19], have reported a tunable slotline resonators printed on a microstrip ground plane to make a low pass filter. The tunability was obtained by actuating arrays of RF MEMS switches located on the slots between ON and OFF states, thereby changing the cutoff frequency of the low pass filter.

Ocera et al. 2006 [20], reported a microstrip bandpass filter using hairpin resonators with direct contact cantilever switches on the end of the resonators. The cantilever switches are used to enlarge the hairpin resonators when the switches are in the ON state, thus tuning the device center frequency.

Ong & Okoniewski [21], also reported a four-resonator microwave bandpass filter**.** The filter frequency response is switched using MEMS cantilever capacitive switches. The filter has insertion losses of 0.6 and 1.3 dB and the frequency response tunes from 16.025 to 13.675 GHz.

Ferroelectric materials can change permittivity values proportionally to an applied DC electric field. Barium Strontium Titanate, $((Ba_x,Sr_{1-x})TiO_3)$,(BST), one of the most intensively studied ferroelectric, represents the state-of-the-art technology for tuning microwave devices. BST is used as a dielectric for fabricating tunable capacitors. It has strong electric-field-dependent permittivity, high power handling capability, and a high value of dielectric constant (300 at room temperature) which allows the fabrication of capacitors with very small footprints. Some works on tunable filters using BST varactors, both in parallel plate (MIM) and InterDigital Capacitors (IDC) configurations are reported below.

Nath et al. [22] have reported a tunable third-order combline band pass filter using thin-film BST IDC. The band pass filter achieved 16% tunability (2.44 to 2.84 GHz) upon the application of 0-200 V bias. The insertion loss was 5 dB at zero bias to 3 dB at 200 V.

Tombak et al. [23] reported tunable lowpass and bandpass filters based on parallel plate BST thin film capacitors. The LPF achieved 40% tunability (120-170 MHz) with the application of 0-9 V DC bias and an insertion loss of 2 dB. The BPF showed a tunability of 57% (176-276 MHz) with 0–6 V bias. The passband insertion loss of the BPF was measured to be 3 dB.

Thus, there exist tradeoffs between the IDC and the MIM structures as stated in these references. In a MIM structure, a BST thin film is sandwiched between two metallic layers, while in an IDC structure, the BST film is directly deposited on the appropriate substrate and metal lines form interdigitated structure on the thin film surface. In general IDCs have small tuning range (as a large part of the electric field passes through air and not the dielectric) and a higher bias voltage is required. Nevertheless, they have better power handling capability. MIMs, on the other hand can achieve maximum tunabillity (electric fields are better confined in the film) at low power level, but at the expense of reduced linearity. Other varactors technologies are currently competing with BST varactors, such as diode varactors and MEMS varactors. MEMS varactors have very high Q value. Yet, they have some disadvantages that include low tunability, slow switching speed and high bias voltage (10 to 100 volts). They also face practical challenges of reliability and expensive hermetic packaging. Diode varactors are highly tunable, however they suffer from Q degradation at higher frequencies. A comparison of the aforementioned varactor technologies is shown in Table 1.2.

Table 1.2 Comparison of varactors technologies [24][25].

| **Properties** | **Varactor diode** | **MEMS varactor** | **Ferroelectric varactor** |
|---|---|---|---|
| Tunability | High | Low | High |
| Quality factor | Moderate | High | Moderate |
| Biasing voltage | Medium | High | Medium |
| Tuning speed | Fast | Slow | Fast |
| Power handling | low | Moderate | High |
| Cost | Moderate/High | High | Low |
| Packaging | Hermetic | Hermetic | Standard |

It is apparent that each technology has its own pros and cons, therefore depending on the application one technology will perform better than other. Applications that favour thin film BST varactors are: 1) Ones requiring rapid, continuous tuning at low voltage, and 2) frequency conversion devices, such as frequency multipliers that exploit the "fast" capacitive non-linearity.

## 1.2 Principles of Various Types of Actuation

### 1.2.1 Electrostatic actuation

Electrostatic actuation is based on the principle of charge attraction. Consider two parallel plates (Fig. 1-4) with an applied voltage (V). The capacitance (C) between the plates is given by:

$$C = \frac{\varepsilon_0 \varepsilon_r A}{d} \qquad 1.1$$

Where $\varepsilon_0$ and $\varepsilon_r$ are the free-space and relative permittivities respectively, A is the area of the parallel plates and d is the distance between the plates. When a voltage is applied between the two plates, the electrostatic energy stored in the capacitor is defined as:

$$W = \frac{CV^2}{2} \qquad 1.2$$

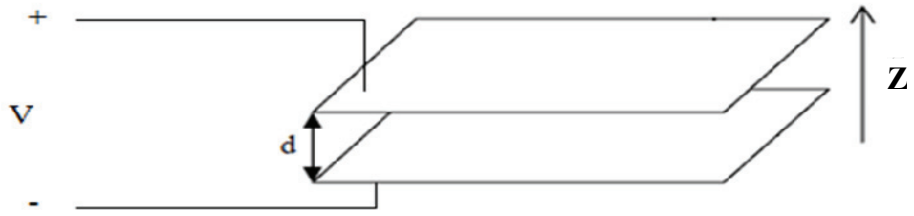


Figure 1-4 Parallel plate capacitor.

Then, the force generated along the Z axis is given as:

$$F = -\frac{\partial W}{\partial Z} = \varepsilon_0 \varepsilon_r \frac{AV^2}{2d^2} \qquad 1.3$$

An example structure of electrostatic switch is shown in Fig. 1-5.

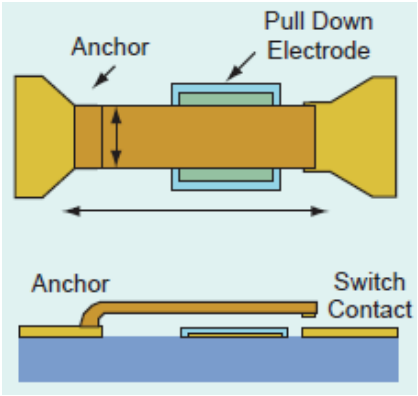


Figure 1-5 Structure of a series electrostatic switch [26].

In this type of series cantilever switch, the bottom electrode is placed underneath the cantilever. By applying an actuation voltage between the membrane and the bottom electrode, an electrostatic force is created to pull the membrane down; the switch ultimately closes when the actuation voltage exceeds the threshold voltage (pull-in voltage). Once the switch closes, the DC electric field will be higher due to the smaller gap between the membrane and bottom electrode.

### 1.2.2 Magnetic actuation

Magnetic actuation offers the possibility of generating torques and attractive forces. Coil structures can create a magnetic field to displace a magnetically coated cantilever. An example of such structure is shown in Fig. 1-6.

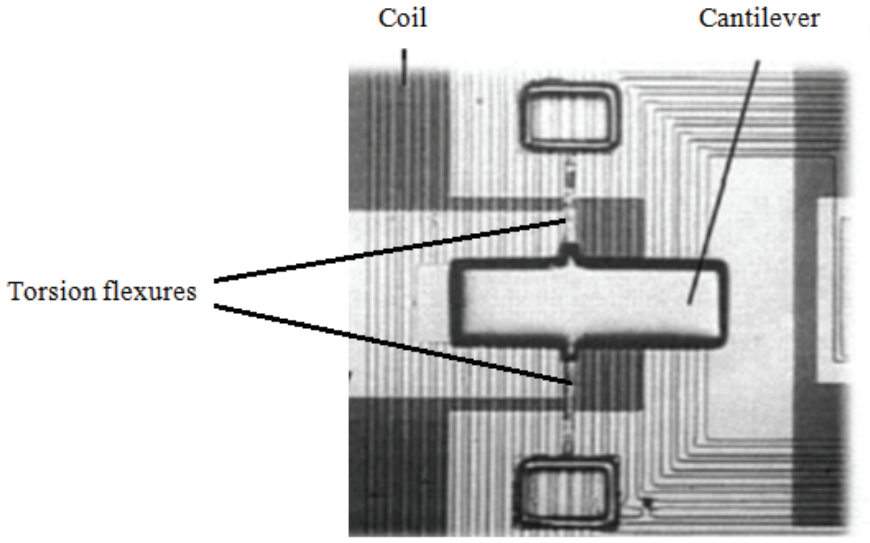


Figure 1-6 Magnetic latching switch [27].

The device consists of a cantilever, integrated planar coil, and a permanent magnet. The cantilever is a bi-layer composite consisting of a soft magnetic material (e.g., permalloy) on its top side and conductive material constitutes the bottom surface. The cantilever is suspended by torsions flexures at its center. Switching between two

stable states is accomplished by energizing the planar coil underneath the cantilever. The switching coil current produces a magnetic field that reverses the direction of the cantilever. Once switched, it is latched by a permanent magnet.

An advantage of this approach is that power is only required while changing the latched state of the device.

The designs proposed in this thesis are also based on this actuation principle. The main difference between this design and the one that will presented in chapters 2 is that our proposed cantilever is fixed at one end and is free to deflect at the opposite. Besides, two coils are used to displace the switching cantilever.

Magnetic actuation can also be done using Lorentz force principle. This principle states that charged particles moving perpendicular to a magnetic field will experience a Lorentz force, that is $\vec{F} = q\vec{v} \times \vec{B}$. Where q is the charge of the particle, v is its speed vector, B is the magnetic flux density.

In engineering applications, Lorentz force can also be expressed as:

$$\vec{F} = \vec{i} \times \vec{B} L \qquad 1.4$$

With $\vec{i}$ is the current that flows through a conductor of length (L). To illustrate this idea, consider a wire loop anchored to two pads with a magnetic field perpendicular to its plane as shown in Figure 1-7. When driven by a current, the wire will be deflected in the direction of Lorentz force.

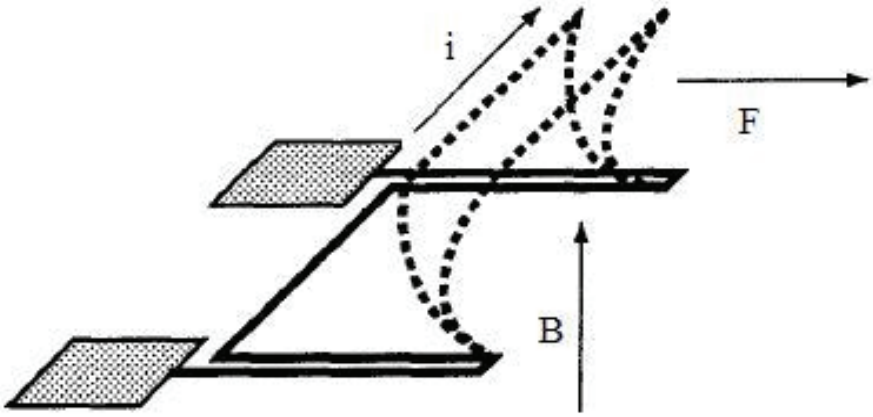


Figure 1-7 Illustration of Lorentz force principle [28].

An example of design is shown in Fig. 1-8, the actuation principle in this device is Lorentz force. The switch is a series type cantilever membrane with coils integrated on the top of it for electromagnetic actuation and a bottom electrode for electrostatic actuation (to minimize power requirements). The bottom electrode is used for holding the membrane in its downward position. The effect of Lorentz force is due to the coils causing the cantilever to deflect up or down depending on the direction of the current (force is proportional to current).

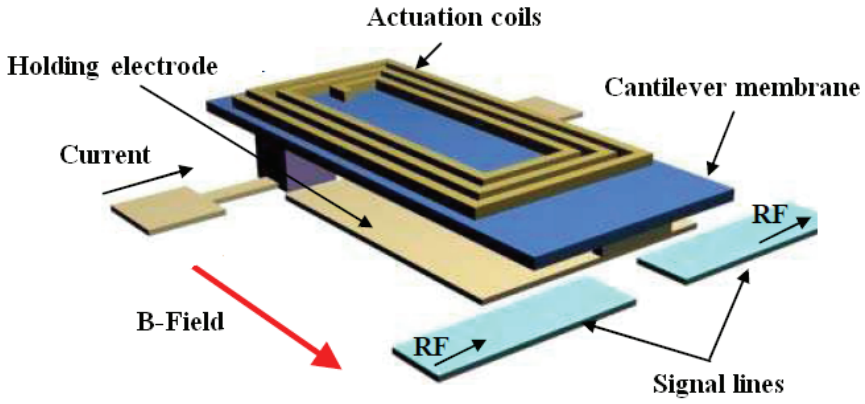


Figure 1-8 cantilever switch based on Lorentz force [29].

### 1.2.3 Piezoelectric actuation

A piezoelectric material generates surface charges when it is subjected to a mechanical stress, which is known as the piezoelectric effect. Inversely, it generates strains if an electric charge is applied to it. This is known as the reverse piezoelectric effect. The governing equations for these two effects are given in Eqs. 1.5 and 1.6:

$$D_i = d_{ij} T_j \qquad 1.5$$

$$S_j = d_{ij} E_i \qquad 1.6$$

Where $D_i$ is the induced electric displacement which is proportional to the piezoelectric coefficient $d_{ij}$ and the applied stress $T_j$ , and $S_j$ is the induced strain which is proportional to the piezoelectric coefficient and the electric field E.

The most common piezoelectric materials are Lead Zirconate Titanate (PZT), Polyvinylidene Fluoride (PVDF) and Zinc Oxide (ZnO). PZT has the largest piezoelectric coefficient.

Piezoelectric actuated switches have been studied by numerous authors including Smits [30], Weinburg [31] and DeVoe [32].

For a piezoelectric cantilever switch, the piezoelectric material is sandwiched between top and bottom electrodes and is poled (polarized) along the polarization "3" axis (see Fig. 1.9). An elastic layer structure is combined with the stack to increase the deformation using the transverse $d_{31}$ or longitudinal $d_{33}$ piezoelectric coefficients to produce bending. For the $d_{31}$ mode, both the polarization and applied electric field point in the thickness direction (along the "3" axis), and the strain is along the "1" axis (orthogonal to the polarization axis). The $d_{31}$ coefficient is therefore used. This kind of actuation mode produces an upward bending displacement. Alternatively, for the $d_{33}$ mode, the polarization, field, and strain lie in the longitudinal direction (along the "3" axis). The $d_{33}$ coefficient is used. Cantilever beams actuated by $d_{33}$ mode produce a downward movement.

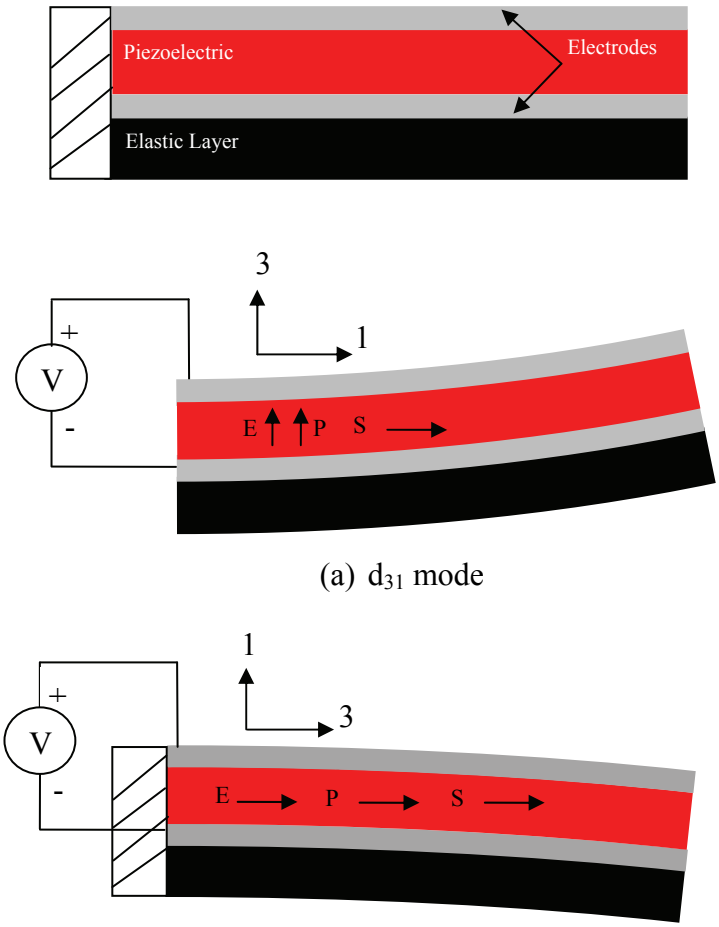


Figure 1-9 Illustration of piezoelectric actuation in a unimorph cantilever for two modes of operation. (a) transverse or $d_{31}$ mode. (b) longitudinal or $d_{33}$ mode. E = Electric field, P = Polarization, S = Strain, V = Voltage.

A piezoelectric microswitch (Fig. 1-10) based on ferroelectric PZT thin film was demonstrated by Gross et al. [33]. The switch used a PZT unimorph cantilever actuator which is composed of a PZT layer on top of an elastic stack of zirconia and silicon nitride. With the Interdigitated (IDT) finger electrodes deposited onto the PZT, the applied field, the polarization and the resulting strain are in the plane of the PZT film. Thus the $d_{33}$ cantilever is downward bending one.

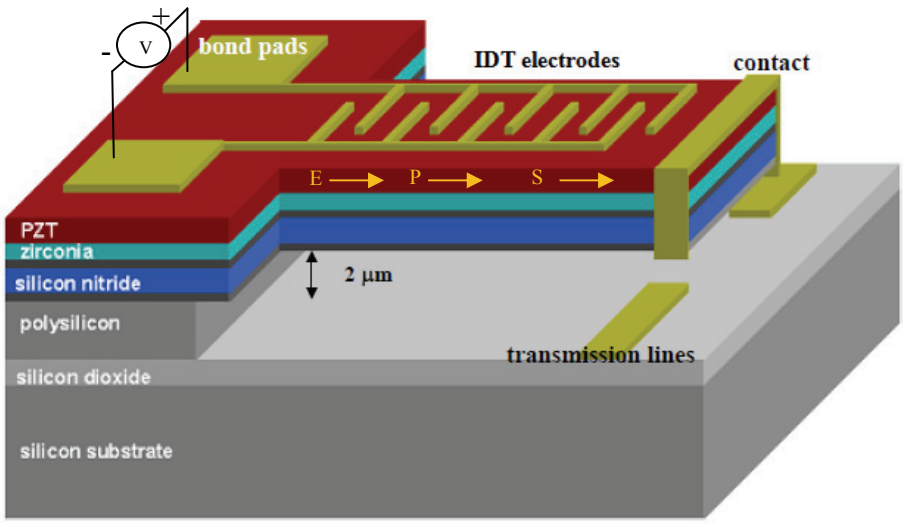


Figure 1-10 An Example of piezoelectric microswitch [33].

### 1.2.4 Thermal actuation

Thermal actuation relies on thermal effect which includes: bimetallic, thermopneumatic, and shape memory alloy (SMA). Bimetallic actuation employs the coefficient of thermal expansion (CTE) mismatch between two layers of different materials to provide bended deformation. In a thermopneumatic actuation, the rise in pressure from a heated fluid (usually a gaz) in a confined cavity is used to deflect a

membrane [34]. Thermo pneumatic actuation is a slow technique but offers very high forces.

Shape memory alloys (SMAs) are materials which exhibit a shape recovery when heated. Some of materials that show the shape recovery effect include: copper, nickel, titanium and zinc alloys. Nickel-titanium alloys is the most used of all SMAs. A shape memory alloy has two solid phases known as martensite and austenite (see Fig. 1-11). The martensite phase occurs at lower temperature. In that phase, the material becomes plastically deformed. When the material is heated up, it transitions to the austenite phase and regains its original shape.

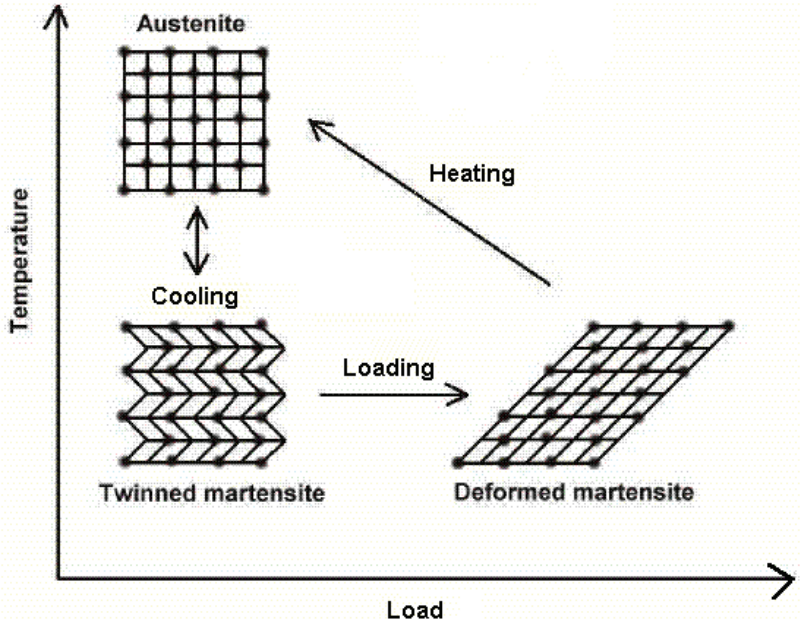


Figure 1-11 Martensite and austenite phases [35].

## 1.3 Summary of the Actuation Mechanisms

RF switches can be actuated either electrostatically, magnetically, thermally or piezoelectrically. Electrostatic actuation is the most common actuation method for

the advantages of low power consumption and ease of integration with a wide variety of fabrication processes, but it may require high voltages to achieve high forces and deflections. Similarly, piezoelectric actuation can offer very high forces but very small deflections with very large voltages. Magnetic actuation is able to provide large forces that produce large deflections, however it is power inefficient. In the case of thermal actuation, the forces are relatively large, but it does tend to increase the switching time and induce noise voltages because of thermal voltage generation effects.

## 1.4 Discussion about Power Handling and Linearity Capabilities

Power handling capability is an important parameter of an RF switch. It indicates that the switch can transmit the power without degradation. Often, power handling and linearity are related; for example the power handling ability for MEMS switch can be limited by the current density causing excessive heat in the circuit, which lead to passive intermodulation product (PIM), a nonlinear effect that will be presented in the next sub-section.

### 1.4. 1 Low and high power switches

In the previous sections, semiconductor (PIN diode - GaAsFET) and MEMS switches have been studied. These devices have power limitations arising from materials properties and/or device design; this prevents them from being used in high-power applications such as in transmitters in satellite and radars. For instance, PIN diode needs large bias current and long switch settling time for high power operation [36]-[37]. GaAsFET transistors suffer from low power capability due to nature of the material [38]. Moreover, MEMS switches have low power handling capability (< 1W). Conversely, switches such as Ferrite waveguide switches are popular for high power applications. Switching is realized by applying magnetic field to change the permeability of the ferromagnetic material. However, they have large

size and mass. Also more energy is required to have the switching magnetic field. Another high power switch is the mechanical switch (e.g. coaxial switch, waveguide switch), which performs switching by moving some metal parts in the waveguide. Mechanical switches can have higher power handling capability as their sizes increase. However, they are unreliable for prolongation applications (e.g. metal parts wear out over time).

### 1.4.2 Nonlinearity problem

In high power RF/microwave systems (e.g. satellite system), passive components such as connectors, switches, cables and antennas are normally considered linear. They can however exhibit nonlinear behaviour when they are subjected to sufficient high power input signals. This nonlinearity generates unwanted signals (interference) at the output, creating harmonics and in-band intermodulation products. This phenomena is called passive intermodulation (PIM) and it appears at frequencies [39]:

$$f_0 = \sum_{i=1}^{M} m_i f_i \qquad 1.7$$

Where $m_i$ are integers and M is the number of the input frequencies. The sum $\sum_{i=1}^{M} |m_i|$ defines the order of the intermodulation product. In the case of two input frequencies $f_1$ and $f_2$ (see Fig. 1-12) equation (1.7) becomes:

$$\begin{aligned} f_0 = m_1 f_1 + m_2 f_2 = f_1 + f_2 + 2f_2 - f_1 + 2f_1 - f_2 + 3f_2 \\ - 2f_1 + 3f_1 - 2f_2 + 4f_2 - 3f_1 + 4f_1 - 3f_2 + ..... \end{aligned} \qquad 1.8$$

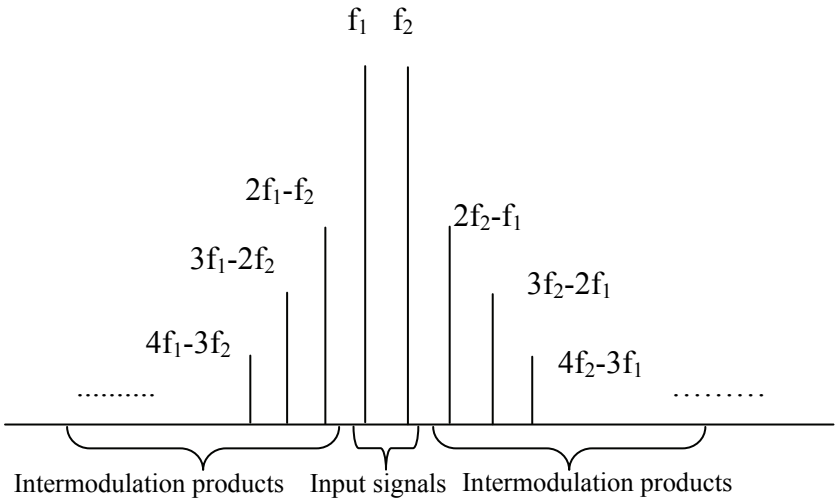


Figure 1-12 Spectral display of non-linearity.

These PIM product can be referred by their order as:

$2f_2-f_1$ and $2f_1-f_2 = 3^{rd}$ order

$3f_2-2f_1$ and $3f_1-2f_2= 5^{th}$ order

$4f_2-3f_1$ and $4f_3-3f_2 = 7^{th}$ order

Typically the lower order PIM products ($3^{rd}$ and $5^{th}$ orders) are of the largest amplitudes and they may create interference. However some of the higher order can also be involved if they are generated by strong signals, which is the case in communications satellites [40].

The sources of PIM include contact nonlinearities and material nonlinearities. Contact nonlinearities involve any contact which presents a nonlinear current/voltage characteristic, typical examples include loose, oxidised and contaminated metallic joint. Many physical mechanisms are responsible for contact nonlinearity, these comprise, high current densities at contacts, electron tunnelling and Schottky effect through thin oxide layers between the metals, and microdischarge across voids and microcracks in metal structures. Material nonlinearities refer to bulk materials such as ferromagnetic and carbon fibres, both of them have nonlinear electrical properties.

An example where PIM problem can occur is illustrated in Figure 1-13, which shows a simplified block-diagram of a satellite antenna subsystem.

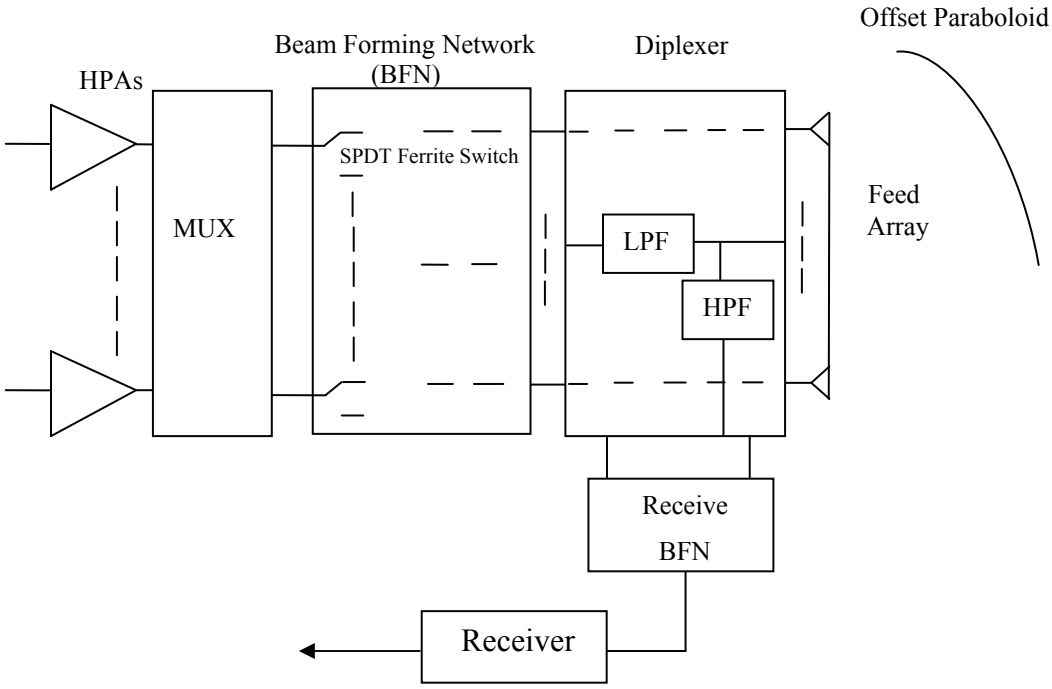


Figure 1-13 Simplified block diagram of antenna subsystem.

In this subsystem, the components multiplexer-Beam forming network-diplexer-antenna-receiver chain, are passive and normally considered to be linear. These components such as metal-to-metal joints, devices having ferrous materials, diplexer filters, reflector surfaces, feed array have been found to be nonlinear to create PIM products of significant magnitude and resulting in the desensitization of the receiver.

# CHAPTER 2. RF SWITCHES USING A POLYIMIDE MEMBRANE

## 2.1 Introduction

As mentioned in the previous chapter, semi-conductors and MEMS switching elements have significant RF performance limitations either at high frequencies or at high power levels. RF MEMS have high isolation, low insertion loss, extreme linearity at frequencies (10-100 GHz) for RF power levels less than 1W. Semi-conductor devices introduce distortions in the input signal at high frequencies (above 1 GHz) and cannot handle high RF power. On the other hand, mechanical switches (coaxial and waveguide) perform well at high frequencies but are power inefficient, bulky and heavy. Furthermore, ferrite latching switches offer low power consumption and good performance at high power, nonetheless, they are heavy. In satellite systems with stringent requirements of size, mass, cost, power handling and power consumption these components require a new solution. Here, we propose novel RF latching switching elements. They may offer potential substitute for the aforementioned devices in space applications. The switches are built from thin polyimide membrane and operate with low currents remaining in steady states with zero DC power consumption. They offer negligible loss and have no bias lines in the propagation media. In addition, their materials are passive and may demonstrate linear behavior at high power levels.

The switches are intended to be implemented in open and closed waveguides. The design aspect is described in section 2.2, the material choice is given in section 2.3, the principle of operation is presented in section 2.4, the mechanical aspect is discussed in section 2.5, the magnetic aspect is considered in section 2.6, the calculated magnetic field is presented in section 2.7, the experimental validation is shown in section 2.8, then the conclusion is stated in section 2.9.

## 2.2 Switches Design

We designed and fabricated two types of waveguide switches. Type 1 is intended to be implemented in a waveguide antenna (Fig. 2.1) while type 2 is meant to be incorporated into a closed waveguide (Fig. 2.2). The switches have a cantilever beam made of Kapton® polyimide substrate (metalized at one side) as the base material. They have fixed and movable beams. For type 1 switch, the movable beam comprises a periodic array of narrow metalized strips printed on the polyimide layer (dielectric). These flexible strips are making a mechanical connection between the rigid part of the movable beam consisting of a magnetic material plate bonded to the base material, and the fixed beam which is also made of metalized polyimide. The copper strips are formed to prevent the unwanted warpage resulting from the stress of switching and to conduct RF current in the OFF state (from the bottom to the top of the waveguide). For type 2 switch, the movable beam however, consists of a first section (flexible beam) of non-metalized polyimide substrate and second section (rigid beam) in which a magnetic plate is bonded to the polyimide substrate. The magnetic plate is responsible for actuating the switch. While the non-metalized substrate is responsible for connecting the fixed and rigid beams and making an easy bending.

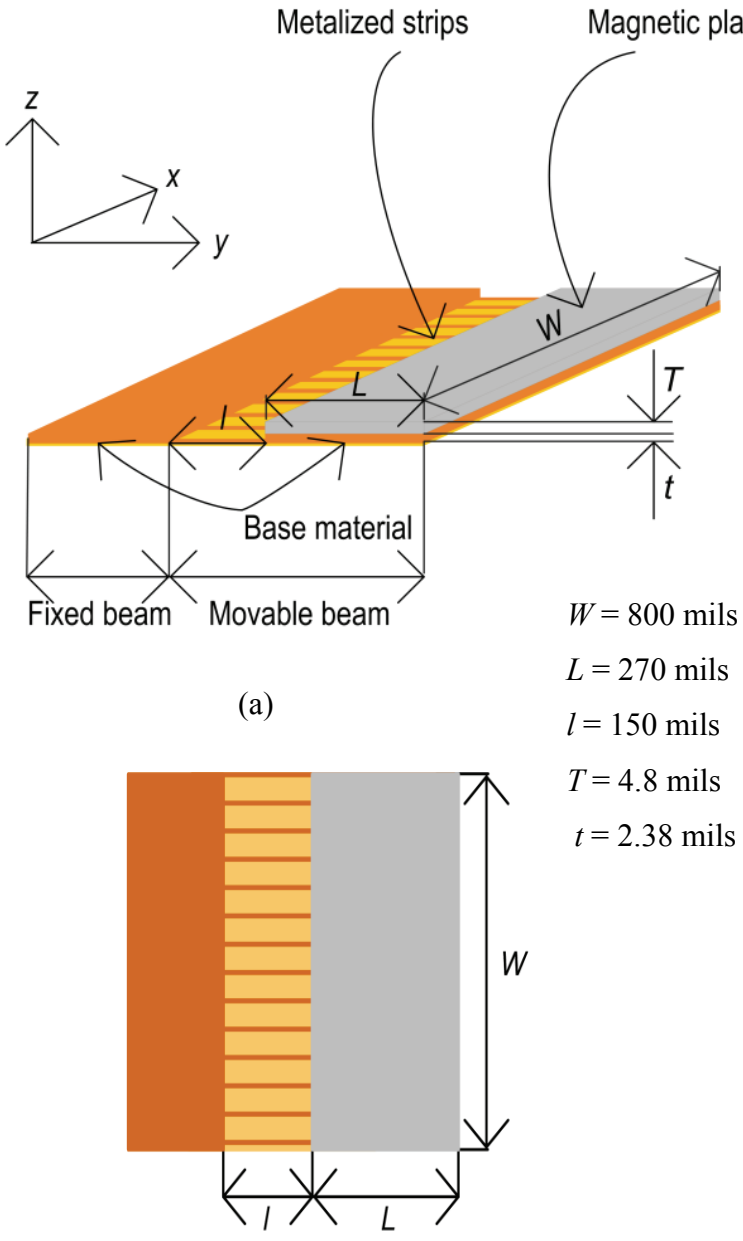


Figure 2-1 Schematic representation of the type 1 switch in the ON state. (a) Perspective view, (b) Top view.

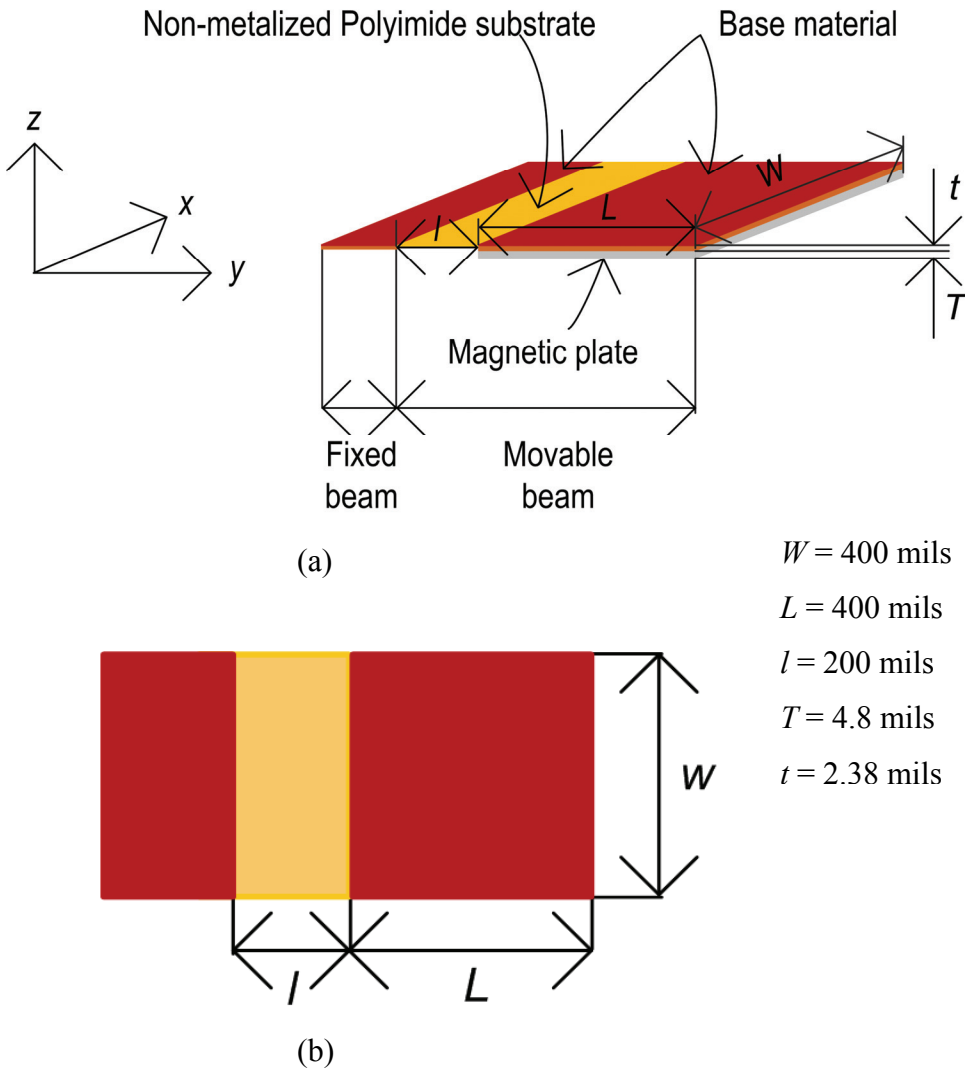


Figure 2-2 Schematic representation of the type 2 switch in the ON state. (a) Perspective view, (b) Top view.

Legend:

$W$: Width of the movable beam

$l$ : Length of the flexible beam

$L$ : Length of the rigid beam

$T$ : Thickness of the magnetic plate

$t$ : Thickness of the base material (polyimide sheet : 1 mil + copper layers : 35 microns)

## 2.3 Material Choice

One concern behind this project was to use as low magnetic field (low drive current) as possible to actuate the switches. For this reason, the material for the switches has to be chosen very carefully. A base material should be flexible, thin, and strong enough to resist the bending stress generated by the switch while a magnetic material needs to have a high permeability. A Single-Sided Copper-Clad polyimide (Dupont) [41] having 35 microns copper layers deposited on a 1 mil (25.4 microns) thick Kapton® sheet was preferred due to the low thickness of the polyimide. Thin films of high-permeability and low remanence material (Metglas 2826MB1 of company Metglas®) [42]) have been chosen, as a magnetic material. It offers a very high permeability ($\mu_r$ > 50 000) which allows high magnetization in a relatively low applied magnetic field.

Prototype switches of different polyimide thicknesses were tested for actuation. With a very thin substrate (0.5 mil), the switch was unstable when subjected to external disturbances. With a greater thickness (2 mils), the switch is less sensitive to disturbances but requires more actuation current.

## 2.4 Principle of Operation

Figures 2-3(a) and (b) show schematically a type 1 switch implemented in an open waveguide (waveguide antenna) and type 2 switch implemented in a closed waveguide respectively. Both waveguides are non-standard WR90 of dimensions 900x80 mils$^2$. The 80 mils height was chosen to have low (DC currents) magnetic fields to actuate the switches. A permanent magnet is bonded to the top broad wall of

the waveguide. The magnet is used to provide the bistability. In addition, two integrated coils are used as electromagnets, one underneath the bottom wall for the ON state and the other above the top wall for the OFF state. The cantilever is initially set to the horizontal position (ON state). When a DC current is passed through the OFF-state coil, a magnetic field is produced that causes the cantilever to move to the vertical position (OFF state). Once switched, the cantilever stays latched by the permanent magnet without any power consumption. The switch returns to its natural (horizontal) position by energizing the ON-state coil.

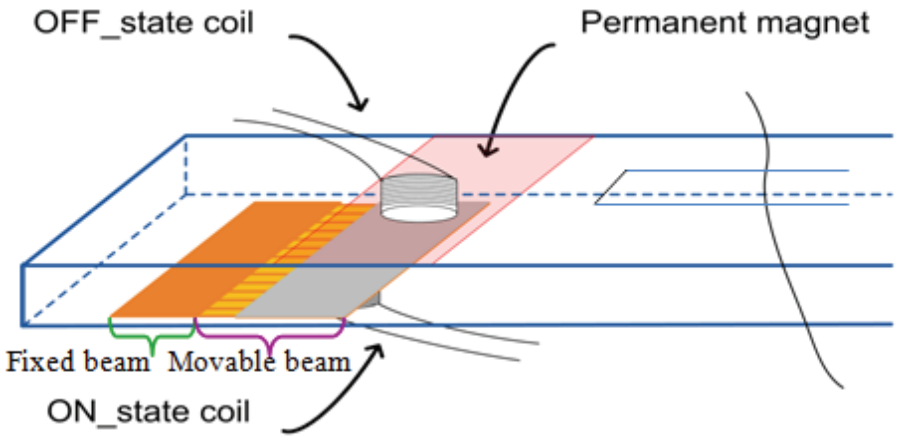


(a)

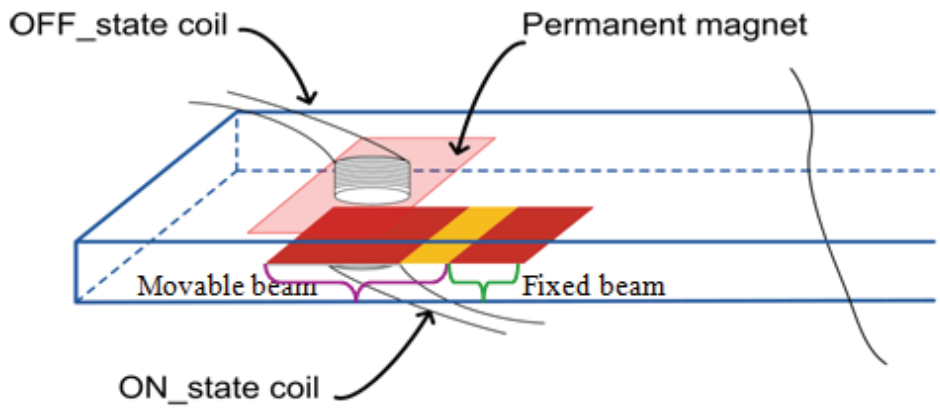


(b)

Figure 2-3 Schematic illustration of the integration of the switches into the waveguides along with the switching and bistability mechanisms. Switches are shown in the ON states, (a) type 1 switch in a waveguide antenna (b) type 2 switch in a closed waveguide.

## 2.5 Mechanical Analysis

In Fig. 2-4, a plate of magnetic material of length $L$ is bonded on a flexible dielectric substrate. It is assumed that the structure is in the vicinity of a magnet (permanent or electromagnet). Initially, if the cantilever is in the horizontal position ($\theta = 0$ in the figure) and the applied $H$ field is vertical and uniform as illustrated, the magnetization in the material will be predominantly vertical. In practice, however the applied $H$ field is never perfectly uniform and it can be assumed that it will have some horizontal component. Given the large length/thickness ratio of the plate, it will have a much stronger demagnetization factor for normal field than for tangential field. Consequently, it can be assumed that a magnetization vector $M$ will develop along the $L$ dimension of the plate even if the horizontal component of the applied $H$

field is small. Then, since the applied $H$ field is predominantly vertical, a magnetic torque $T_m$ will develop on the magnetic plate and cause the cantilever to bend.

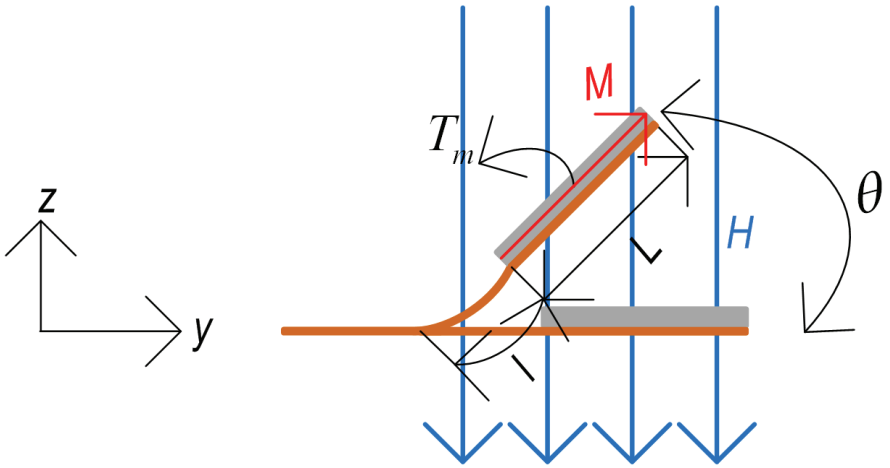


Figure 2-4 Cantilever switch under an applied magnetic field.

Since the beam of length $L$ is much thicker ($t+T \leq 7.18$ mils) and stiffer than the beam of length $l$ ($t \leq 2.38$ mils), it is considered to be rigid while the latter is taken to be flexible. Based on this assumption, the magnetic torque can be translated to the bottom side of the plate (unconstrained torque). Therefore, the mechanical analysis can be simplified to the deformation of a cantilever beam which is fixed at one end and has a torque at the other, as shown in Figure 2-5.

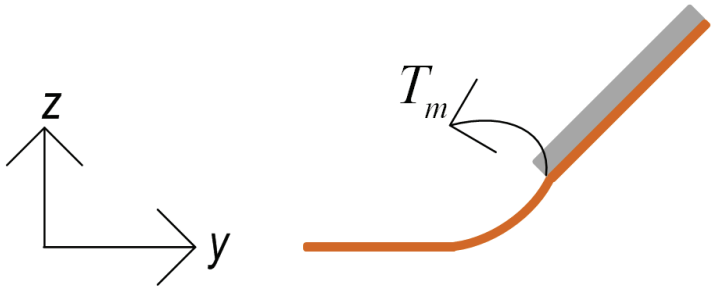


Figure 2-5 Simplified mechanical model of the cantilever switch.

The application of a torque causes a deflection of the cantilever beam along an arc of circle with radius of curvature *R* that is determined by [43]. (see Fig. 2-6).

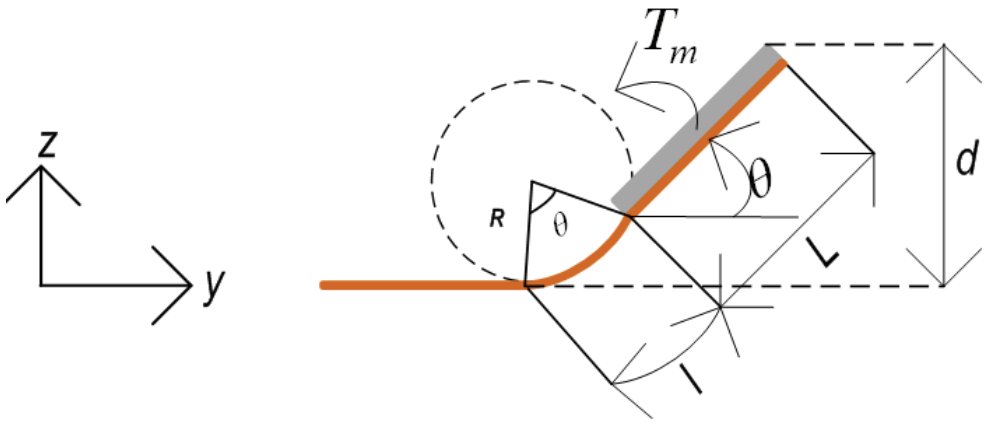


Figure 2-6 Schematic illustration of the cantilever switch under an applied torque.

$$R = \frac{EI}{T_m} \qquad 2.1$$

Where *E, I* are the Young's modulus, the surface moment of inertia of the flexible beam respectively.

The angular mechanical deflection can be expressed as:

$$\theta = \frac{l}{R} \qquad 2.2$$

With l is the length of the flexible beam.

Its relationship with the applied torque $T_m$ is given by:

$$\theta = \frac{l}{EI} T_m \qquad 2.3$$

The moment of inertia *I* depends on the cross section of flexible beam. The latter has a rectangular cross section (see Figure 2-7). For the flexible beam of the type 1 switch, the copper metallization is thicker than the polyimide layer and it has a much

higher Young's modulus. Therefore the analysis can be simplified by ignoring the presence of the polyimide layer in the analysis. In this case $I$ is given by [44].

$I = \frac{W_c t_c^3}{12}$, where $W_c = \sum w_i$ is the total width of all the strips and $t_c$ is the thickness of the copper layers. In the type 2 switch, the flexible beam is only made of polyimide of thickness $t_p$ and width $W_P$. In this case, the moment of inertia is given by $I = \frac{W_p t_p^3}{12}$


(a)


(b)

Figure 2-7 Flexible beams cross-sections: (a) region of strips and (b) polyimide beam.

## 2.6 Magnetic Analysis

In Figure 2-8, we assume that the magnetic plate is homogeneously magnetized with a saturation magnetization $M_S$ .This magnetization results in two equivalent magnetic charges $+q_m$ and $-q_m$ residing on the north and south poles of the Metglas plate respectively. These charges experience equal but opposite forces when they are placed in a uniform magnetic field *H:*

$$F_N = +q_m H \quad and \quad F_S = -q_m H$$

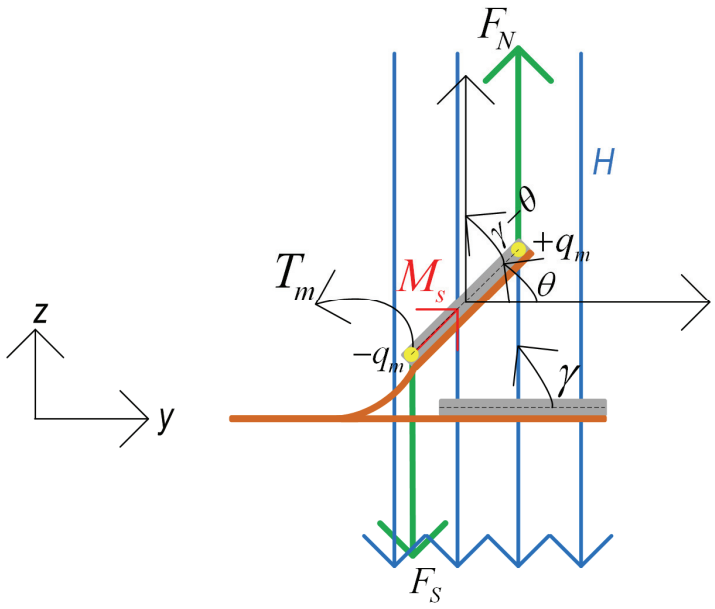


Figure 2-8 Presentation of the magnetic charges, the uniform magnetic field lines and their effect on the displacement of the cantilever switch.

The angle between the initial direction of the magnetic plate and the direction of the magnetic field is $\gamma$ .

Due to the applied torque, the magnetic plate is oriented at an angle $\theta$. The forces $F_N$ and $F_S$ generate a torque that can be expressed as:

$$T_m = q_m HL \sin(\gamma - \theta) = M_S WTLH \sin(\gamma - \theta) = M_S V H \sin(\gamma - \theta)$$

Where $V$ and $M_S$ are the volume and saturation magnetization of the metglas plate respectively.

We will assume that the magnetic field is held constant $(\gamma = 90°)$. This leads to

$$T_m = M_S V H \sin(90 - \theta) = M_S V H \cos\theta \qquad 2.4$$

This expression indicates that as the deflection angle increases the torque decreases and eventually an equilibrium is reached between the applied magnetic torque and the deflection resistance of the flexible beam.

## 2.7 Magnetic Field Density Calculation

Equating eq. 2.3 and 2.4 yields the relationship between $H$ and $\theta$

$$H = \frac{EI}{M_S l V \cos\theta}\theta \quad A/m \qquad 2.5$$

The magnetic flux density can be written as :

$$B = \mu_0 H = \mu_0 \frac{EI}{M_S l V \cos\theta}\theta \quad Tesla \qquad 2.6$$

For type 1 switch, Eq. 2.6 can be written as:

$$B = \mu_0 \frac{E W_c t_c^{\,3}}{12 M_S l V \cos\theta}\theta \qquad 2.7$$

For type 2 switch, it can be expressed as:

$$B = \mu_0 \frac{EW_p t_p^{\,3}}{12 M_S l V \cos\theta}\theta \qquad 2.8$$

The angular deflection $\theta$ can be determined by solving the following equation obtained by simple geometrical analysis from Figure 2.6.

$$d = L\sin\theta + \frac{l}{\theta}(1-\cos\theta) \qquad 2.9$$

Where *d, l, L* are maximal tip deflection, length of the flexible beam and length of the rigid beam respectively.

Based on equation 2.7 for type 1 switch, and using the numerical values in Table 2.1, the minimum flux density necessary to move the tip of the cantilever from the bottom wall to the top wall of the 80 mils thick waveguide is 12.6 mT.

Table 2.1 Parameters used to calculate the magnetic flux density.

| Parameters | Dimensions |
|---|---|
| *L*: Length of the magnetic plate | 270 mils |
| *W*: Width of the magnetic plate | 800 mils |
| *T*: Thickness of the magnetic plate | 4.8 mils |
| $W_c$ : Total width of the copper strips | 224 mils |
| *l*: Length of the copper strips (flexible beam) | 150 mils |
| $t_c$ : Thickness of the copper strips (flexible beam) | 1.38 mil (35μm) |
| $M_S$ : Saturation magnetization of the Metglas | 0.88 tesla [42] |
| *E*: Young's modulus of copper strips | 117 GPas [45] |
| *d*: Maximal tip deflection | 80 mils (2 mm) |
| $\theta$: Angular deflection for contact | 0.234 rad |

## 2.8 Experimental Validation

An MG-501 Magma teslameter was used on the realized switch prototype at the OFF state, the measured flux density was 12 mT, which is close to the calculated value. The teslameter probe was positioned on the bottom wall of the waveguide as shown in Figure 2-9.

We have chosen a waveguide of height 80 mils (2 mm) to have a lowest possible magnetic field (DC current). From equations 2.6 and 2.9, it can be seen that as $d$ increases, so does $\theta$ and $B$. If an array of switches is set into the waveguide, more current will be needed for controlling the displacement, and if the latter becomes higher, additional DC power is required.

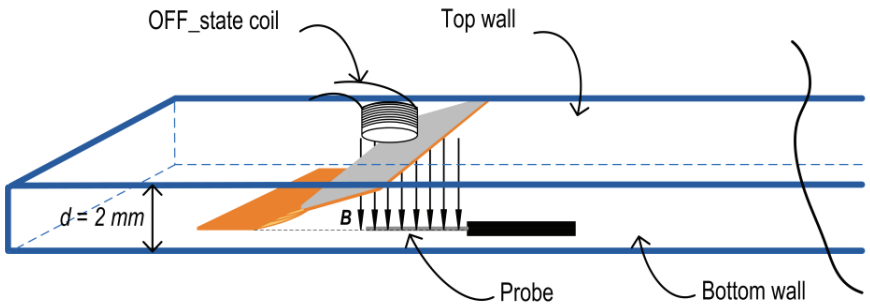


Figure 2-9 Teslameter probe used to measure the magnetic field density generated by the coil that causes the cantilever to move to the top wall of the waveguide.

## 2.9 Conclusion

The following parameters have influence on the magnetic field.

1) Volume of the magnetic plate: $V$

2) Length of the flexible beam: $l$

3) Thickness of the flexible beam: $t_c, t_p$

4) Width of the flexible beam: $W_p, W_c$

The volume of the magnetic plate highly influences the amount of the necessary magnetic field because $\mathrm{B} \propto \frac{1}{V}$, as seen in eq. 2.6. Hence, the practical way to lower the field is to increase the volume. This is not true if gravitational force is taken into account. If $V$ is increased, an additional weight will have to be lifted and $B$ will increase. Furthermore, the thickness $t$ of the base material (copper or polyimide) is very crucial as $B$ is proportional to $I$ ( $B \propto I = \frac{Wt^3}{12}$ ). So, for a lower magnetic field density, it is important that the cantilever is fabricated as thin as possible.

# CHAPTER 3. LEAKY WAVE ANTENNA USING A MEMBRANE SWITCH

## 3.1 Introduction

An antenna that is capable to alter its radiation characteristics, such as operating frequency, polarization or radiation pattern is referred to as a reconfigurable antenna. It provides a unique way to serve different functionalities at different frequency bands, which may lead to considerable saving in size, weight and cost. The reconfiguration can be achieved through switches and variable capacitors. In some design [46]-[47] MEMS switches or PIN diodes are used to change the length of an antenna element such as dipole or a slot, thereby shifting the frequency of operation (resonant frequency). Other approaches make use of varactors to steer or tune the beam of an antenna [48].

The work described here deals with the design, implementation and measurement of a leaky wave antenna in which a membrane switch is incorporated. Strictly speaking, the capability to switch the antenna between ON and OFF states cannot be considered as reconfigurability. However, by incorporating an array of switches in a beam forming network it becomes possible to reconfigure the radiation pattern. Consequently, the switch presented in this chapter should be considered as a building block enabling the synthesis of reconfigurable antennas.

## 3.2 Leaky Waveguide Antenna Theory

A longitudinal slot cut into the broad wall of a rectangular waveguide is known as one of the leaky waveguide antennas. A wave traveling along the waveguide leaks (or radiates) energy as it propagates. The angle at which the leakage occurs is given by:

$$\sin\theta = \frac{\lambda_0}{\lambda_g}$$

Where $\lambda_0$ is the free space wavelength and $\lambda_g$ is the guided wavelength inside the structure. Since the amplitude of the leaky wave decays as the wave propagates, the amount of radiation decreases with increasing x (see Figure 3-1).

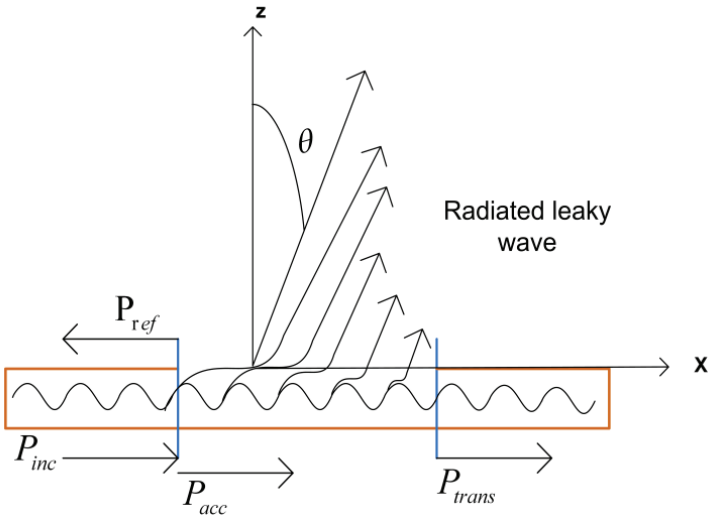


Figure 3-1 Leaky wave structure showing principal beam angle.

The $TE_{10}$ mode incident power $P_{inc}$ from the input waveguide, is partially reflected towards the source at the slotted section with reflection coefficient $S_{11}$. The accepted power by the radiating structure depends on the input impedance mismatch, $P_{acc} = P_{inc} - P_{ref} = P_{inc}(1-|S_{11}|^2)$. The radiated power depends on the portion of the transmitted power (absorbed in the matched load). $P_{rad} = P_{acc} - P_{trans} = P_{acc}(1-|S_{21}|^2)$ Where $|S_{21}|^2$ is the power transmitted to a matched load at the end of the waveguide.

## 3.3 Switchable Antenna Design 1

The intention of this work was to demonstrate the possibility of implementing a reconfigurable antenna using a slotted rectangular waveguide (leaky waveguide antenna) with an embedded membrane switch. A number of design approaches described herein have been tried. These designs have been studied by simulations using the Ansoft HFSS simulator. In one design, a longitudinal slot is made on one of the waveguide's broad walls and two pivoting plates, whose angles with respect to the bottom wall of the guide can be switched, are placed along the length to alter the antenna radiation patterns (Fig. 3-2). In the simulations, the switched plates are considered as infinitely thin perfect electric conductors (PEC). When they are in the down position, the antenna radiates a negligible amount of power, owing to the symmetry of the current distribution along the edges of the centered slot. Similar behaviour is obtained when the switches are in the up position. These cases are referred to as the OFF state. The ON state is obtained by operating with the two plates in opposite positions (i.e. one up and the other down) in order to break the symmetry, as shown in Fig. 3.2. In this case the radiated $E_{\Phi}$ field component in XZ plane increases by 48 dB (see Figure 3-3). In these simulations the width, thickness and length of the rectangular waveguide are 900 mils, 80 mils and 5360 mils respectively. The slot has a length of 5360 mils and a width of 200 mils.

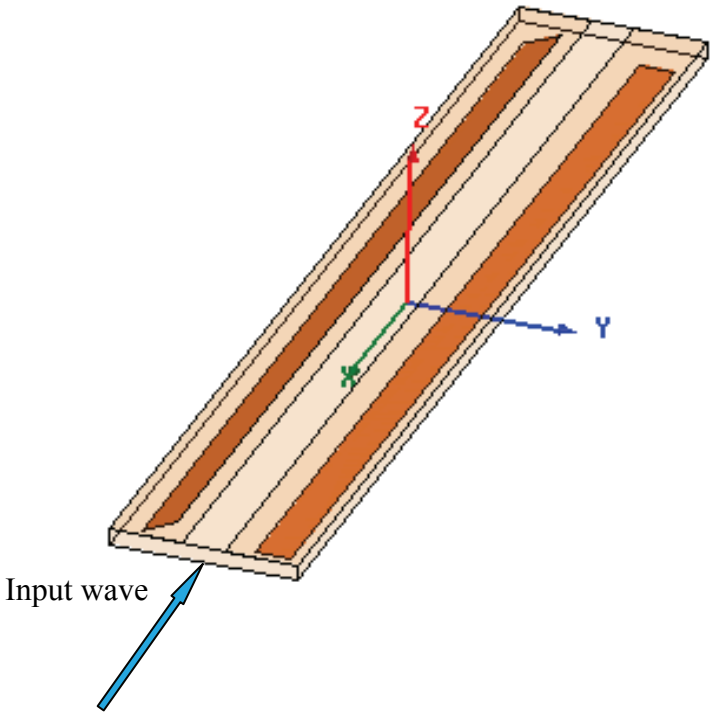


Figure 3-2 Slotted waveguide with two flexible plates, one is in the up position and the other is in the down position. The antenna is in the ON state.

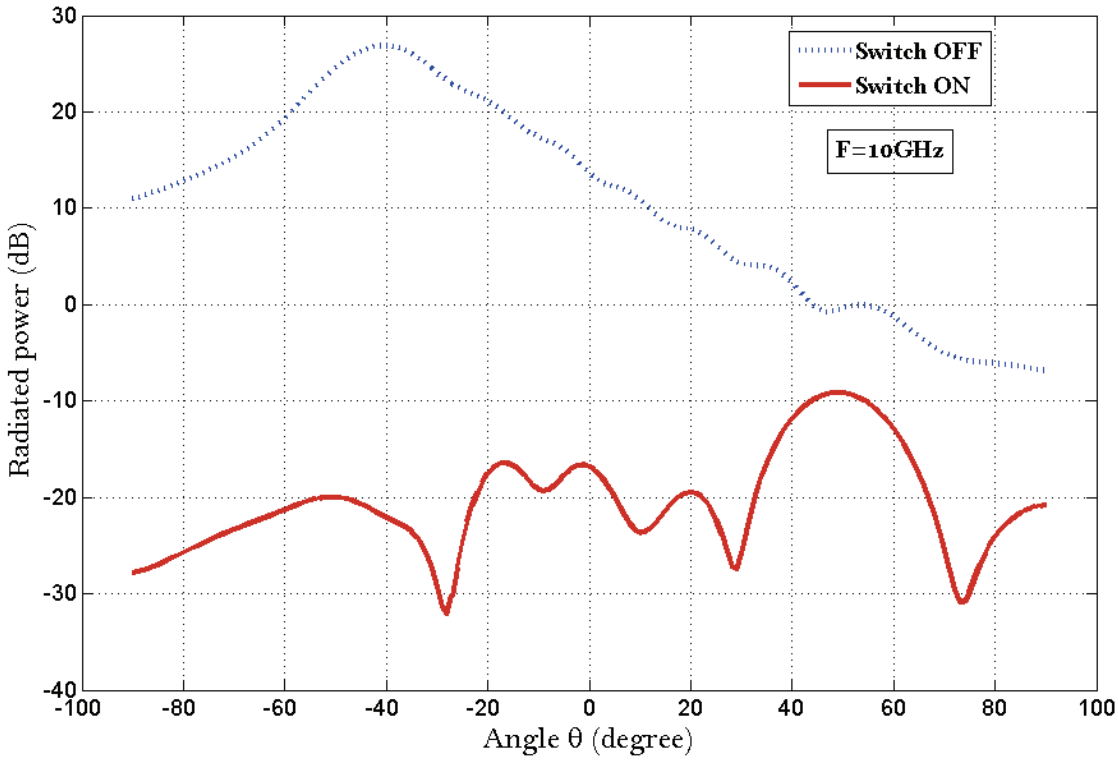


Figure 3-3 Simulated $E_\Phi$ field pattern in XZ plane (H-plane) in the ON and OFF states for antenna geometry 1.

As the presence of two flexible plates is not really needed to alter the symmetry of the fields, we envisaged the design shown in Figure 3-4. In this model, the slot is made asymmetric about the centerline to have a large amount of leakage. The flexible pivoting plate implements a switch of type I, presented in the previous chapter. However, it has different dimensions. Again when the switch is in the down position (lying on the bottom wall of the guide), the antenna radiates. By displacing the switch to the upper position as shown in the figure, the antenna exhibits an insignificant radiation. In other words, the $E_\Phi$ field magnitude when the switch is ON is higher than when the switch is OFF. Figure 3-5 depicts the simulated $E_\Phi$ patterns in H-plane of the ON and OFF switch states. Evidently, there is a 30 dB change in the pattern of $E_\Phi$ between the two states.

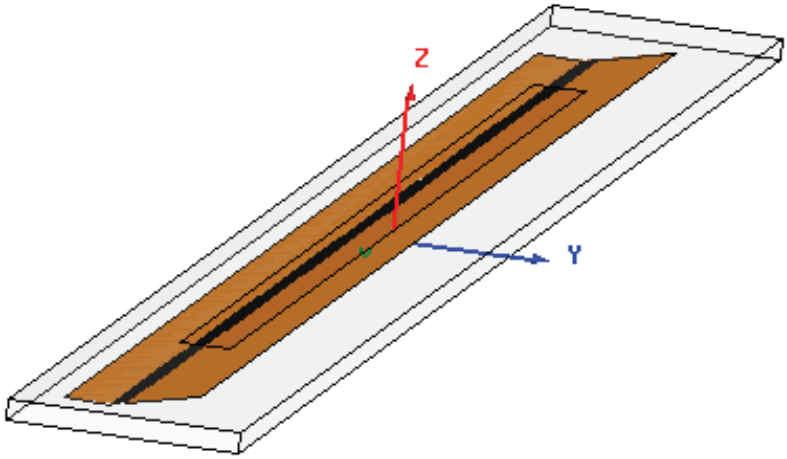


Figure 3-4 Slotted waveguide with one switch in OFF state: geometry 2.

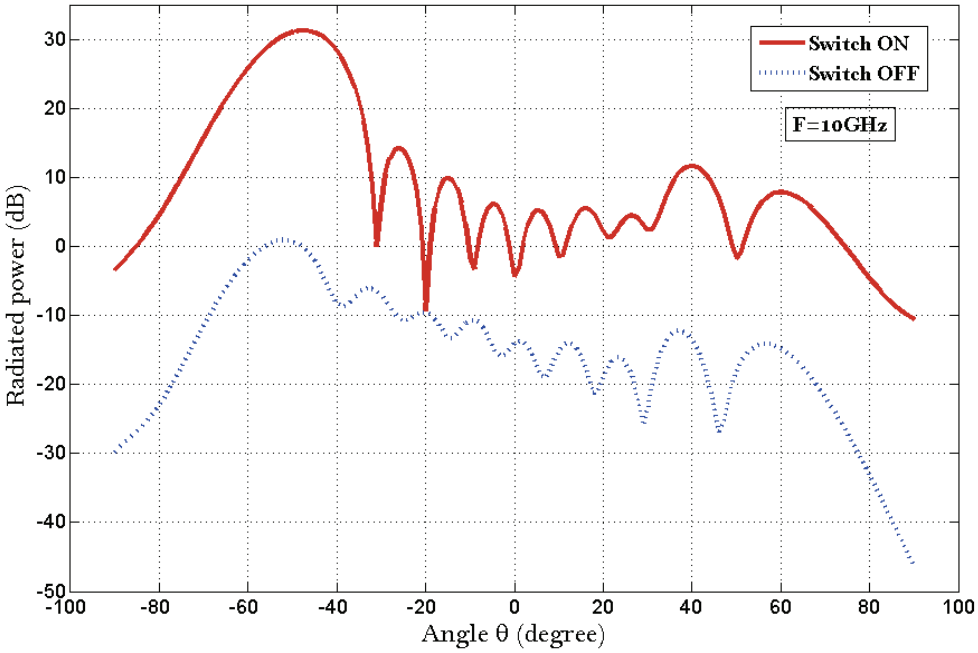


Figure 3-5 Simulated $E_\Phi$ field pattern in H-plane (XZ plane) of the switch operations (ON/OFF) for antenna geometry 2.

A prototype switch of small size was tested for actuation as well as to investigate the energy needed to control the antenna. Experiments show a switching current of 43 mA and 150 mA for moving the plate up and down respectively. Once the device is in the up position, it has been observed that the upper edge of the flexible membrane does not make a uniform physical contact with the broad wall. This allows more radiated power in the OFF state, which is not a desired behaviour. Therefore, it would not be practical to implement an antenna with a long switch or an array of switches. To that end, this design approach was not pursued, and was replaced by the one described below.

## 3.4 Switchable Antenna Design 2

The proposed antenna consists of a (900x80x9760) $mils^3$ slotted rectangular waveguide and uses the membrane type I switch presented in chapter 2 (see Fig. 3-6). The fixed and movable plates implementing the switch are modeled as PEC plates with zero thickness. The switch is placed 540 mils away from the waveguide input port (before the slot) and 50 mils from the waveguide sidewalls. The 800x150 $mils^2$ movable part is composed of thin conducting strips which are spaced apart from one another by air gaps of size $\boldsymbol{s}$ = 45 mils. There are 14 strips, and each strip is of width $\boldsymbol{w}$ = 15 mils.

The slot (Fig. 3-7) is 6760 mils long, 200 mils wide and is asymmetric about the center line. The asymmetry provides a single narrow beam whereas the chosen length and width allow a high gain. It is etched from the copper cladding on the upper side of the waveguide (broad wall). The latter is made of 10 mils RT/duroid 6002 material with a relative dielectric constant of 2.94 and a loss tangent of 0.0012. In order to fasten the broad wall to the waveguide, two screwed metal bars are incorporated into the design. For this aim, the upper side has to be wider (1500 mils) than the waveguide (900 mils) as it can be seen from Figures 3-6 and 3-7.

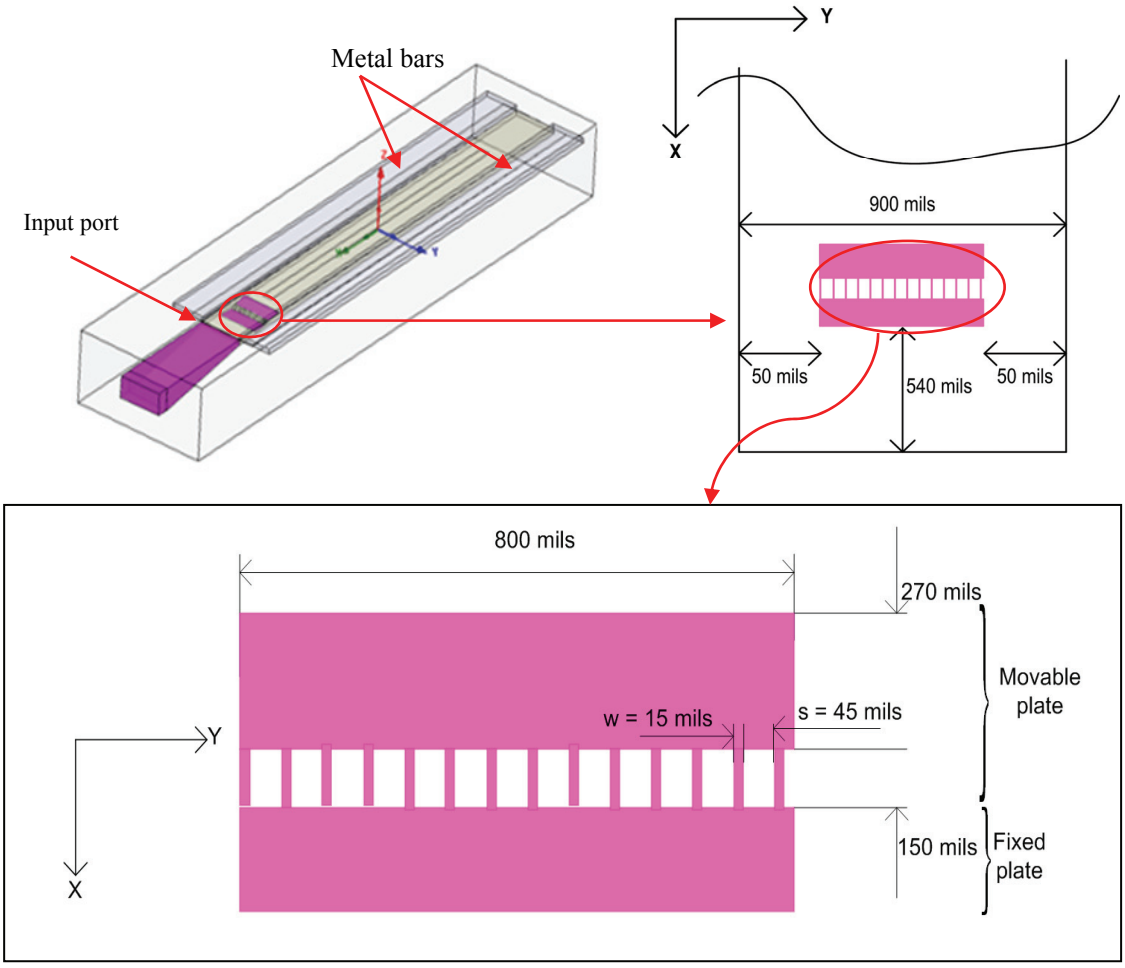


Figure 3-6 A screen shot of the HFSS antenna model showing the arrangement of the switch and its dimensions. Drawing is not to scale.

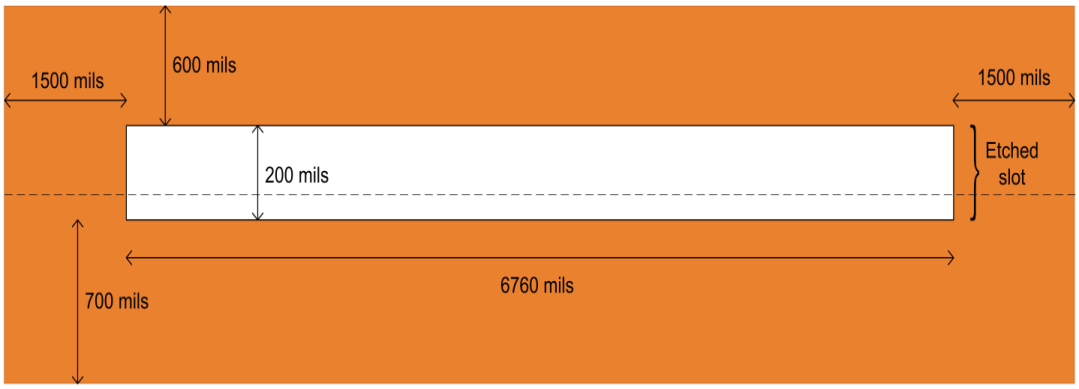


Figure 3-7 Upper side of the waveguide showing the slot dimensions.

As this antenna is a traveling-wave antenna, the output port of the waveguide must be matched. For this reason, waveports at both ends of the waveguide are used to insure a match at both ends of the antenna. To excite the $TE_{10}$ mode in the waveguide using a standard WR90 adaptor, a tapered transition was designed as shown in Figure 3-8 (a). Figure 3-8 (b) depicts the S-parameters simulation results for this transition.

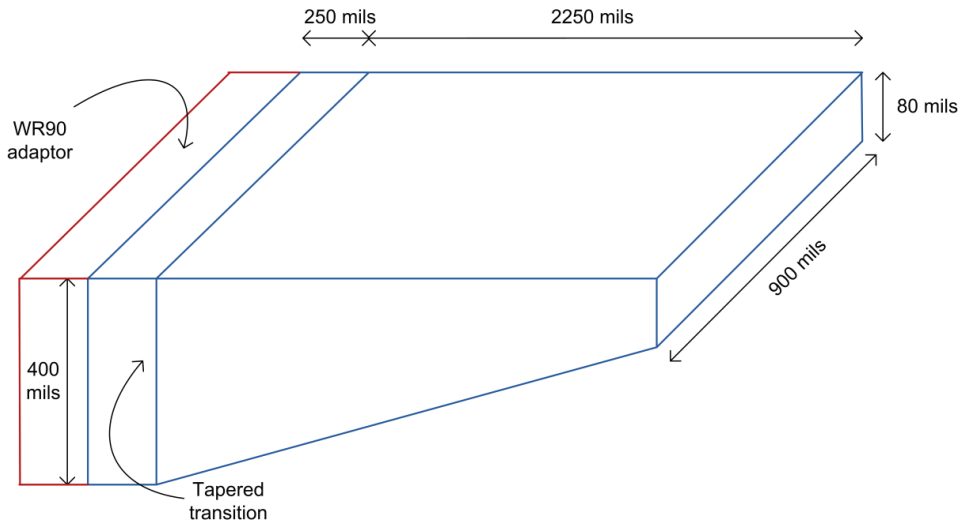


(a)

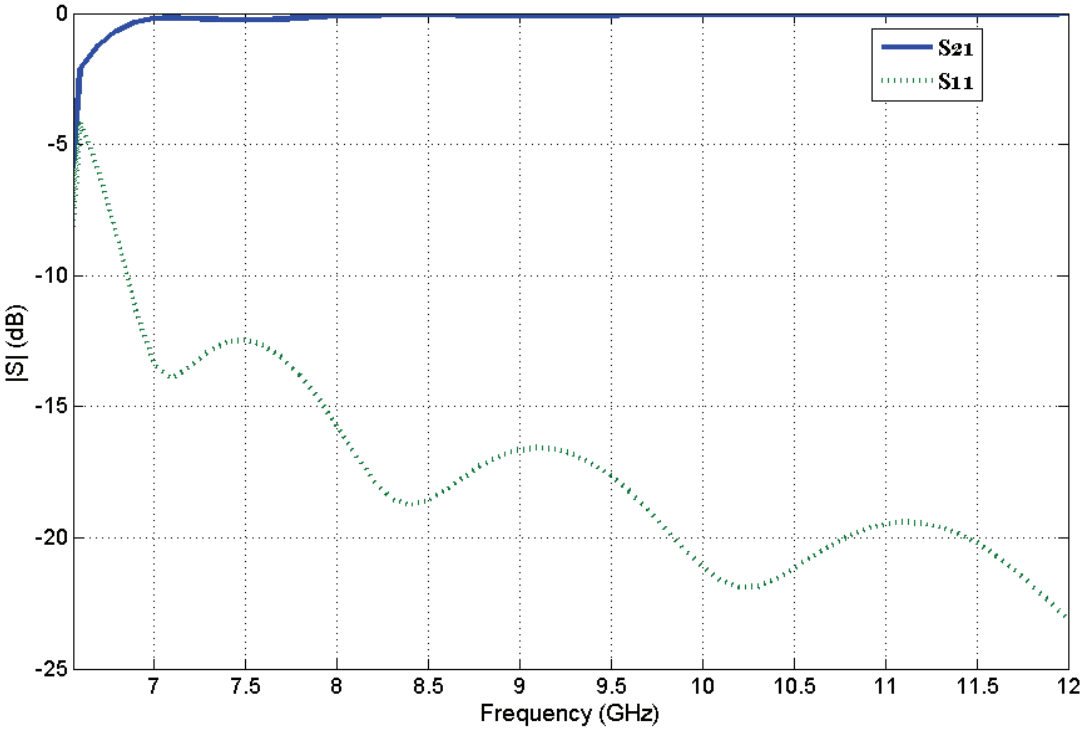


(b)

Figure 3-8 (a) WR90 adaptor and tapered transition (b) Simulated S-parameter results of the transition.

## 3.5 Switchable Antenna Structure and Functionality

Figure 3-9 shows a schematic drawing of the prototype antenna with the membrane cantilever switch. A thin (24 mils) permanent magnet of 2.55 mT (measured at the surface) is bonded to the top broad wall of the waveguide. This magnet is used to provide the bistability. In addition, two integrated coils are used as electromagnets, one underneath the bottom wall for the ON state and the other above the top wall for the OFF state. When a current is momentarily applied to the OFF-state coil, the cantilever is moved to the vertical position where it makes an electrical contact with the inner side of the top broad wall (shorten the waveguide) and remains

latched by the permanent magnet, the switch is OFF and the incident wave is reflected. Therefore, the antenna does not radiate, this is referred to as the OFF state.

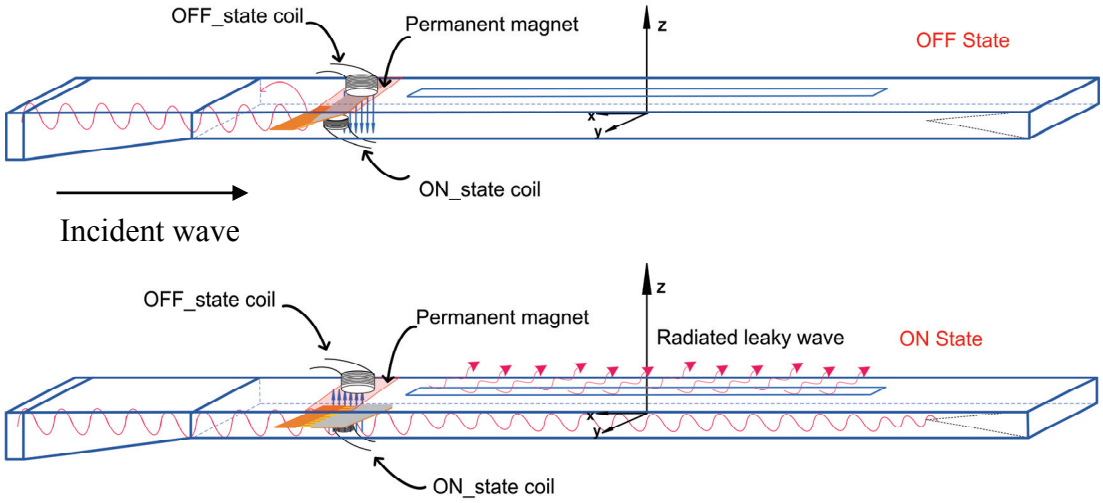


Figure 3-9 principle of antenna operation.

By energizing momentarily the ON-state coil, the cantilever is displaced to the horizontal position. The switch is ON and the wave propagates along the antenna where it leaks energy through the slot. This is referred to as the ON state. The switching currents used for switching to the OFF and ON states were 40 mA and 140 mA respectively.

The antenna was fabricated as a proof of concept. Figure 3-10 (a) shows a photograph of the fabricated antenna along with integrated coils and permanent magnet. A photograph of the membrane switch positioned in the waveguide is shown in Figure 3-10 (b).

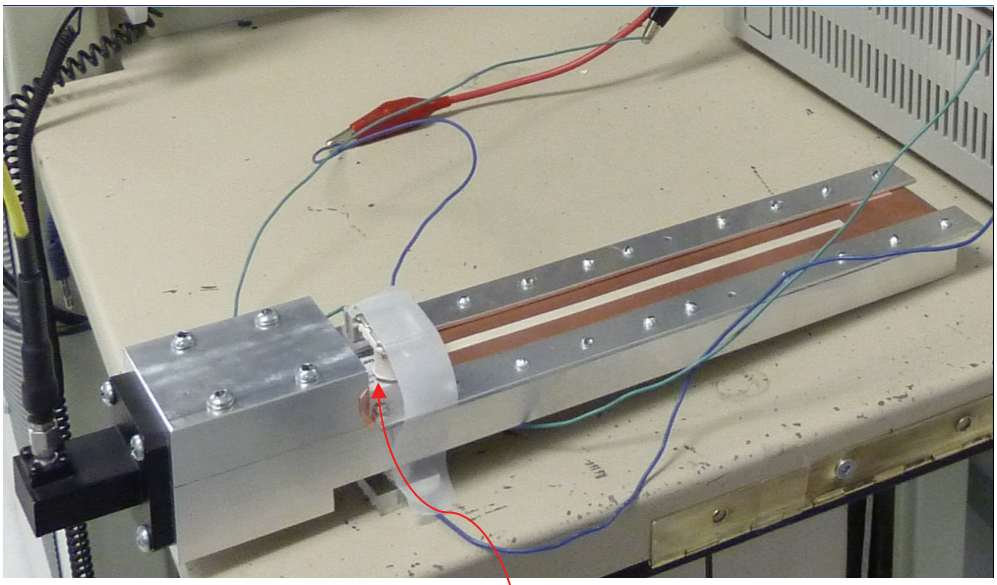

(a)

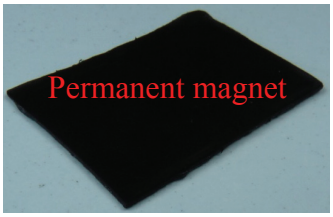


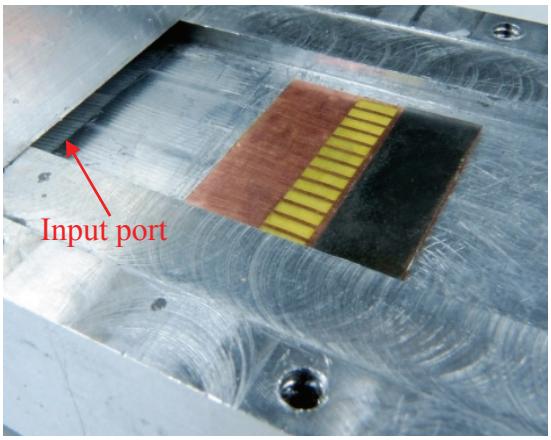


(b)

Figure 3-10 (a) A Photograph of the fabricated antenna with integrated coils and permanent magnet, (b) A photograph of the fabricated switch inside the waveguide.

## 3.6 Results

The simulated return loss characteristic is plotted in Figure 3-11. The switch was modeled in two states. First, it was in the down position ‘’ON state’’ that acts as an open circuit and in the up position ‘’ OFF state’’ which shorts the waveguide. Those results are compared to the measured ones shown in Figure 3-12. As it can be seen, the frequency band defined by the reflection loss lower than -10 dB is from 8.8 to 11.1 GHz for both ON state-graphs, which indicates that the antenna radiates fairly well in this range. However, there is a noticeable difference between the OFF state-graphs, specifically at the frequency of the design 10 GHz, where the simulated and measured return losses differ by 2.2 dB. This difference can be attributable to a non-ideal contact between the inner side of the broad wall and the end of the movable beam. This non-ideal contact is due to the fact that the upper edge of the movable beam touches the upper waveguide wall only at some points but not all along the edge.

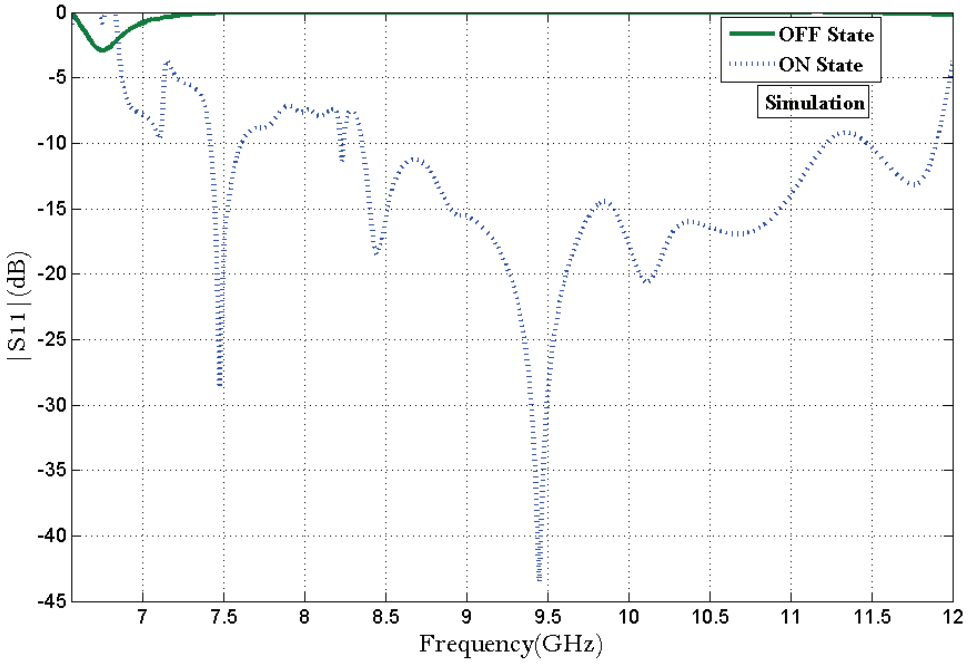


Figure 3-11Return loss simulations for both states of the switchable antenna.

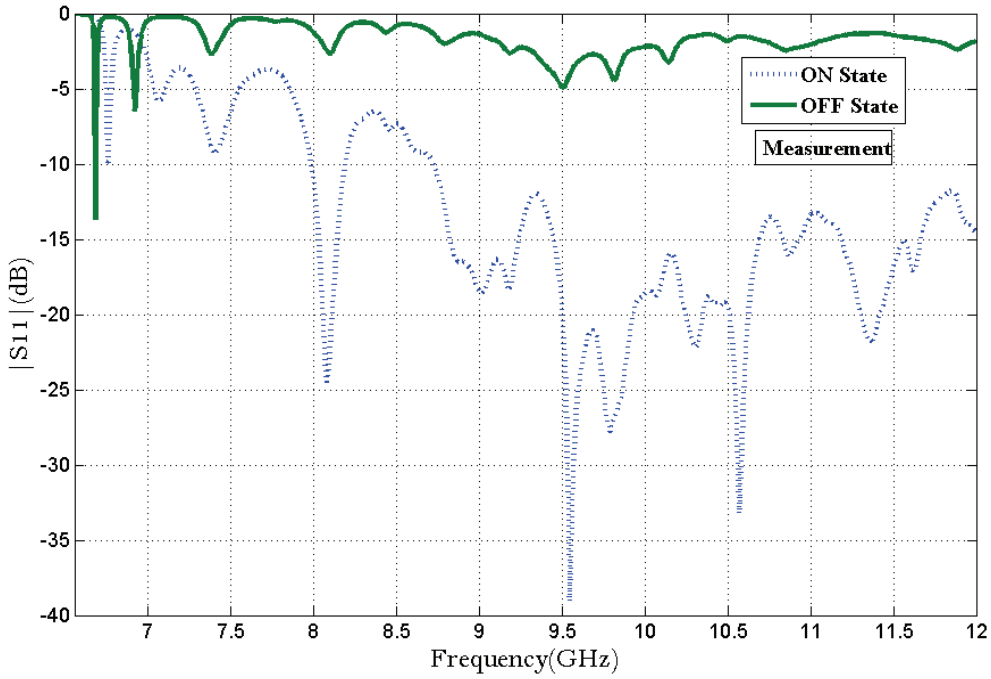


Figure 3-12 Return loss measurements for both states of the switchable antenna.

Measured normalized pattern of the antenna in H-plane for the frequency of operation 10 GHz in the ON state is given in Figure 3-13. The simulated pattern obtained from HFSS in XZ plane (H plane) is also given in the same graph. A good match can be observed between the two patterns in the main lobe region. The back lobe at angles greater than 40 degrees observed in the measured pattern and occurring near 40 degrees in the simulations could be due to a partially reflected wave at the end of the slot and, in the case of the experimental results, to a reflection caused by the non ideal matched load at the end of the waveguide.

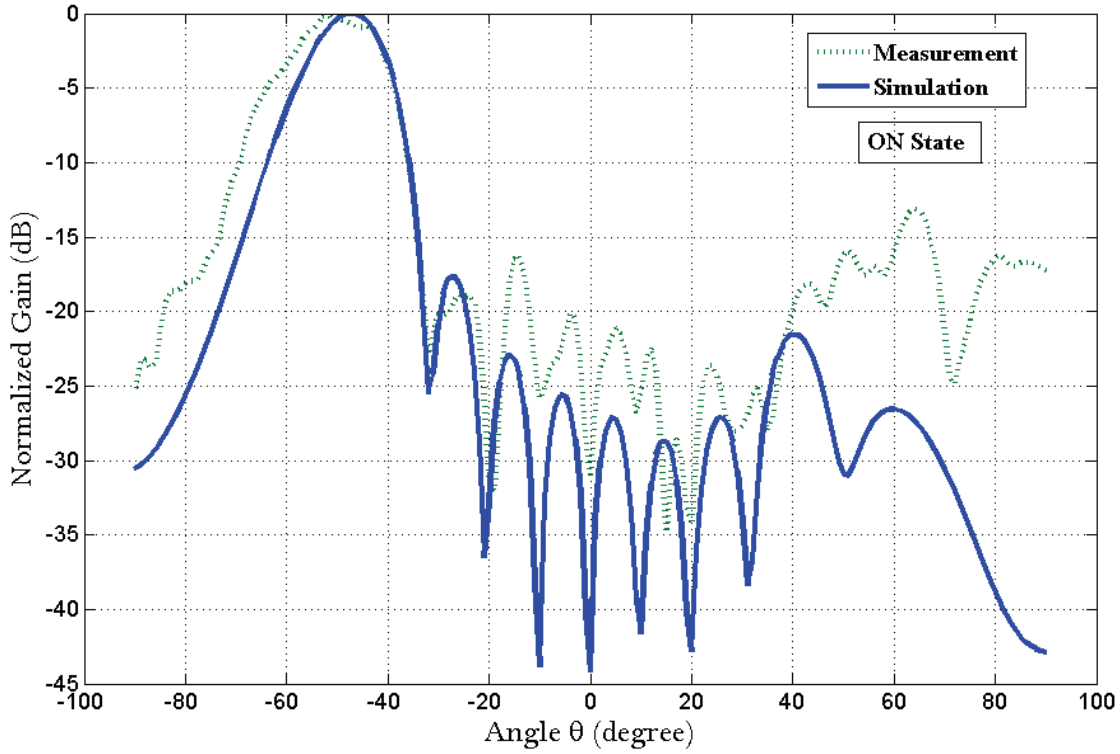


Figure 3-13 Simulated and measured normalized gain in H plane for ON state at 10 GHz.

A screen shot of 3-D simulated HFSS realized gain polar pattern (in linear scale) at 10 GHz is provided in Figure 3-14. It can be seen that the beam is quite narrow due to the large slot aperture (6760 mils), it tilts towards the –x axis from the +z axis at an angle $\theta_{max}$ = - 48.7°.

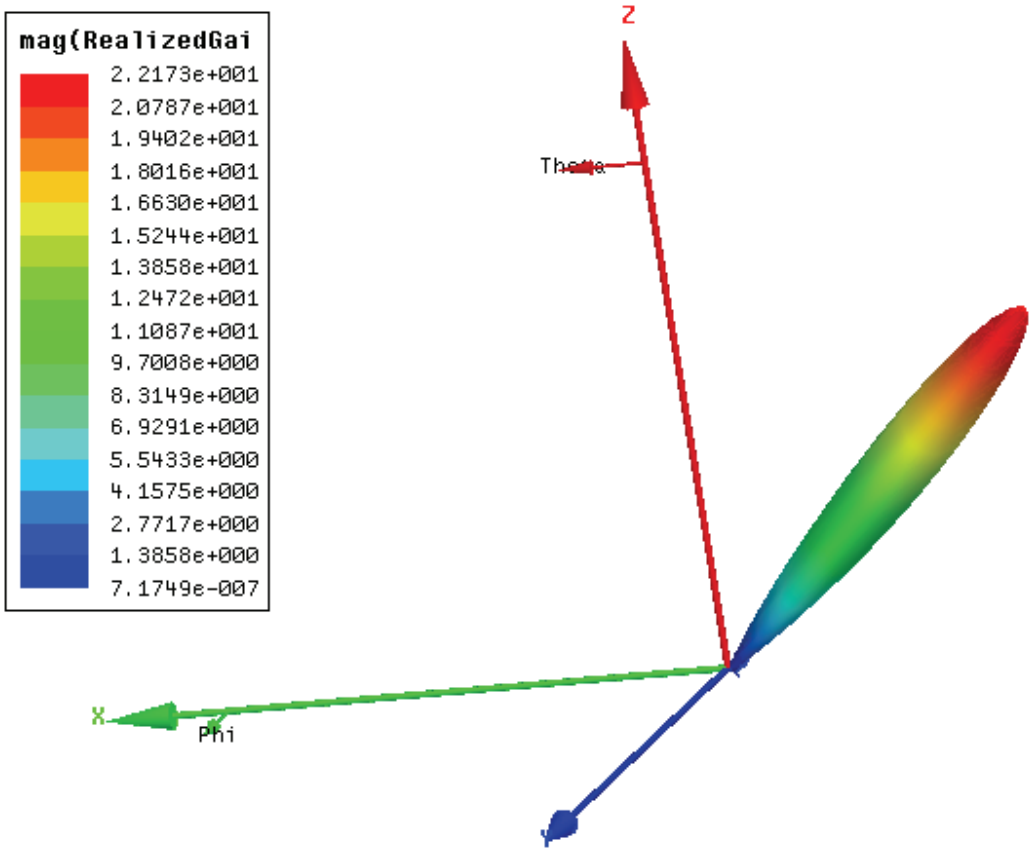


Figure 3-14 A 3-D simulated HFSS realized gain polar pattern (in linear scale).

The simulated realized gain (gain including mismatch) patterns at Φ = 0 (XZ plane) for the ON and OFF states at the design frequency are shown in Figure 3-15 and the measured gain patterns are given in Figure 3-16. Simulations indicate 62.2 dB gain difference between the two states, whereas measurements show a difference of only 12.8 dB. As already mentioned, it is believed that this discrepancy is due to a poor contact of the cantilever with the top waveguide wall. This will be discussed in details in the foregoing paragraphs. As will be discussed in the following paragraphs, the maximum extinction ratio (i.e. extinction ratio is used here to characterize the switch, instead of gains in states ON-OFF) of 62.2 dB obtained in simulations can be improved by increasing the width of the strips connecting the fixed and movable parts of the beam. Also, the overall width of the cantilever is 800 mils whereas the WR90 waveguide's width is 900 mils. Leakage through the gaps on both sides of the cantilever could be reduced by using a wider cantilever.

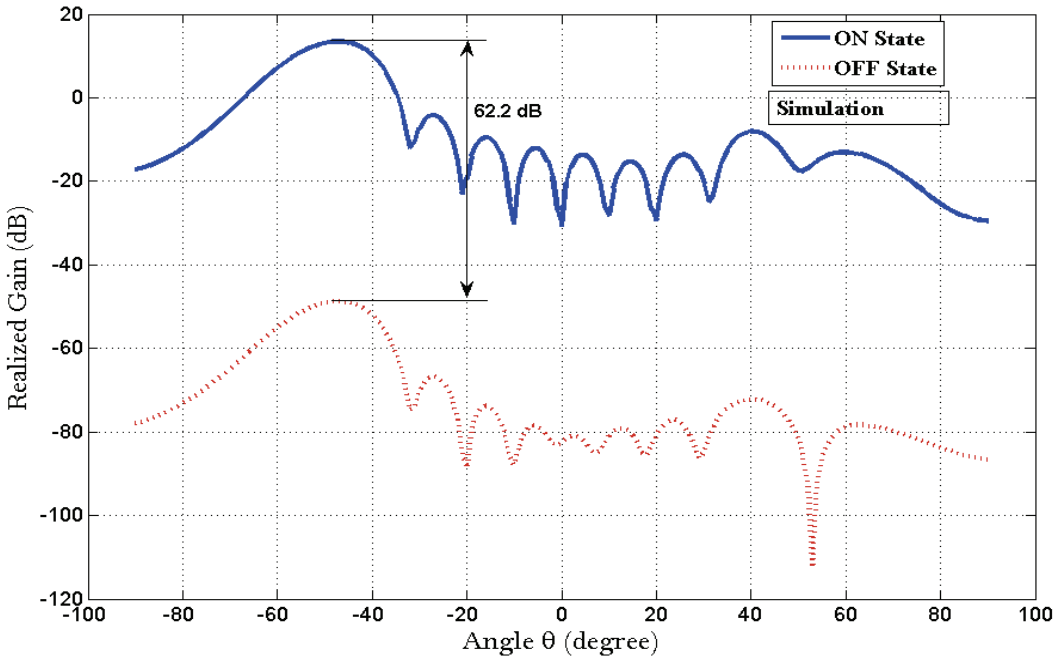


Figure 3-15 Simulated realized gain (XZ plane, Φ = 0) for ON and OFF states at 10 GHz

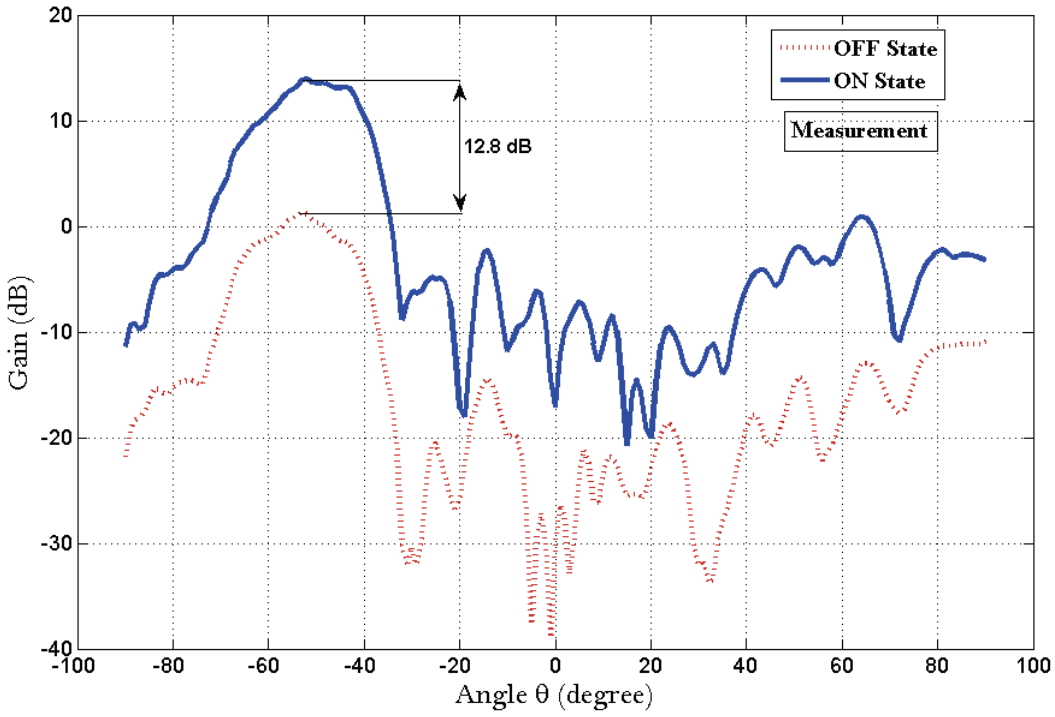


Figure 3-16 Measured gain (H plane) for ON and OFF states at 10 GHz.

Extinction ratios for 8.8, 9.2, 9.6, 10 and 10.4 GHz are indicated in Figure 3-17 to see how the antenna behaves over this frequency range. The ON state patterns are similar at 9.6, 10 and 10.4 GHz. However, a shift of the main lobe is observed at 8.8 and 9.2 GHz.

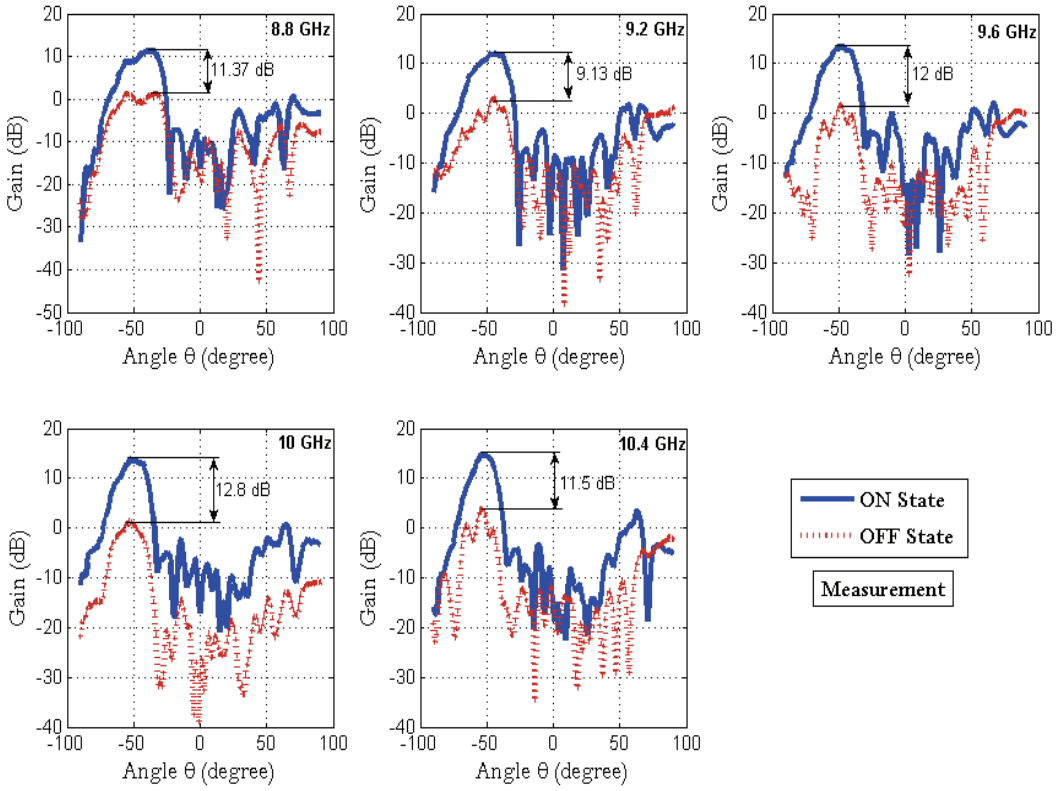


Figure 3-17 Measured gain (H plane) for ON and OFF states at different frequencies.

No YZ plane ($\Phi = 90°$) radiation pattern for ON state was measured. Nevertheless, the simulated pattern is obtained and shown in figure 3-18 (a). $E_\Phi$ field is weaker and wider in YZ plane then in XZ plane (Fig.3.18(b)) due to the smaller antenna aperture in YZ plane.

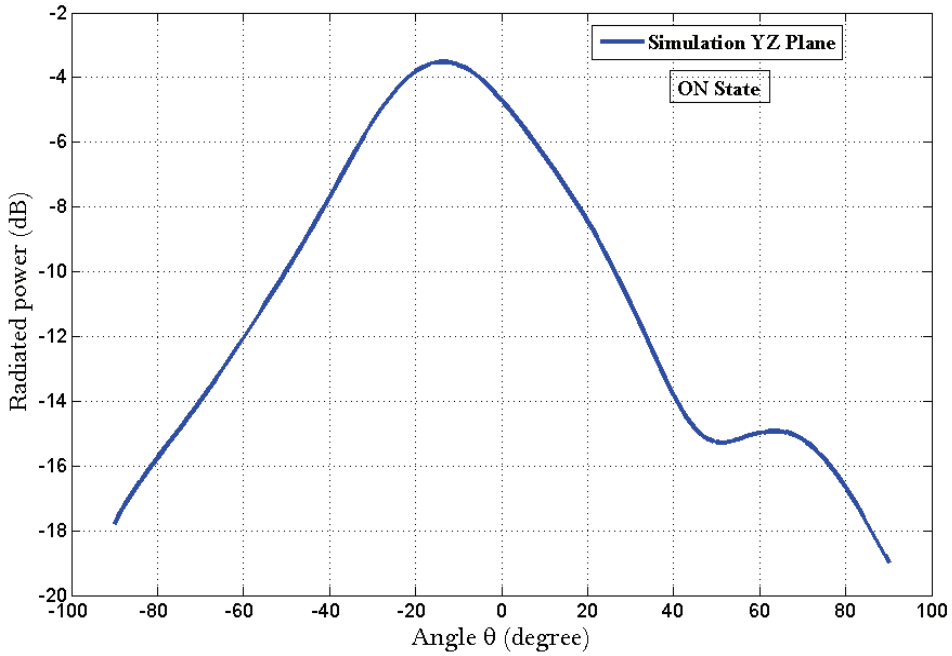


(a)

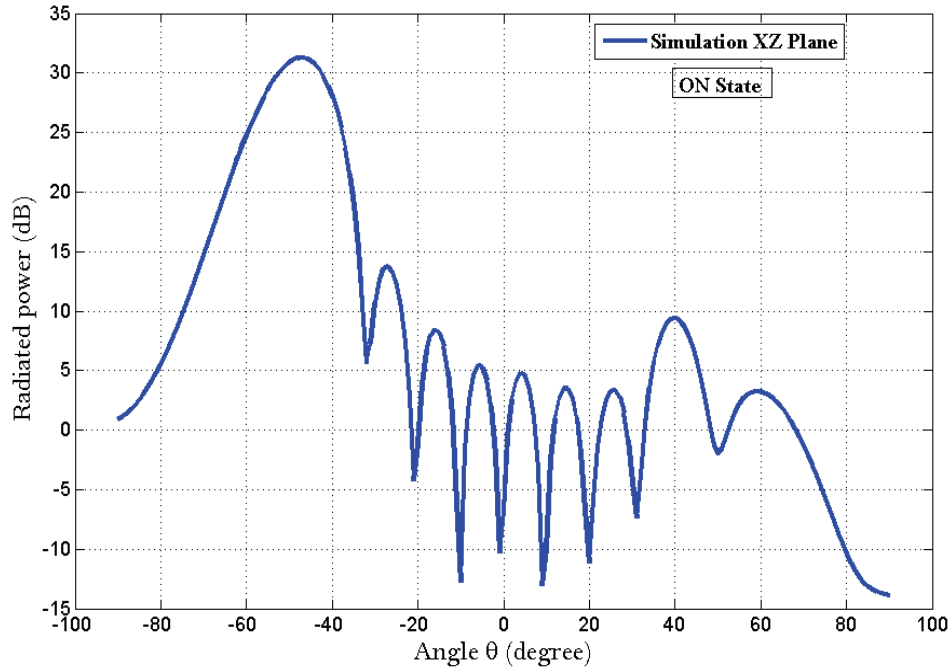


(b)

Figure 3-18 Simulated $E_\Phi$ field patterns (a) in YZ and (b) XZ planes.

## 3.7 Discussions

### 3.7.1 Effect of switch contact

As seen in the previous section, the realized switch had an extinction ratio of about 12.8 dB whereas a value of about 62 dB was expected from simulations. More simulations were done to verify if this is due to the effect of poor switch contact. In practice, the magnet holding the cantilever in its upper (OFF) state cannot create a strong torque to enhance the contact. So, instead of having a contact over the full width of 800 mils, it is more likely that only few randomly distributed points of the cantilever will touch the waveguide. Everywhere else there will be a separation, possibly of few microns between the surfaces, with accompanying capacitive coupling. It was not possible to accurately model these detailed micron scaled structures in HFSS. Instead, we considered a 0.5 mil gap between the surface broadwall and the beam (see Figure 3-19).

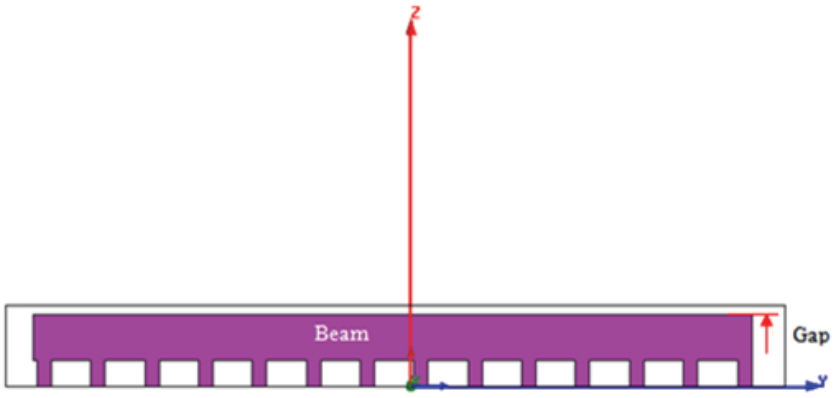


Figure 3-19 A front view (YZ plane) of the switch inside the waveguide showing a gap between the surface broadwall and the beam. The switch is in the OFF state.

The simulation results in Figure 3-20 show that the realized gain for the OFF state increases even when a gap of only 0.5 mil is present, the extinction ratio decreases from 62.2 dB to 25.3 dB.

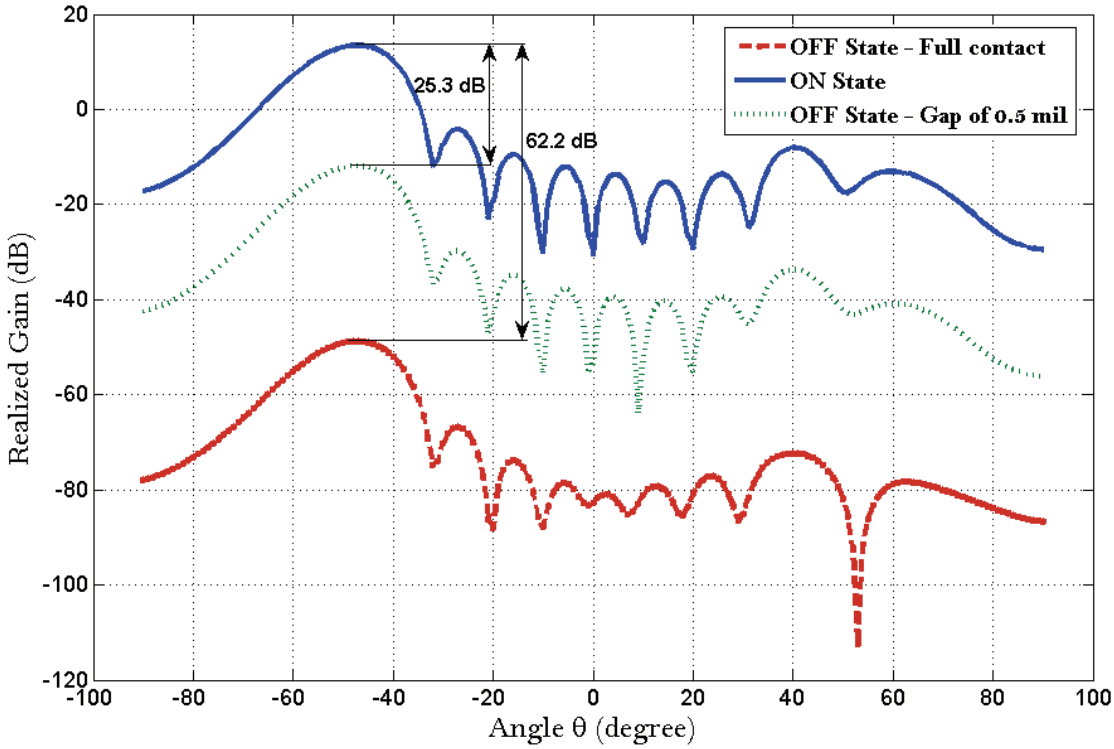


Figure 3-20 Effect of switch contact on realized gain.

### 3.7.2 Effect of switch proximity to the slot

In the 6.5 to 13 GHz range, only one mode can propagate without attenuation in the guide. However, if the switch is set too close to the slot some attenuated higher-order modes can reach the slot and contribute to radiation. To investigate this possibility, simulations were done by placing the switch at different distances *d* from the input port, before the slot. The $E_\Phi$ field patterns of the antenna in XZ plane is illustrated in Figure 3-21. It is observed that larger separation between the switch and

the input port (smaller distance between the switch and the slot) yields higher radiated power. This confirms the presence of higher-order modes in the vicinity of the switch.

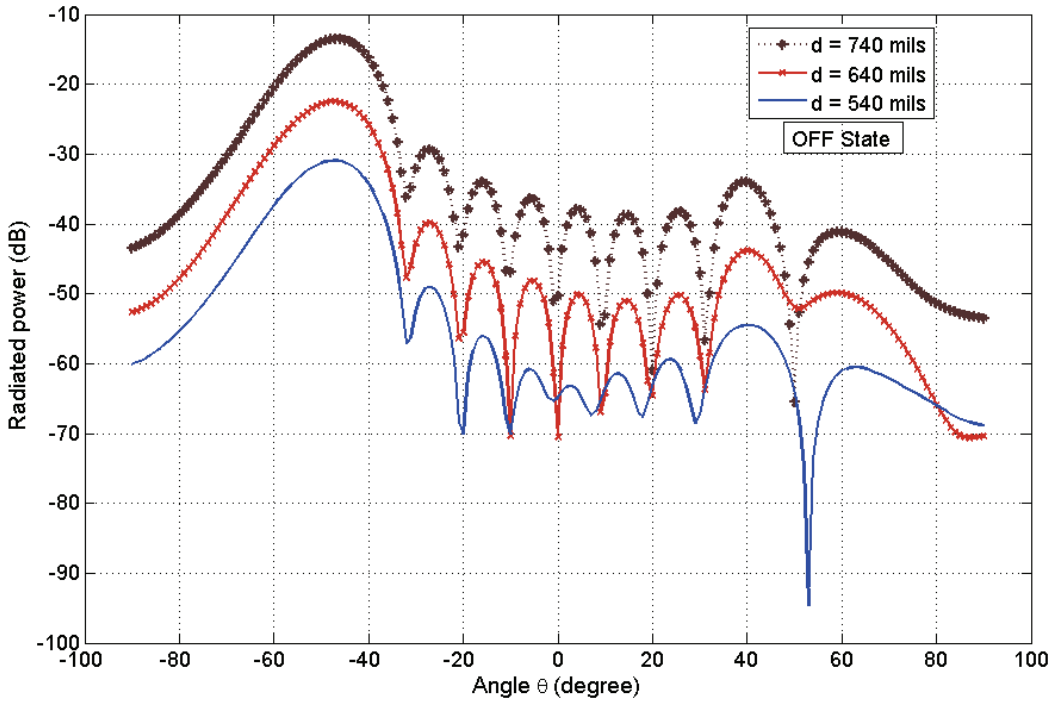


Figure 3-21 $E_\Phi$ field patterns (XZ plane) for OFF state at different switch positions. Parameter d is the distance between the switching plate and the waveguide input port.

### 3.7.3 Effect of strips width

The width of the strips (w = 15 mils) previously illustrated in Figure 3-6 was chosen in order to achieve the minimum possible radiation in the OFF state. Simulations were done by varying the strips width, hence changing the air gaps width. The results of Figure 3-22 show that the radiation increases with the decrease of the strip width. This is an expected situation as the input power leaks from the air gaps and transforms to radiation.

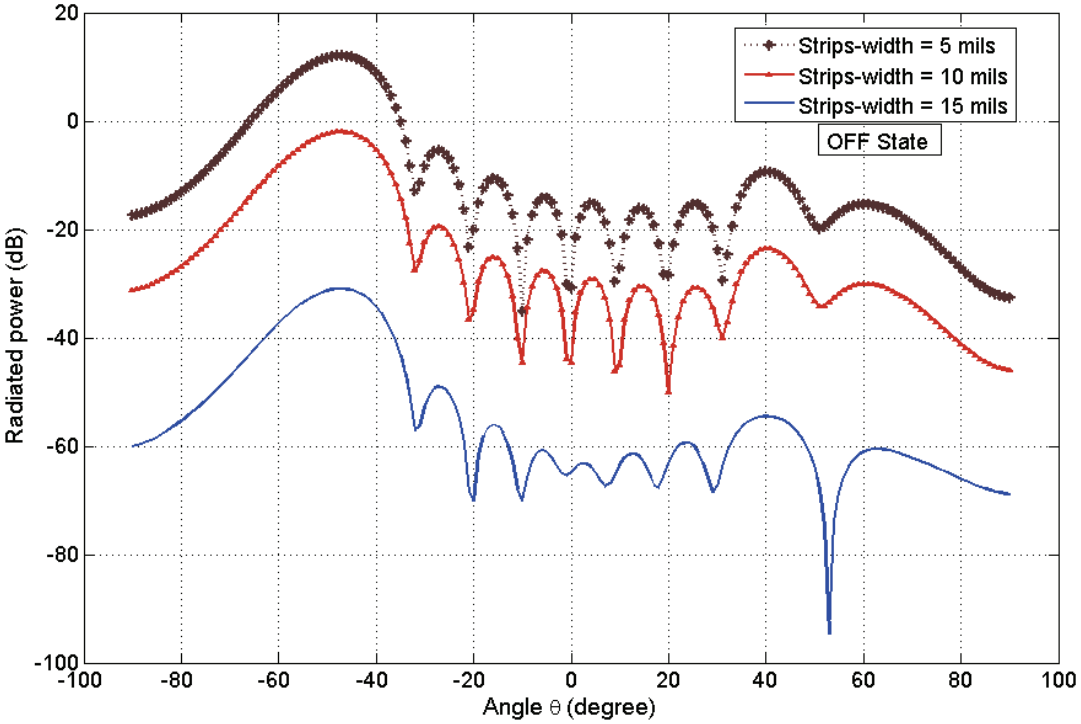


Figure 3-22 $E_\Phi$ field patterns (XZ plane) for OFF state at different strip widths.

## 3.8 Summary

In the work reported here we addressed issues concerning the development of a switchable leaky waveguide antenna prototype. After investigating several design approaches, we decided to implement the one that appeared the most practical. For this proof of concept demonstration, a bistable magnetic membrane switch was considered. The switch allows two different antenna configurations ON and OFF. Switching is accomplished through activation of magnetic field drive coils. Simulated radiation patterns and return loss in each of the two states of the antenna are comparable to the measured ones. Design issues affecting the OFF state radiation such as poor contact, switch arrangement and dimensions have been investigated.

# CHAPTER 4. MEMBRANE-BASED SWITCHED WAVEGUIDE FILTER

## 4.1 Introduction

Chapters 2 and 3 have concentrated on a switch membrane and its incorporation with a leaky waveguide antenna. We have demonstrated its design, operational principles and implementation. One of the main limitations of the proposed switch was the difficulty to make a good electrical RF contact between the moving edge of the cantilever and the waveguide wall. On the other hand, even with a poor contact, or no contact at all, the presence of a vertical cantilever within the rectangular waveguide introduces reactive loading. The objective of this chapter is to investigate the possibility of making use of this switchable reactive element into waveguide filters. In fact, rectangular waveguide filters are often made of capacitive irises that are only partially covering the waveguide cross section, i.e. without an electrical contact from the top to the bottom walls of the guide. The situation is however somewhat different with our cantilever switch because instead of being normal to the wall as in irises, our cantilever is making an angle of only 7.66 degrees with the bottom wall. Consequently, the cantilever in its raised position, which occupies a length of approximately 1.5 centimeters along the guide, cannot be represented as a shunt capacitive loading. It is nevertheless a low-loss component and it may therefore have potential for application in a switched filter. One important feature of this component is that the electromagnets used to change the state are located outside the guide. Therefore there are no bias lines inside the propagating media, as it would be the case with other switching elements such as MEMS, semiconductor and ferroelectric-based devices used in tuneable filters. This can be a significant advantage to simplify the design. Furthermore, the cantilever materials are passive and can therefore exhibit linear operation at higher power levels.

In this chapter, we discuss a technique of employing a switch membrane in a closed waveguide and the potential of this technique in filter design. The switch geometry is introduced and then used to show a band-stop filter.

## 4.2 Design and Operation

In order to demonstrate the feasibility of a band stop filter, Figures 4-1(a), (b) and (c) show the proposed switch incorporated into a closed rectangular waveguide. We kept the pre-existing waveguide used to demonstrate the antenna prototype in the previous chapter and added a second transition to the waveguide in order to measure the transmission. The switch is of type 2, as presented in Figure 2-2. It uses a 1 mil thickness polyimide (Kapton®) dielectric membrane on one part of the cantilever while the other part is a single sided copper clad polyimide beam bonded to a metglas magnetic plate (Fig. 4-1(b)). In the HFSS simulations, the dielectric membrane is modeled as vacuum (i.e. the membrane is transparent and thin that the wave can pass through) and the beam along with the metglas are modeled as a PEC.

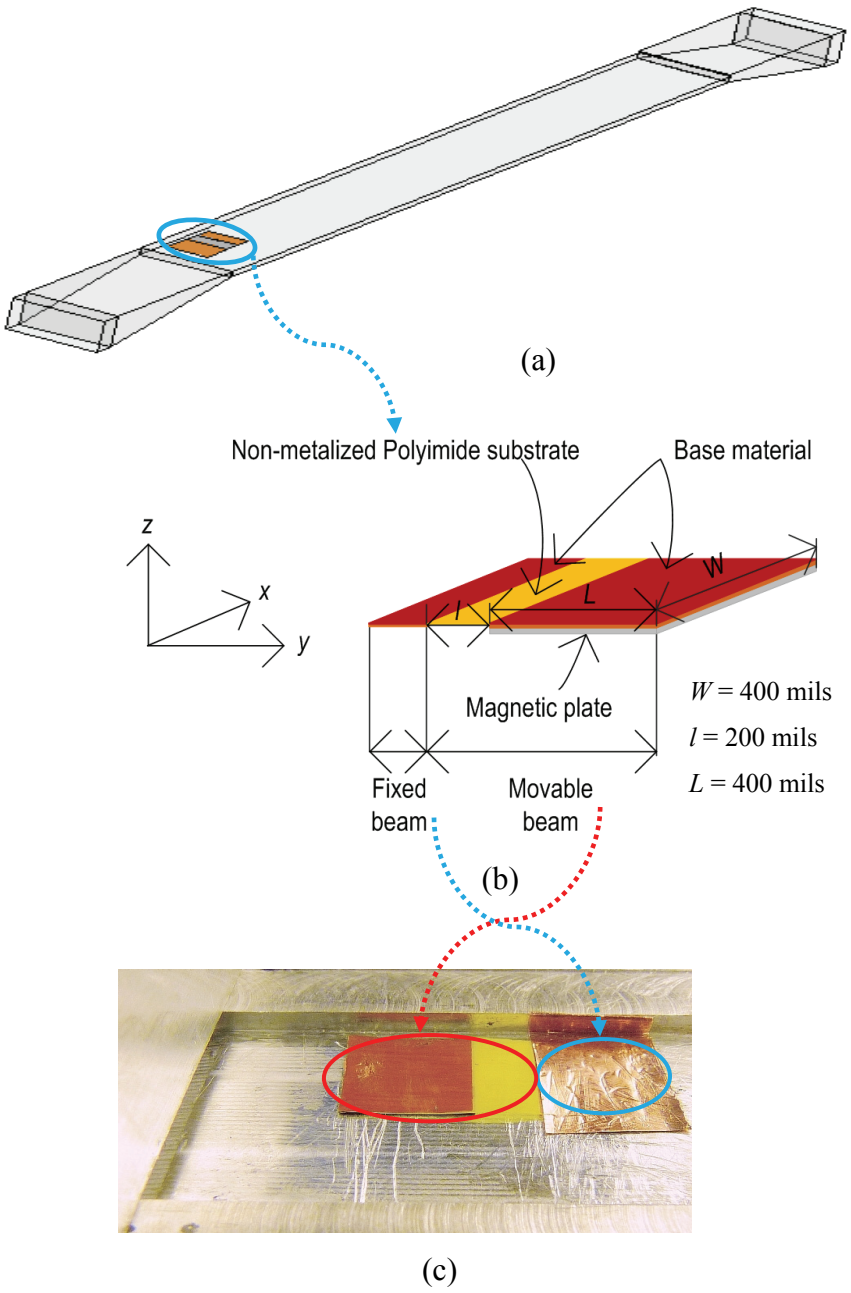


Figure 4-1 Membrane switch geometry: (a) screen shot of the HFSS model of the switch inside the waveguide. (b) Its schematic diagram. The design parameters are labeled within the drawing. (c) A photograph of the fabricated switch set in the waveguide.

In the ON state, the switch is in the down position and the wave propagates through the waveguide. In the OFF state, the movable beam is actuated to move upward, where its tip makes a dielectric-metal contact with the waveguide broad wall. This creates reactive loading in the guide that prevents part of the signal from reaching the output port. It is to be mentioned that in order to avoid the contact problem encountered in the antenna implementation, the switch in its natural position (horizontal) is set in a way that the polyimide side of the single sided copper clad polyimide beam faces the upper broad wall, while its metallic (metglas) side faces the bottom wall of the waveguide (Fig. 4-1(c)).

In the HFSS simulations, when the switch is in the OFF state, a gap of 1 mil (polyimide thickness) separates the metallic broad wall and the tip of the movable beam. Superior gap distances (thicker polyimide) could also be used in order to facilitate the switch fabrication. However, more energy would be required to actuate the cantilever.

The switch is magnetically actuated through the magnetization of the Metglas piece and the switching mechanism introduced in Chapter 3 is used to implement the displacement of the cantilever and the bi-stability function. The switching currents used for switching to the OFF and ON states were 30 mA and 110 mA respectively.

## 4.3 Effect of Switch Length and Position

### 4.3.1 Effect of varying the length of the movable beam

Simulations were performed for changing the membrane dielectric length *l* (Figure 4-1*)* by keeping the length *L* of the PEC plate at 400 mils. It was observed that the variation of the length *l* enables the adjustment of the filter's center frequency. When the length is increased from 100 mils to 250 mils in 50 mils step, the filter presents the following center frequencies: 10.2 GHz, 10.6 GHz, 10.8 GHz

and 11GHz respectively. The return loss and insertion loss characteristics of the filter when the cantilever in the up (OFF) position are illustrated in Fig. 4-2.

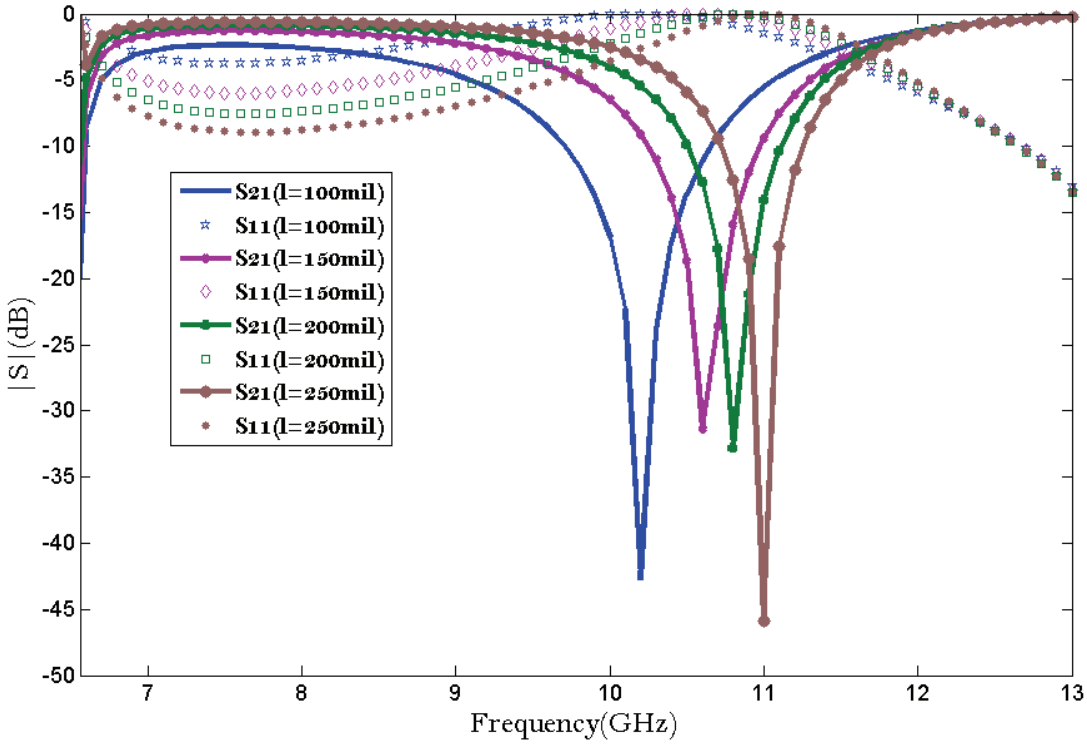


Figure 4-2 Simulated S-parameters for the waveguide, showing the effect of modifying the length of the dielectric beam. The switch is in the up position.

We adopted the same approach to explore the effect of changing the length *L* of the PEC plate and maintaining the dielectric membrane length *l* at 200 mils. The simulation results of Figure 4-3 show that as the length decreases, the center frequency shifts to a higher value.

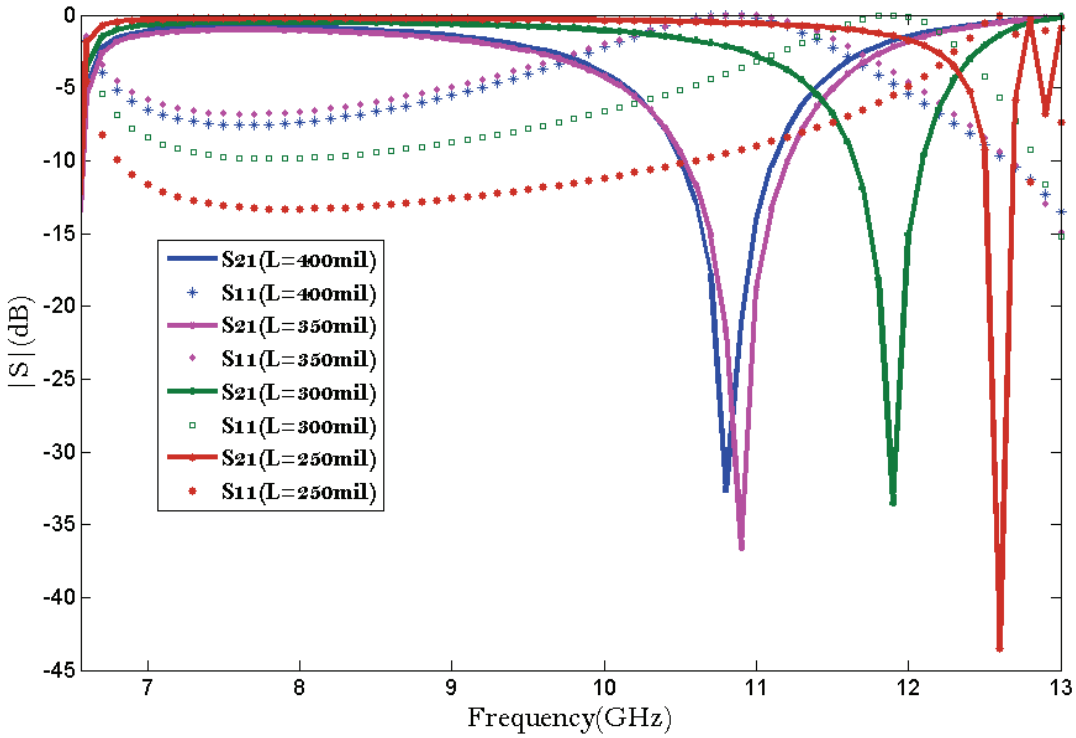


Figure 4-3 Simulated S-parameters for the waveguide, showing the effect of modifying the length of the metallic plate. The switch is in the up position.

### 4.3.2 Effect of the switch location

The switch was placed at different distances *d* from the waveguide sidewall (see Fig. 4-4) to characterize the effect of the switch placement, and the results are shown in Figure 4-5. It is noted that the notch frequency shifts to higher value as *d* is increased until it reaches 250 mils, where the switch is in the middle. By symmetry, the same behaviour can be obtained if the switch is set to the same distances from the opposite sidewall.

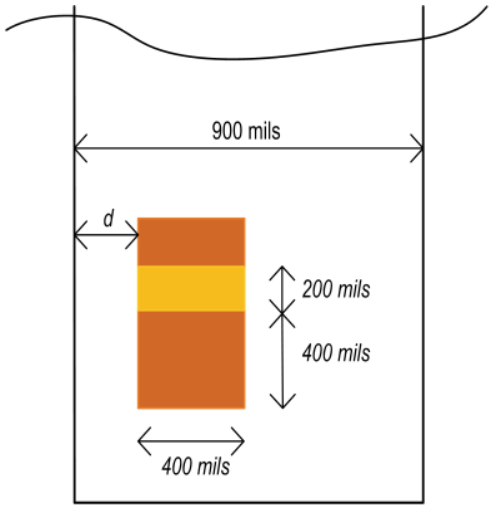


Figure 4-4 Switch position in the waveguide.

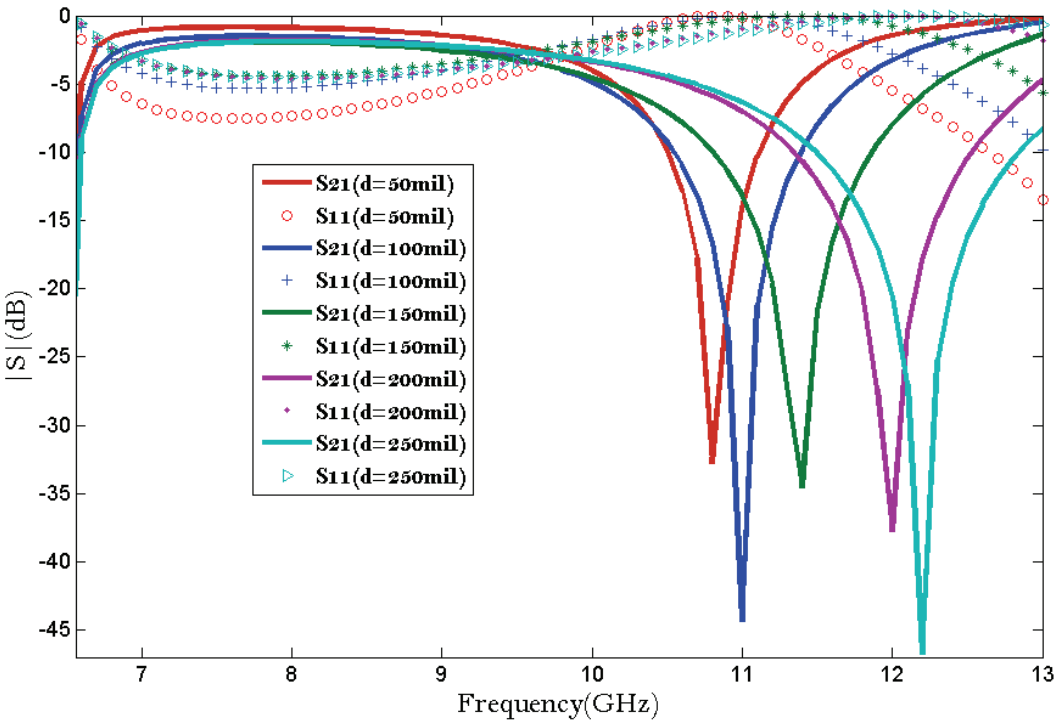


Figure 4-5 Simulated S-parameters for the waveguide with variation in the switch position. The Switch is in the up position.

## 4.4 Simulations and Measurements Results

### 4.4.1 One switch integration

Figure 4-1(c) above shows a photograph of the prototype switch, when it is placed at distance d = 50 mils from the waveguide sidewall. The measured RF characteristics, namely, return loss and insertion loss are depicted in Figure 4-6 and Figure 4-7 for the ON and OFF states respectively. These measurements were taken with an Anritsu 37369D vector network analyzer after a full two-port calibration at the coaxial ports. Therefore there is no de-embedding of the coaxial port to waveguide transitions and of the transitions between the WR90 and the thin waveguide section. As can be seen in Figure 4-6, the transmission and reflection of the ON state (when the switch is the down position) are closely correlated to the ones for an empty waveguide (without switch). It can be seen that the empty waveguide has an insertion loss level of about 3 dB, which is due to the fact that the transitions were not taken into account in the calibration. Comparison of the insertion loss without switch and with the switch in the ON state clearly shows that the cantilever membrane does not introduce insignificant losses in the structure. The simulated ON state results are presented in Figure 4-8. Observing the plots in both figures, it can be seen that there is a noticeable change. This can be attributed to the coax-to-waveguide and tapered waveguide transitions.

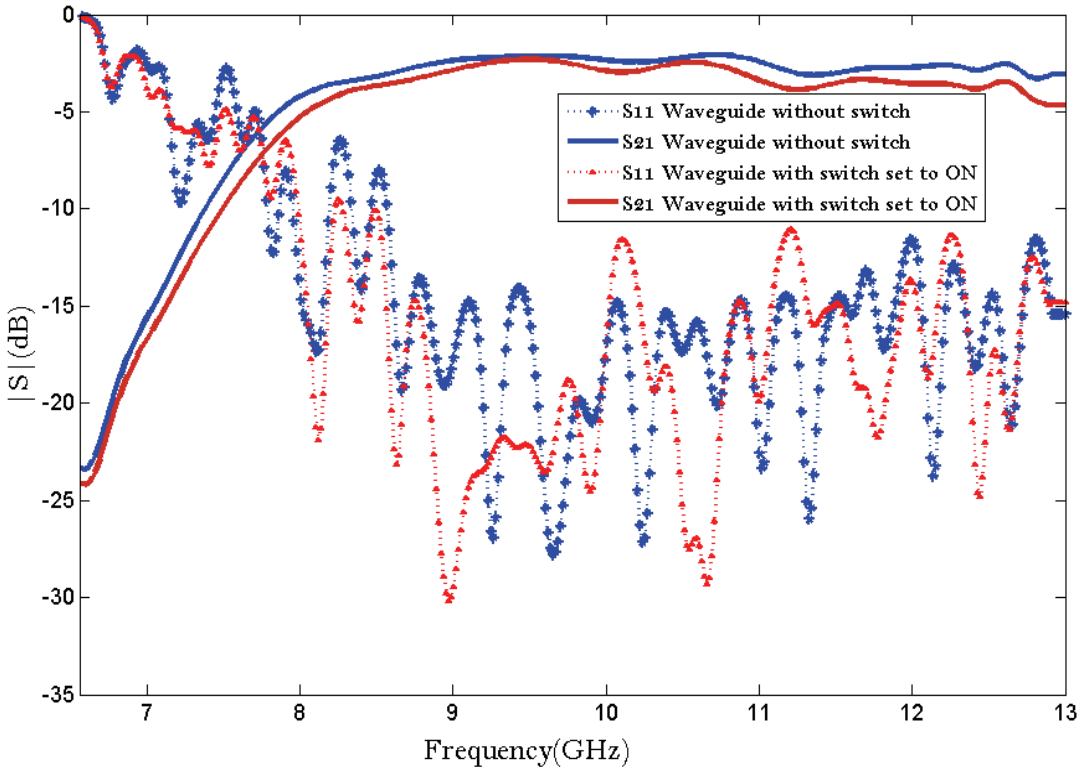


Figure 4-6 Measured S-parameters of the waveguide with switch in the ON state and without switch.

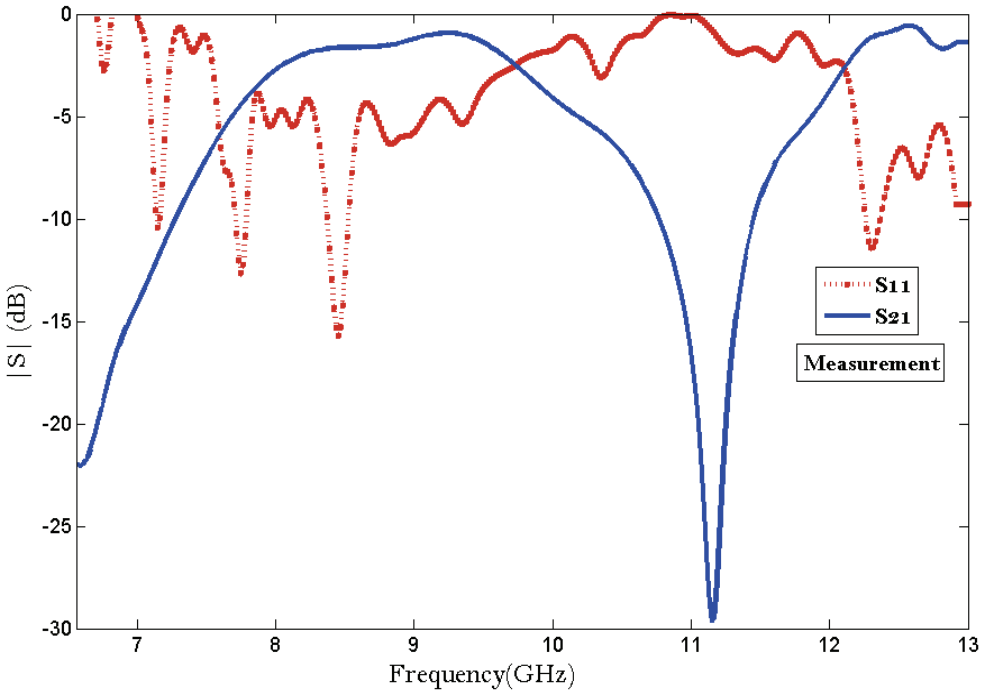


Figure 4-7 Measured S-parameters when the switch is OFF. 3 dB transitions losses were assumed and subtracted.

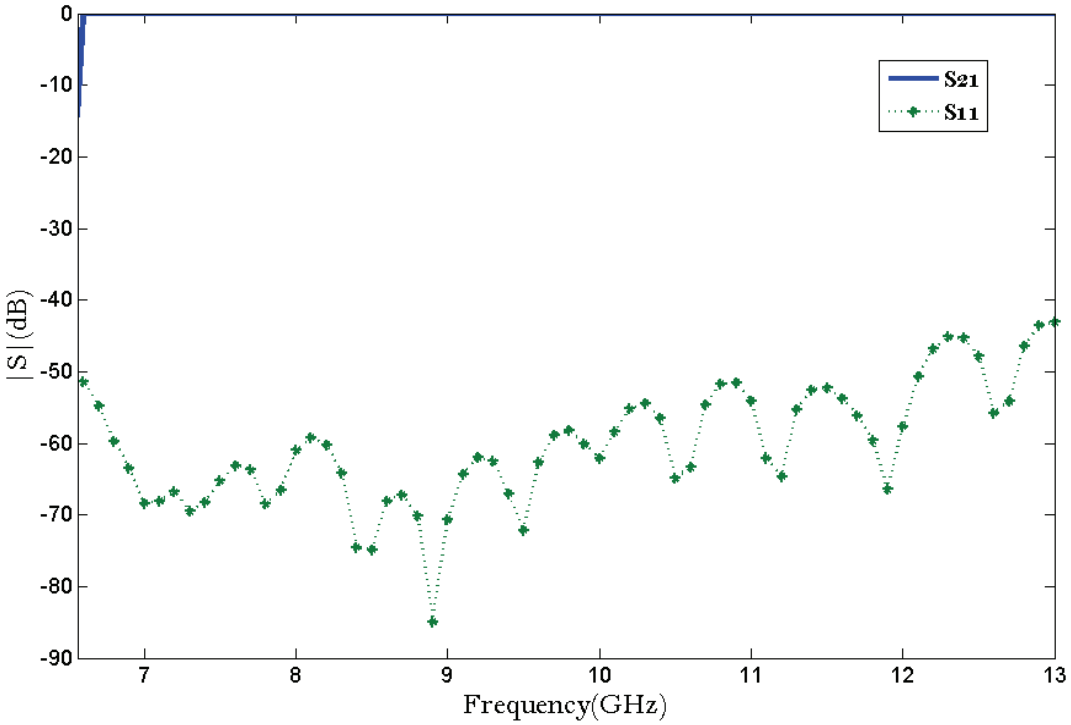


Figure 4-8 Simulated S-parameters when the switch is ON.

Figure 4-9 shows the simulated S-parameters of the OFF state. As expected from Figs. 4-2 to 4-5 the switch exhibits a stop-band behaviour. In the plotted frequency range of 7 - 13 GHz, we can see that the 20 dB stop-band is from 10.72 to 10.92 GHz, the notch frequency is at 10.8 GHz with -33 dB of insertion loss and 0 dB of return loss. These results are compared with the measured values given in Figure 4-7 (transition losses are taken into account by adding 3 dB to the original measured data). The shift in the notch frequency may be owing to a non-perfect switch fabrication or non-ideal position of the switch in the waveguide (the switch is set up by hand). As can be seen from Figures 4-3 and 4-5, a small change of the length of the metallic beam or the switch location makes the notch frequency shift noticeably.

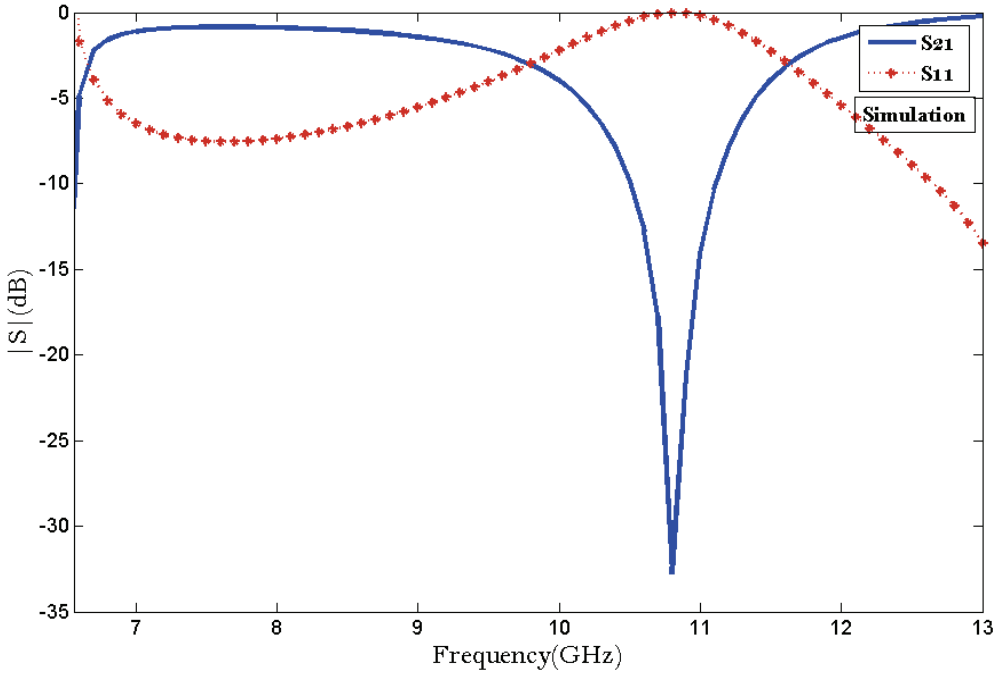


Figure 4-9 Simulated S-parameters when the switch is OFF.

### 4.4.2 Two switches incorporation

Using only one switch can be limiting if the system requires additional bandwidth. It would be advantageous to add multiple switches to obtain more flexible bandwidth. For example, as a frequency band is needed, the appropriate switches are activated. To demonstrate the utility of using more than one switch, another membrane switch that is identical to the one presented in Figure 4-1 was integrated to the waveguide structure. The second switch was set at a distance of 260 mils from the first one as illustrated in Figure 4-10. If this distance is less than 260 mils, the structure exhibits similar behaviour as in Figure 4-11. The difference is in the insertion loss at the notch frequency 10.6 GHz, it takes values between -33 dB and - 48 dB as the distance goes from 100 mils to 260 mils respectively. If the separating distance is greater than 260 mils, the stop-band presents one notch frequency at 10.9 GHz but at significant insertion loss (less than -60 dB).

As before, when only one of the switches is activated to be OFF, the simulated transmission exhibits a 20 dB stop-band bandwidth of 0.2 GHz. However, when the two switches are activated, this 20 dB bandwidth is extended to 0.9 GHz. Frequency responses of the modeled $S_{11}$ and $S_{21}$ magnitudes are shown in Figure 4-11. Those results are compared to measurements shown in Figure 4-12. From this Figure, it can be noticed that the 20 dB stop-band bandwidth is of 0.2 GHz when only one switch is operated to be OFF, and 0.9 GHz when both switches are OFF (the 3 dB transition losses are taken into consideration). Therefore, the simulated 20 dB stop-band bandwidth follows closely the measured ones. A comparison of measurements and simulations of the proposed switches shows that except for the 20 dB stop-bandwidth, the measured results show inferior pass-band and stop-band performance compared to the modeled ones. The $S_{21}$ notch has changed to 11.1 GHz from of 10.8 GHz. The reason for this discrepancy could be attributed to the aforementioned aspects such as switch fabrication uncertainties, non ideal switch placement and the use of the tapered transitions.

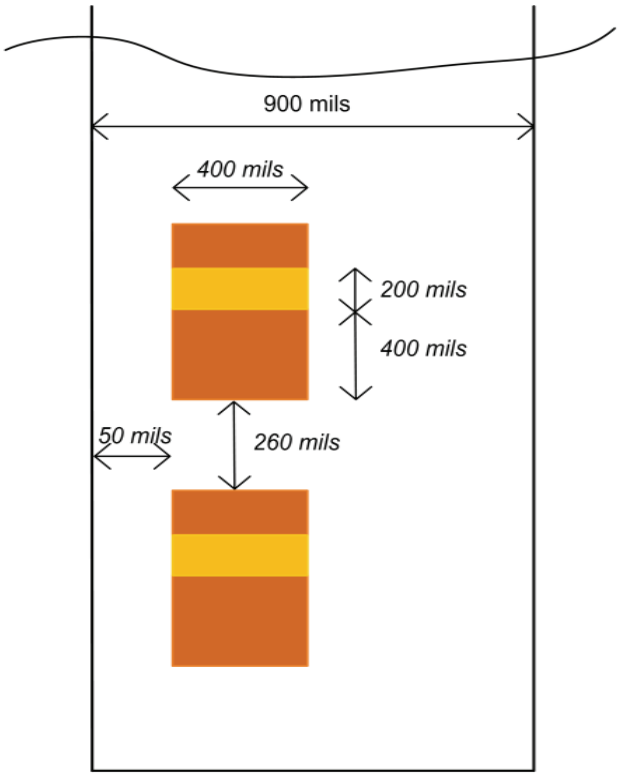


Figure 4-10 Switches arrangement in the waveguide. Drawing is not to scale.

.

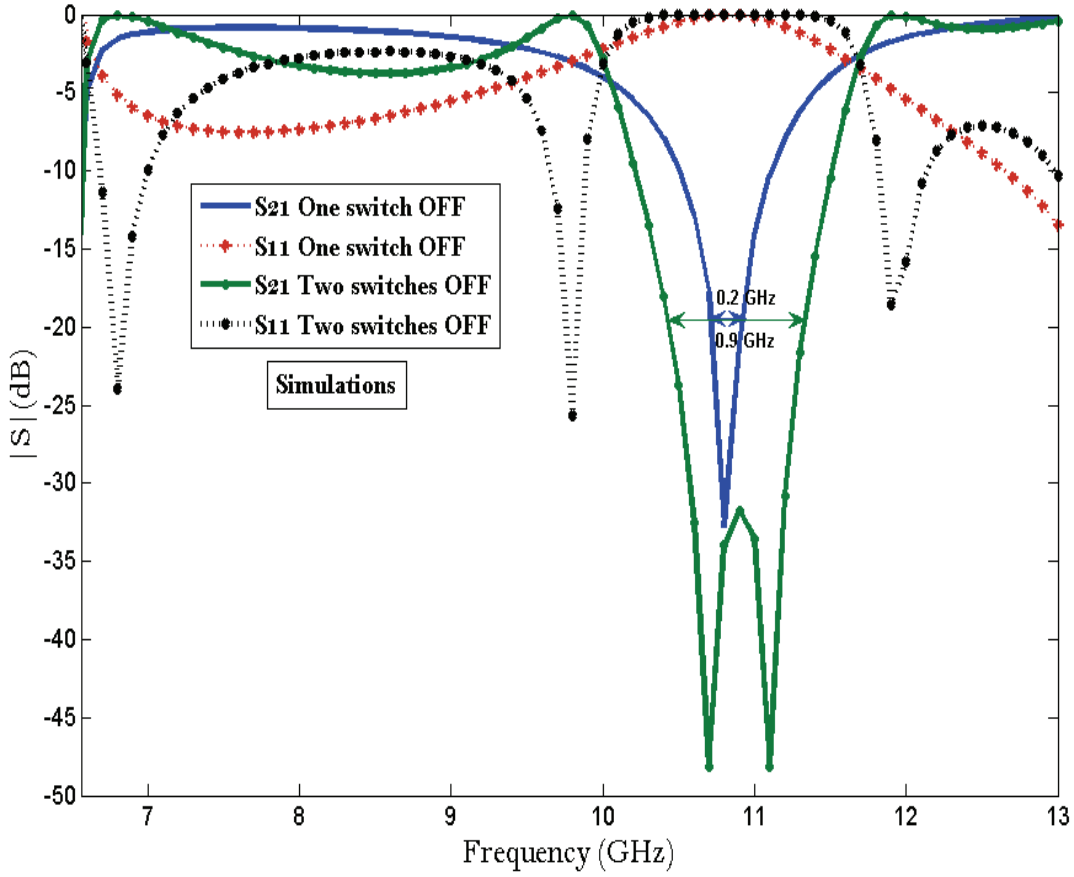


Figure 4-11 Simulated S-parameters when the switches are OFF, showing the effect of switch operation on the bandwidth.

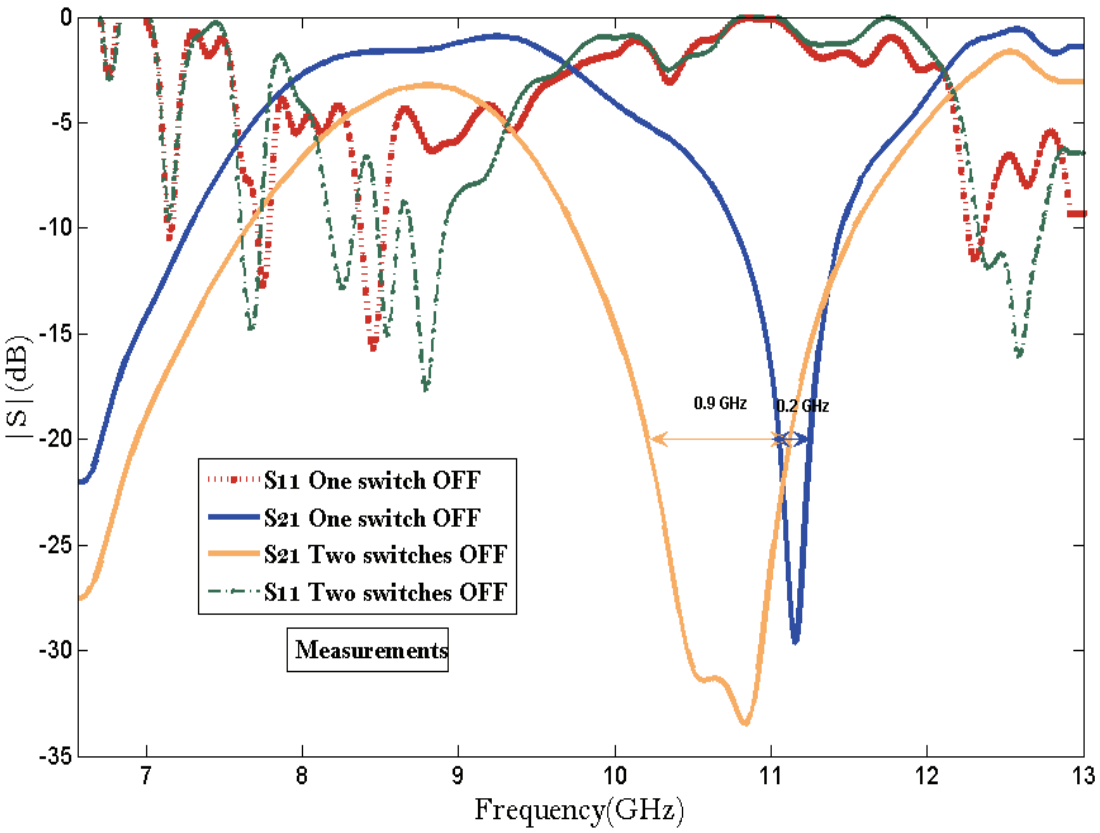


Figure 4-12 Measured S-parameters when the switches are OFF, showing the effect of switch operation on the bandwidth.

### 4.4.3 Switching time measurement

The switching time was measured using a measurement set up as shown in Figure 4-13. A 5 dBm RF signal at 11.017 GHz was applied to the input port of the waveguide. A switch actuation signal was generated by an Agilent 33250 with unipolar square waveform of period 0.6 Hz and 5V amplitude. The RF signal was detected at the output port by a DSO81204B Agilent oscilloscope with bandwidth of 12 GHz.

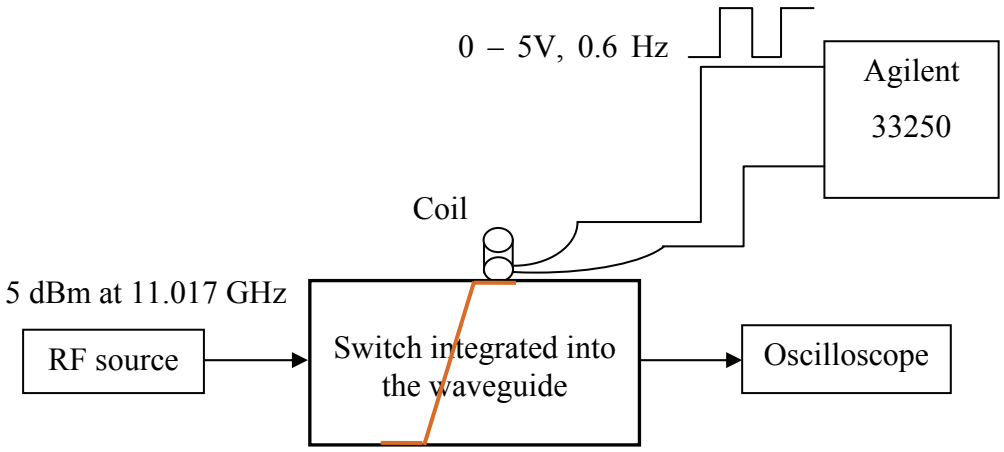


Figure 4-13 Switching time measurement setup.

Figure 4-14 shows the detected RF signal and Figures 4-15(a) and (b) illustrate the measured switching times $t_{off}$ and $t_{on}$ respectively. The $t_{off}$ is 80 ms for the transition from the ON to the OFF state and $t_{on}$ is 3ms for the transition from the OFF to the ON state. This difference is due to the mechanical oscillations (bouncing) that occur before the switch settles into the upper position (OFF state).

This test was running for 1 hour duration with no RF performance degradation, nor switch deformation. Therefore, the fabricated switch showed good mechanical performance.

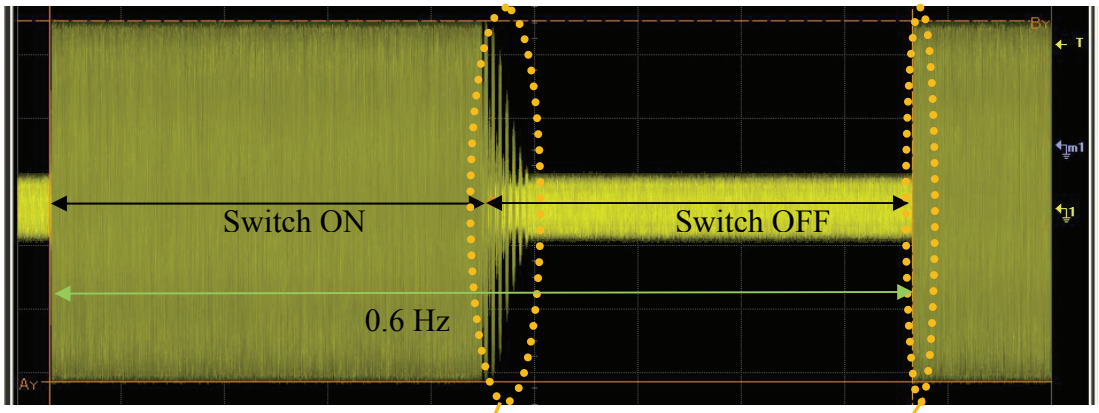


Figure 4-14 Detected RF signal when the switch is ON and OFF.

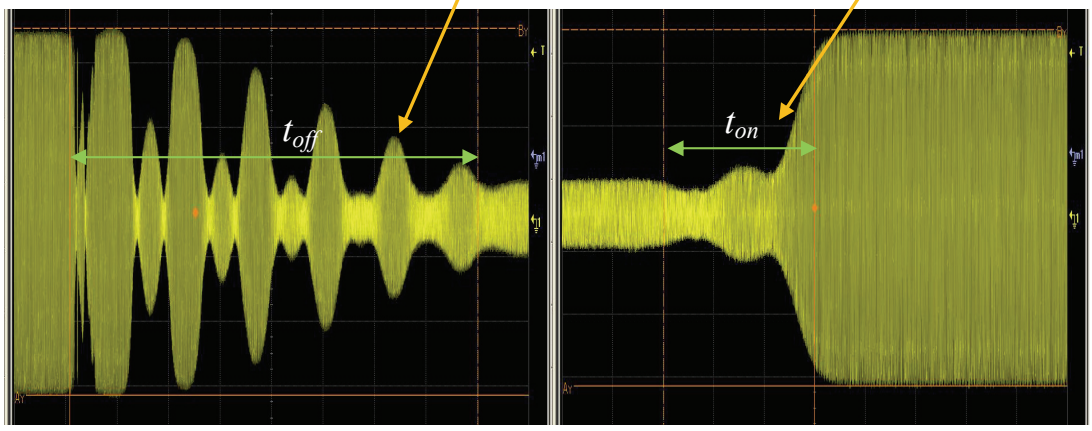


(a) (b)

Figure 4-15 Illustration of the measured switching time: (a) $t_{off}$ and (b) $t_{on}$.

## 4.5 Conclusion

In this chapter, a demonstration of the stop-band (notch) filtering capability of cantilever membrane switches in a rectangular waveguide is presented. This structure can be used in an application that requires channel selection. Using only one switch, the measured notch frequency is at 11.1 GHz with -29.7 dB of insertion loss and the 20 dB stop-band bandwidth is of 0.2 GHz. By cascading two similar switches, the 20 dB stop-band is as wide as 0.9 GHz. The measured results showed lower pass-band

and stop-band performance when compared to the simulated ones, owing to the switch fabrication uncertainties. The measured switching times are 3 ms for the transition from the OFF to the ON state and 80 ms for the transition from the ON to the OFF state.

# CHAPTER 5. CONCLUSIONS

## 5.1 Thesis Contributions

This project has focused on developing a latching magnetic RF waveguide switch built on a flexible membrane. Two distinct switch geometries have been investigated by simulations and experiments: one in a leaky waveguide antenna and the other in a closed waveguide filtering structure. Both geometries offered an out-of plane displacement of 2 mm of the flexible membrane at driving currents of 40 mA (max.) for switching from ON to the OFF state and 140 mA (max.) for switching from the OFF to the ON state. The latched state was maintained with a permanent magnet generating a flux density of 2.55 mT in the vicinity of the magnetically actuated membrane.

A switched antenna was designed, fabricated and tested. Simulations and measurements showed similar gains (~13 dB) and comparable radiation patterns when the switch is in the ON state. However, the experimental characterization highlighted the difficulty of achieving the OFF state antenna characteristics predicted by simulations. This was due to a non-perfect electrical contact between the tip of the cantilever and waveguide broad-wall. Overall, the concept of a switched antenna using this type of switch was proven but more work is needed to overcome this contact problem.

The demonstrated membrane switch could be a potential candidate for reconfigurable antennas. As this switch does not have any electronic components, the interference coming from its environment will not be a concern. One of the most interesting characteristics of the proposed switch is its negligible loss. This allows its integration into antenna feeding networks.

The second part of this research dealt with the demonstration of a stop-band filter, implemented using a variable reactance membrane switch in a closed rectangular waveguide. Fortunately, with this switch configuration, we were able to surmount the aforementioned metal-metal contact problem, as the moving cantilever makes a dielectric-metal contact with the waveguide broad-wall. The measured results verify the concept demonstrating an insertion loss of -29.7 dB at a notch frequency of 11.1 GHz and a 20 dB stop-band bandwidth of 0.2 GHz. By using two cascaded switches, this bandwidth was extended to 0.9 GHz. Measured switching time were 3 ms from the OFF to the ON state and 80 ms from the ON to the OFF state.

## 5.2 Future Work

Even though the proposed switches demonstrated promising results, a few issues still need to be further addressed.

**Antenna switch**

The reconfigurable antenna did not work as expected. This is due to a non perfect contact between the tip of the cantilever and the waveguide broad-wall in the OFF state. Future efforts can be directed towards developing a technique to enhance this electrical contact.

**Variable reactance switch**

For improving the switching time from ON to OFF, suppression of bounce duration is required. An approach to minimize this duration may be the use of a very high permeability magnetic material. This will provide low actuation voltage and fast settling time. It has been demonstrated in section 4.3 that different sized membranes give varied notch frequencies. By cascading set of dissimilar (in dimensions) membrane switches, a tunable band stop filter can be implemented. This would be a completion of what has been done in this work regarding variable reactance

membrane switch. Another possible research direction could be to derive an equivalent electric circuit model of the flexible beam in the upright position. With such a model, it would be possible to use filter synthesis software tools to assist in the design of the proposed reconfigurable filters. Without such models, design would only be possible with time consuming electromagnetic simulations.

As indicated in Chapter 1, the majority of the devices currently used in reconfigurable RF components (MEMS, PIN diodes, varactors, FETs) have severe power limitations. The switching elements presented here are operating in a rectangular waveguide which is well known for its high power handling capability. In addition, all the parts of the switch exposed to the RF field are passive. We can therefore anticipate that it will exhibit linear operation at high power levels before deleterious effects such as passive intermodulation or electrical breakdown occur. Unfortunately, it was not possible to verify this conjecture because high-power X-band generators are not available in our laboratory. Should such generators become available to the research team, future work should then include tests to verify the real power handling of the flexible switch devices we have proposed.

# REFERENCES

[1] D. Lichodziejewski, R. Cravey, G. Hopkins, "Inflatably Deployed Membrane Waveguide Array Antenna for Space" AIAA 2003-1649, 4th Gossamer Spacecraft Forum, April 7-10, 2003, Norfolk, VA.

[2] M. Leipold, H. Runge, and C. Sickinger, "Large SAR Membrane Antennas with Lightweight Deployable Booms," 28th ESA Antenna Workshop on Space Antenna Systems and Technologies, ESA/ESTEC, May 31 –June 03, 2005.

[3] D. Fralick, R.L. Cravey, G. Hopkins, D. Lichodziejewski, M. C. Bailey, "Performance Evaluation of a Membrane Waveguide Array Antenna", IEEE-2003-1148 IEEE Aerospace Conference, March 8 2003, WY

[4] M.C. Bailey and T. G. Campbell, "Inflatable Membrane Waveguide Antenna Array for Space applications" IUTAM-IASS Symposium on Deployable Structures, Cambridge, UK, September 6-9, 1998.

[5] A.Di. Maria, M. Limbach, R. Horn, A. Reigber, "Reflectarray membrane study for deployable SAR antenna," *Antennas and Propagation, 2009. EuCAP 2009. 3rd European Conference on*, vol., no., pp.3720-3723, 23-27 March 2009

[6] B.M. Kendall, M.C. Bailey, L.C. Schroeder, "Inflatable antenna microwave radiometer for soil moisture measurement," *Combined Optical-Microwave Earth and Atmosphere Sensing, 1995. Conference Proceedings., Second Topical Symposium on* , vol., no., pp.217-219, 3-6 Apr 1995

[7] M. Leipold, M. Eiden, CE. Garner, L.Herbeck, "Solar Sail Technology Development and Demonstration", 4th IAA International Conference on Low-Planetary Missions, May 2-5, 2000, Johns Hopkins University, Maryland, USA, IAA 2000, Paper 0707

[8] G.M. Rebeiz, *RF MEMS: Theory, Design and Technology*; Wiley: Hoboken, NJ, USA, 2003.

[9] J.B. Rizk, E. Chaiban, G.M. Rebeiz "Steady state thermal analysis and high-power reliability considerations of RF MEMS capacitive switches," *Microwave Symposium Digest, 2002 IEEE MTT-S International* , vol.1, no., pp.239-242, 2002

[10] W.Thiel, K. Tornquist, R. Reano, L.P.B "Katehi A Study of Thermal Effects in RF-MEMSwitches Using a Time Domain Approach", In *Proceedings of the IEEE MTT-S International Microwave Symposium*, Seattle, WA, USA, 2002; pp. 235-238.

[11] C.T.-C. Nguyen, L.P.B. Katehi, G.M. Rebeiz, "Micromachined devices for wireless communications," *Proceedings of the IEEE* , vol.86, no.8, pp.1756-1768, Aug 1998

[12] P.M. Zavracky, N.E. McGruer, R.H. Morrison, and D. Potter, "Microswitches and Microrelays with a View Toward Microwave Applications, " International Journal of RF and Microwave Computer Aided Design, vol. 9, no. 4, pp. 338– 347, July 1999.

[13] S. Duffy, C. Bozler, S. Rabe, J. Knecht, L. Travis, P. Wyatt, C. Keast, M. Gouker, "MEMS microswitches for reconfigurable microwave circuitry," *Microwave and Wireless Components Letters, IEEE* , vol.11, no.3, pp.106-108, Mar 2001

[14] C.L. Goldsmith, Z. Yao, S. Eshelman, and D. Denniston, "Performance of Lowloss RF MEMS Capacitive Switches, " IEEE Microwave and Guided Wave Letters, vol. 8, no. 8, pp. 269–271, August 1998.

[15] S.J. Gross, Q.Q. Zhang, S. Trolier-McKinstry, S. Tadigadapa, T.N. Jackson, "RF MEMS piezoelectric switch," Device Research Conference, 2003 , vol., no., pp. 99- 100, 23-25 June 2003

[16] G.M. Rebeiz, *RF MEMS: Theory, Design and Technology*, John *Wiley* & Sons, Inc., Hoboken, NJ, USA, 2003

[17] R.R. Mansour, "RF MEMS for space applications," MEMS, NANO and Smart Systems, 2005. Proceedings. 2005 International Conference on, vol., no., pp. 191- 192, 24-27 July 2005

[18] Z. Jun, L. Chang, J. Schutt-Aine, C. Jinghong, K. Sung-Mo, "Development of a wide tuning range MEMS tunable capacitor for wireless communication systems," *Electron Devices Meeting, 2000. IEDM Technical Digest. International*, vol., no., pp.403-406, 2000

[19] R. Zhang, R.R Mansour, "Novel digital and analogue tunable lowpass filters," *Microwaves, Antennas & Propagation, IET* , vol.1, no.3, pp.549-555, June 2007

[20] A. Ocera, P. Farinelli, P. Mezzanotte, R. Sorrentino, B. Margesin, F. Giacomozzi, "A Novel MEMS-Tunable Hairpin Line Filter on Silicon Substrate," *Microwave Conference, 2006. 36th European*, vol., no., pp.803-806, 10-15 Sept. 2006

[21] C.Y. Ong; M. Okoniewski, "Low loss switchable coupled resonator bandpass filter," *Microwave Symposium Digest, 2008 IEEE MTT-S International* , vol., no., pp.137-140, 15-20 June 2008

[22] J. Nath, D. Ghosh, J.-P. Maria, A.I. Kingon, W. Fathelbab, P.D. Franzon, M.B. Steer, "An electronically tunable microstrip bandpass filter using thin-film Barium-Strontium-Titanate (BST) varactors," *Microwave Theory and Techniques, IEEE Transactions on* , vol.53, no.9, pp. 2707- 2712, Sept. 2005

[23] A. Tombak, J.-P. Maria, F.T. Ayguavives, Jin. Zhang Jin, G.T. Stauf, A.I. Kingon, A. Mortazawi, "Voltage-controlled RF filters employing thin-film barium-strontium-titanate tunable capacitors," *Microwave Theory and Techniques, IEEE Transactions on* , vol.51, no.2, pp. 462- 467, Feb. 2003

[24] Y.Lu " RF MEMS Devices and their applications in reconfigurable RF/Microwave circuits", Ph.D. dissertation, University of Michigan, 2005.

[25] R. Jakoby, P. Scheele, S. Muller, C. Weil, "Nonlinear dielectrics for tunable microwave components," *Microwaves, Radar and Wireless Communications, 2004. MIKON-2004. 15th International Conference on*, vol.2, no., pp. 369- 378 Vol.2, 17-19 May 2004

[26] G.M. Rebeiz, J.B. Muldavin, "RF MEMS switches and switch circuits," *Microwave Magazine, IEEE*, vol.2, no.4, pp.59-71, Dec 2001

[27] M. Ruan, J. Shen, and C.Wheeler, "Latching Micro Electromagnetic Relays," Solid-State Sensor and Actuator Workshop (Hilton Head 2000), Hilton Head Island, SC (June 4-8, 2000), pp.146-149

[28] R. Holzer, I. Shimoyama, H. Miura, "Hybrid electrostatic/magnetic microactuators," Robotics and Automation, 1995. Proceedings, 1995 IEEE International Conference on , vol.3, no., pp.2941-2946 vol.3, 21-27 May 1995

[29] C. Il-Joo, S. Taeksang, B. Sang-Hyun, Y. Euisik, "A low-voltage and low-power RF MEMS series and shunt switches actuated by combination of electromagnetic and electrostatic forces," *Microwave Theory and Techniques, IEEE Transactions on* , vol.53, no.7, pp. 2450- 2457, July 2005

[30] J.G. Smits, S.I. Dalke, "The constituent equations of piezoelectric bimorphs," *Ultrasonics Symposium, 1989. Proceedings., IEEE 1989*, vol., no., pp.781-784 vol.2, 3-6 Oct 1989

[31] M.S. Weinberg, "Working equations for piezoelectric actuators and sensors," Microelectromechanical Systems, Journal of , vol.8, no.4, pp.529-533, Dec 1999

[32] D.L. DeVoe, A.P. Pisano, "Modeling and optimal design of piezoelectric cantilever microactuators," *Microelectromechanical Systems, Journal of* , vol.6, no.3, pp.266-270, Sep 1997

[33] S.J. Gross, S. Tadigadapa, T.N. Jackson, S. Trolier-McKinstry, Q.Q. Zhang, "Lead-zirconate-titanate-based piezoelectric micromachined switch," *Applied Physics Letters* , vol.83, no.1, pp.174-176, Jul 2003

[34] F.C.M van de Pol, H.T.G van Lintel, M. Elvenspoek, J.H.J. Fluitman, “Thermopneumatic micropump based on micro-engineering techniques,” Sensors and Actuators A, 21, pp.198, 1990.

[35] http://webdocs.cs.ualberta.ca/~database/MEMS/sma_mems/sma.html [Consulted on August 9, 2010]

[36] N. Camara, K. Zekentes, L.P. Romanov, A.V. Kirillov, M.S. Boltovets, K.V. Vassilevski, G. Haddad, "Microwave p-i-n diodes and switches based on 4H-SiC," Electron Device Letters, IEEE , vol.27, no.2, pp. 108- 110, Feb. 2006

[37] E.W. Jacobs, D.W. Fogliatti, H. Nguyen, D.J. Albares, C.K. Sun, C.T. Chang, "Photo-injection PIN diode switch for high power RF switching," Solid-State and Integrated-Circuit Technology, 2001. Proceedings. 6th International Conference on, vol.2, no., pp. 1274- 1279 vol.2, 22-25 Oct. 2001

[38] K. Miyatsuji, S. Nagata, N. Yoshikawa, K. Miyanaga, Y. Ohishi, D. Ueda, "A GaAs high-power RF single-pole double-throw switch IC for digital mobile communication system," Solid-State Circuits Conference, 1994. Digest of Technical Papers. 41st ISSCC., 1994 IEEE International , vol., no., pp.34-35, 16-18 Feb 1994

[39] Eng Kai Eng, T. Stern, "The Order-and-Type Prediction Problem Arising from Passive Intermodulation Interference in Communications Satellites," Communications, IEEE Transactions on , vol.29, no.5, pp. 549- 555, May 1981

[40] Kai Y. Eng, On-Ching Yue, "High-Order Intermodulation Effects in Digital Satellite Channels," Aerospace and Electronic Systems, IEEE Transactions on , vol.AES-17, no.3, pp.438-445, May 1981

[41] http://www2.dupont.com/Pyralux/en_US/products/laminate/index.html [Consulted on October 15, 2009]

[42] http://metglas.com/products/page5_1_2.htm [Consulted on November 5, 2009]

[43] R. Frisch-Fay, Flexible Bars, London, U.K: Butterworth, 1962.

[44] Crandall, S. H, Dahl, N. C. & Lardner, T. J. (1978) An Introduction to the Mechanics of Solids (McGraw–Hill, New York).

[45] http://en.wikipedia.org/wiki/Young's_modulus [Consulted on November 5, 2009]

[46] J.H. Schaffner, R.Y. Loo, D.F. Sievenpiper, F.A. Dolezal, G.L. Tangonan, J.S. Colburn, J.J. Lynch, J.J. Lee, S.W. Livingston, R.J. Broas, M. Wu, "Reconfigurable aperture antennas using RF MEMS switches for multi-octave tunability and beam steering," Antennas and Propagation Society International Symposium, 2000. IEEE, vol.1, no., pp.321-324 vol.1, 2000

[47] K.C. Gupta, Li. Jun, R. Ramadoss, W. Chunjun, "Design of frequency-reconfigurable rectangular slot ring antennas," Antennas and Propagation Society International Symposium, 2000. IEEE , vol.1, no., pp.326 vol.1, 2000

[48] D. Sievenpiper, J. Schaffner, B. Loo, G. Tangonan, R. Harold, J. Pikulski, R. Garcia, "Electronic beam steering using a varactor-tuned impedance surface ," Antennas and Propagation Society International Symposium, 2001. IEEE , vol.1, no., pp.174-177 vol.1, 2001